EPFL

Thèse n° 9854

Telomere protection against oxidative stress

Présentée le 22 septembre 2023

Faculté des sciences de la vie
Unité du Prof. Lingner
Programme doctoral en approches moléculaires du vivant

pour l'obtention du grade de Docteur ès Sciences

par

Thu Trang NGUYEN

Acceptée sur proposition du jury

Prof. P. Gönczy, président du jury
Prof. J. Lingner, directeur de thèse
Prof. C. M. Azzalin, rapporteur
Prof. L. Krejcí, rapporteur
Prof. D. Suter, rapporteur

École
polytechnique
fédérale
de Lausanne

2023

Acknowledgements

"Everything will be okay in the end. If it's not okay, it's not the end."

John Lennon

Here I am reaching the end of my PhD journey, and I would probably have never made it without my family, friends and colleagues, to whom I would like to express my deepest gratitude.

I would like to first thank my supervisor Prof. Joachim Lingner for giving me an opportunity to do my PhD in his lab, for all of his support and guidance during the last 5 years, his patience, encouragement and understanding during difficult time, for giving us the freedom to pursue our own research questions, and just as importantly, for his humor. To all the past and present members of Lingner lab, I owe special thanks to them for always being supportive and helpful. I would like to express my appreciation to Wareed, whom I shared a desk with for two years. Wareed was the one who taught me many experimental techniques when I first joined the lab, always open for discussion not only about science and experiments but also politics, environment, life, etc., and he gave me critical insights and suggestions about my project even after he left the lab. I would also like to thank my "Telo cool kids" comrades: Efty and Thomas for always saying "yes" when I asked for favors, and for lightening up my lab life. Thomas with his jokes and positivity, and his help in collecting liters of cells for my QTIP experiments and running a million of agarose gels made my lab life much easier and enjoyable, and Efty has always been the one who I came to for scientific and personal advices. I would also like to thanks Efty for generating the cell line containing Halo-tagged TRF1 which I used in my live-cell imaging experiments. To Rita, Anna and Patricia, thank you very much for being my PhD fellows, for always being helpful, for sharing not only the PhD frustration but also many good laugh and joyful moments in and outside of the lab, and for our friendship. I am also thankful to Samah and Suna for all of their scientific feedback and suggestions, their encouragement and support, and for our lunchtime together. To Galina who patiently answered all of my questions about QTIP and Mass Spectrometry when I first started, and always gave constructive and practical comments about my project, I would like to thank you very much for that. To Gabriela who was very warmly welcoming from the beginning, thank you for sharing your knowledge and expertise, for being reassuring and comforting, and for giving me all the addresses of good Asian groceries and restaurants. I would also like to express my gratitude to Marianna, Aleks and Anna Briod for their helpful advices and intriguing discussions. Also, I thank Joachim, Wareed, Galina and Rita for their comments on this thesis, and Samah for her help in translating the abstract.

My appreciation also goes to Prof. Ylli Doksani and his lab for hosting me for my three-month internship. Ylli's encouragement and engaging attitude, and the hospitality from the lab made me feel very welcoming. I would like to particularly thank Giulia for her guidance and her help in experimental work both during my time in the lab and after I left, and for proofreading part

of my thesis, Elia for sharing the struggle of being a PhD, as well as Martina, Lorenzo and Eleftherios for all of the interesting discussion and support.

I would like to express my appreciation to Prof. Pierre Gönzy, the president of my thesis committee, as well as Prof. David Suter, Prof. Claus Azzalin and Prof. Lumír Krejčí for their interest in my research project and their participation as members of my thesis committee. I am also thankful for all valuable insights and suggestions from Prof. Elisa Oricchio – my mentor and the president of my candidacy exam and mid-thesis meeting, Prof. Etienne Meylan – my previous mentor and member of my candidacy exam and mid-thesis meeting, Prof. Susan Smith – member of my mid-thesis meeting and Prof. David Shore – member of my candidacy exam committee.

My gratitude also goes to EPFL core facilities including Bioimaging and Optics Platform (BIOP) and Proteomics Core Facility (PCF), as well as Protein Analysis Facility in the University of Lausanne for all the support provided. I am also thankful to Nicole, Natalia and Tatiana for their help in administrative duties.

In addition, I would like to thank the Marie Skłodowska-Curie Action Innovative Training Networks for funding part of my PhD study, and the ITN-aDDRess consortium and my ITN-aDDRess fellows for all insightful scientific discussion and support.

My enthusiastic journey with biology started since I was in high school, and lasts until now thanks to my high school teacher Ms. Xuan, my IBO professors and trainers, my undergraduate project supervisor Dr. Stephan Gasser, my internship supervisor Prof. Fuyuki Ishikawa, as well as my bachelor thesis supervisor Prof. Takaomi Sanda. I am deeply thankful to them.

To all of my friends here in Switzerland and all over the worlds, thank you very much. To Lieu, my best friend who is also courageously doing her PhD, thank you for all of the fun trips that we had together, for encouraging me during my difficult time, and for providing me a place that makes me feel like home where I can go and rest when I feel tired. To Van, my big sister here in Lausanne, thank you for being caring and supportive, for checking up on me from time to time to make sure that I am doing okay, and for all of the silly moments that we shared. To Tho, Tin and Hoang, thank you for your care and for making my life outside of the lab joyful. I am thankful to all of you for making my life away from home more endurable and enjoyable.

To my boyfriend Guillaume, thank you very much for always being supportive and believing in me, for cheering me up when I felt down, for patiently enduring my (sometimes unreasonable) grumpiness, and for always being there for me during the last few difficult months.

And no word can describe my gratitude to my family, who has been loving and supporting me unconditionally. I would like to thank my parents who have been always undoubtedly believing in me even when I did not myself, my brother for his “annoying” friendship and care, my aunt and uncle – my second parents, for raising me as their own child, and my cousins with whom I shared very interesting childhood, and my grandmother who took care of me since I was born and still does. To all of them, I owe my deepest appreciation.

Abstract

Telomeres are nucleoprotein structures at the ends of linear chromosomes. Telomeres have a unique structure which distinguishes chromosome termini from DNA damage sites. Telomeres are essential for the maintenance of genomic integrity. Shelterin complexes are the most abundant proteins associated with telomeric DNA. They prevent intact telomeres from being recognized as double-stranded DNA breaks, thus preventing the inappropriate activation of DNA damage signaling. The shelterin protein complex consists of 6 subunits: TRF1, TRF2, TPP1, POT1, Rap1 and TIN2. In addition to shelterin, a very large number of additional proteins have been detected at telomeres. The function of many of these is less well characterized. Despite the heterochromatin features present at telomeric and subtelomeric regions, telomeres are transcribed into the long non-coding telomeric repeat containing RNA TERRA.

Telomeric DNA is particularly susceptible to oxidative damage due to the repression of some DNA repair pathways at intact telomeres, triple-G-containing 5'-TTAGGG-3' repeats, which are highly prone to oxidation, and 3' overhangs, which cannot be repaired by the base excision repair pathway due to the lack of a complementary strand. Reactive oxygen species (ROS) trigger telomeric DNA strand breaks and nucleotide oxidation, causing telomerase inhibition, telomere shortening and cellular senescence. Several DNA repair factors and antioxidant enzymes have been reported to protect telomeres from oxidative damage. However, it is not well understood how telomeres counteract ROS and how telomeric oxidative lesions are repaired. In my thesis, I aimed at elucidating the molecular mechanisms underlying telomere protection against oxidative damage by studying the changes in telomeric chromatin composition and structure upon oxidative stress induction.

Using menadione, which damages mitochondria and mimics endogenous oxidative stress, we successfully induced damage at telomeres indicated by the accumulation of single-stranded telomeric DNA breaks. We observed elevated levels of telomeric RNA:DNA hybrids (R-loops) upon menadione treatment, coinciding with upregulation of TERRA transcription. The elevation in telomeric R-loop levels was not only mediated by increased telomeric transcription but also due to an increase in TERRA recruitment to damaged telomeres. In addition, we discovered by 2D gel electrophoresis and Electron Microscopy the accumulation of internal loop structures at damaged telomeres. Interestingly, our findings show that the telomeric protein TRF1 dissociates from telomeres upon oxidative damage possibly to render the damaged telomeres accessible to damage signaling and repair. Several mechanisms for TRF1 dissociation can be envisaged. Oxidative lesions in telomeric DNA may reduce the binding affinity of TRF1. In addition, as TRF1 protein cannot bind R-loops, the increase in R-loop levels at damaged telomeres may prevent TRF1 from binding. Also, upregulated TERRA levels may sequester nucleoplasmic TRF1 protein, thereby reducing the concentration of telomere-binding competent TRF1.

We also examined the changes in the whole telomeric chromatin upon oxidative stress induction implementing a two-step quantitative telomeric chromatin isolation protocol (QTIP)

combined with Mass Spectrometry analysis. We detected the recruitment of DNA repair proteins, antioxidant enzymes, chromatin remodelers and post-translational modification (PTM) enzymes. Overall, our results uncover that oxidative damage induces drastic remodeling of the telomeric chromatin composition to orchestrate protection, repair and DNA damage signaling pathways.

Keywords: telomeres, oxidative stress, TRF1, TERRA, R-loop, i-loop, QTIP, DNA damage

Résumé

Les télomères forment une structure nucléoprotéine située à la fin des chromosomes. Les télomères ont une structure unique qui distingue la fin des chromosomes d'un dommage à l'ADN. Les télomères sont essentiels pour la maintenance de l'intégrité génomique. Les complexes shelterins sont les protéines les plus abondantes associées à l'ADN télomérique. Ils empêchent les télomères d'être reconnus comme des cassures doubles brins d'ADN, et ainsi empêche l'activation inappropriée de la voie de signalisation des dommages à l'ADN. Le complexe shelterin est composé de 6 protéines : TRF1, TRF2, TPP1, POT1, Rap1 et TIN2. En plus de la shelterin, un grand nombre d'autres protéines ont été détectées aux télomères. La fonction de la plupart de ces protéines reste encore méconnue. Malgré le statut hétérochromatinique présent aux régions télomériques et subtélomériques, les télomères sont transcrits en ARN longs non-codant, TERRA.

L'ADN télomérique est particulièrement sensible aux dommages causés par un stress oxydatif en raison de : la répression de certaines voies de réparation de l'ADN aux télomères intacts, de la présence de 3 guanines consécutives dans la séquence répétées télomérique (5'-TTAGGG-3') sensibles à l'oxydation et d'une extrémité 3' sortantes qui ne peux pas être prises en charge par une voie de réparation basée sur l'excision (BER) dû au manque du brin complémentaire. Les dérivés réactifs de l'oxygène (ROS) entraine des cassures double brin au niveau de l'ADN télomérique et l'oxydation de nucléotide, causant : l'inhibition de la télomérase, le raccourcissement des télomères et la senescence cellulaire. Plusieurs facteurs et enzymes antioxydantes ont été identifié comme important pour protéger les télomères du dommage oxydatif. Cependant, la compréhension de comment les télomères contrecarrent les ROS et comment les lésions oxydatives sont réparées, reste très méconnue. Dans le cadre de ma thèse, j'ai cherché à élucider le mécanisme moléculaire sous-jacent à la protection des télomères contre le dommage oxydatif en étudiant les changements dans la composition et la structure de la chromatine télomérique après induction d'un stress oxydatif.

En utilisant le ménadione, qui endommage les mitochondries et qui mimique le stress oxydatif endogène, nous avons réussi à induire un dommage aux télomères indiqué par l'accumulation de cassures simple brin aux télomères. Nous avons observé un niveau élevé d'hybride d'ARN/ADN (R-loops) aux télomères après traitement avec le ménadione qui coïncide avec une régulation positive de la transcription de TERRA. L'élévation des R-loops aux télomères n'est pas seulement dû à une augmentation de la transcription télomérique mais aussi à une augmentation du recrutement de TERRA aux télomères endommagés. De plus, nous avons découvert par électrophorèse à 2-dimension et microscopie électronique l'accumulation de structure en boucle interne (i-loop) aux télomères endommagés. De façon intéressante, nos travaux montrent que la protéine TRF1 après stress oxydatif, se dissocie des télomères probablement dans le but de rendre les télomères endommagés accessible à la réponse aux dommages à l'ADN et à la réparation. Plusieurs mécanismes de dissociation de TRF1 des télomères peuvent être envisagés. Les lésions oxydatives au niveau de l'ADN télomériques peuvent affecter l'association de TRF1 aux télomères. De plus, puisque la protéine TRF1 ne

peut pas se lier aux R-loops, l'augmentation du niveau de R-loops aux télomères endommagés peut empêcher la liaison de TRF1. Aussi, la régulation positive du niveau de TERRA peut séquestrer la protéine TRF1 nucléoplasmique, et ainsi réduire la concentration de la protéine TRF1 capable de se lier aux télomères.

Nous avons aussi examiné les changements dans l'entièreté de la chromatine télomérique après induction d'un stress oxydatif en utilisant un protocole qui permet d'isoler la chromatine télomérique appelé aussi QTIP (quantitative telomeric chromatin isolation protocol) combiné avec l'analyse par spectrométrie de masse. Nous avons détecté le recrutement de protéines de réparation de l'ADN, des enzymes antioxydantes, des protéines impliquées dans la réorganisation de la chromatine et des enzymes de modifications post-traductionnelles. Globalement, nos résultats ont permis de mettre en évidence une importante réorganisation de la composition de la chromatine télomérique lors d'un dommage oxydatif afin de permettre la protection, la réparation et d'éviter d'activer la signalisation des dommages à l'ADN.

Mots clefs : Télomères, stress oxydatif, TRF1, TERRA, R-loop, i-loop, QTIP, Dommage à l'ADN

Table of content

Chapter 1. Introduction

1.1. Telomere structure, function and maintenance

Telomeres are nucleoprotein structures at the end of chromosomes in eukaryotes, functioning in protection of genomic integrity. The term “telomeres” was coined by Muller in 1938, derived from Greek “end part” (“telos” = end and “méros” = part). The interest in telomeres started with the fundamental observation by Muller and McClintock that chromosome ends are physiologically distinctive from breaks induced by X-ray irradiation (Barbara, 1941, 1939; Muller, 1938).

The discovery of DNA double helix structure by Watson and Crick in 1953 suggested a DNA replication mechanism, which was then further characterized by Meselson and Stahl to propose the semi-conservative DNA replication mechanism which ensures the proper segregation of the genetic material into two identical daughter cells (Meselson and Stahl, 1958; Watson and Crick, 1953). However, further studies about DNA replication machinery and DNA polymerase activity reveal that DNA could not be replicated fully at the end of chromosomes, leading to loss of genetic material with each cycle of replication, which is recognized as the end replication problem. This provides an explanation for Hayflick’s observation of limited replication potential of somatic cells in culture, which is now known as Hayflick limit or replicative senescence (Hayflick, 1965). However, certain cell types, including stem cells and tumor cells, bypass this limitation by using telomere maintenance mechanisms.

Since the late 1970s, it has been discovered that eukaryotic chromosome ends consist of repetitive DNA sequence, and the number of repeats varies significantly depending on species (de Lange et al., 1990; Hastie et al., 1990; Moyzis et al., 1988). This repetitive nature of telomeric DNA allows it to act as a buffer which can be sacrificed during DNA replication and cell division. In human cells, telomeres are composed of 2 to 15 kb of $(TTAGGG)_n$ terminating into a 3’ single-stranded overhang of 50 – 300 nt, in which the G-rich strand is longer than the C-rich strand (Henderson & Blackburn, 1989; Klobutcher et al., 1981; Makarov et al., 1997). This single-stranded overhang can loop back and invade the double-stranded region, displacing the G-rich strand to form a structure named t-loop (Figure 1). T-loop formation is facilitated by TRF2 protein – a component of the most abundant telomeric protein complex named shelterin, which is the central solution for the end protection problem. This will be discussed in more detail in the following section.

Subtelomeres are chromosome-arm-specific sequences locating immediately upstream of the repetitive telomeric tract. They comprise telomeric-like repeats and segmentally duplicated tracts (Riethman et al., 2005). A subset of human subtelomeres contains promoters from which the telomeric long non-coding RNAs (TERRA) are transcribed (Azzalin et al., 2007) (Figure 1).

1.1.1. Telomere-specific shelterin protein complex (Figure 1)

Shelterin protein complexes are the most abundant telomere-specific proteins, consisting of six subunits (de Lange, 2005). TRF1 (telomeric repeat binding factor 1) and TRF2 (telomeric repeat binding factor 2) proteins bind double-stranded DNA (dsDNA) region of telomeres as homodimers through Myb domain (Bilaud et al., 1997; Broccoli et al., 1997; Chong et al., 1995; König et al., 1998; Zhong et al., 1992). Rap1 protein (repressor-activator protein 1) binds constitutively TRF2 (Li et al., 2000). TIN2 protein (TRF1-interacting nuclear protein 2) links TRF1 and TRF2 proteins (Houghtaling et al., 2004; Kim et al., 1999; Liu et al., 2004a), and also associates with TPP1 protein (also known as ACD, adrenocortical dysplasia protein homolog) (Houghtaling et al., 2004; Liu et al., 2004b; Ye et al., 2004). TPP1 in turn recruits the single-stranded DNA (ssDNA) binding protein POT1 (protection of telomeres 1), which binds the telomeric G-rich overhang through OB (oligonucleotide binding) folds (Baumann and Cech, 2001; Liu et al., 2004b; Ye et al., 2004). The shelterin protein complexes protect intact telomeres from being recognized as dsDNA breaks, thus preventing the inappropriate activation of DNA damage signaling.

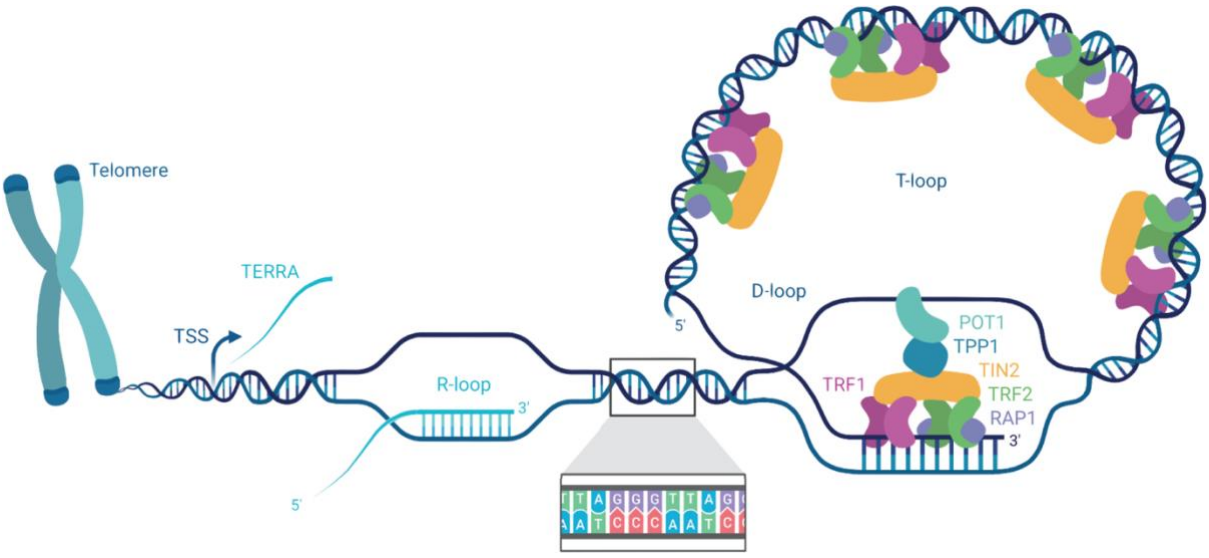

Figure 1: The nucleoprotein composition of telomeres (adapted from Fernandes et al., 2021). Human telomeres consist of tandem 5'-TTAGGG-3' repetitive double-stranded DNA, followed by a 3' single-stranded overhang which can loop back and invade the double-stranded region, base-pairing with the C-rich strand to form a telomeric D-loop (termed t-loop). Telomeres are bound by a large number of proteins, among which the most abundant ones are shelterin protein complexes. They contain six protein components: the dsDNA-binding proteins TRF1 and TRF2, the ssDNA-binding protein POT1, TPP1 and TIN2 connecting POT1 to TRF1 and TRF2, and Rap1 which binds TRF2 protein. The telomeric 5'-TTAGGG-3' repeats are preceded by subtelomeric sequences. Some of them contain transcription start sites (TSS) from which the long non-coding RNA TERRA is transcribed. TERRA can bind to telomeres through direct base-pairing, forming R-loop structures, leaving a displaced G-rich DNA strand.

1.1.2. Chromosome end protection mechanism

Due to the resemblance of chromosome ends to double-stranded DNA breaks (DSBs), unprotected telomeres can trigger DNA damage responses (DDR) through the activation of ATM and ATR kinases, classical and alternative non-homologous end joining (c-NHEJ and alt-NHEJ) and homologous recombination (HR) [reviewed in (de Lange, 2018)].

TRF2 protein is known to suppress ATM and NHEJ activation at chromosome ends. TRF2 depletion leads to ATM activation at telomeres and chromatin end fusion. As TRF2 mediates t-loop formation (Doksani et al., 2013), the suppressive effect of TRF2 on DDR activation is possibly via sequestration of the 3' overhang by t-loops. This shelterin protein blocks the dismantlement of t-loops throughout the cell cycle except S-phase during which RTEL1 helicase unwinds t-loops for DNA replication (Sarek et al., 2019, 2015; Vannier et al., 2012). Unfolded t-loops can be substrates of ATM and NHEJ signaling independently or collectively, depending on the level of TRF2 protein remaining at telomeres, structural states of telomeres and cell cycle (Cesare et al., 2009; Hayashi et al., 2012; Orthwein et al., 2014; Van Ly et al., 2018). T-loop structures conceal chromosome ends from being recognized as DSBs by the MRN complex (Mre11-NBS1-RAD50) – the first sensor of DSBs. It recruits and activates ATM kinase (ataxia-telangiectasia mutated) (Lee and Paull, 2005), which in turn phosphorylates downstream proteins such as H2AX, CHK2 and 53BP1 (Banin et al., 1998, 1998; Burma et al., 2001; Chapman et al., 2013; Matsuoka et al., 2007, 2000). TRF2 depletion results in the accumulation of phosphorylated H2AX (γH2AX) and 53BP1 at telomeres, forming so-called telomere dysfunction-induced foci (TIFs) which can be visualized by immunofluorescence staining (Takai et al., 2003). Apart from ATM signaling pathway, TRF2 also counteracts the activation of c-NHEJ via preventing the oligomerization of Ku70/80 and the accumulation of 53BP1 at telomeres (Okamoto et al., 2013; Ribes-Zamora et al., 2013). In TRF2-deficienct cells, telomeres become substrates of c-NHEJ pathway resulting in chromosome end-to-end fusions (Celli and de Lange, 2005; van Steensel et al., 1998). It leads to genomic instability due to mis-segregation during mitosis (Barbara, 1941).

The shelterin protein POT1 blocks the binding of RPA (replication protein A) to the telomeric single-stranded 3' overhang, thereby preventing the activation of ATR signaling (Baumann and Cech, 2001; Liu et al., 2004b; Ye et al., 2004). Although POT1 protein is less abundant, it can effectively exclude RPA probably because of its shelterin-mediated enrichment at telomeres. Upon POT1a depletion in MEFs (Mouse Embryonic Fibroblasts), RPA binds to single-stranded telomeric DNA, leading to the recruitment and activation of ATR, followed by the phosphorylation of its downstream proteins such as Chk1, eventually leading to cell cycle arrest (Denchi and de Lange, 2007). In addition to ATR signaling suppression, POT1 protein also plays a role in inhibiting homology-directed repair (HDR) at telomeres (Glousker et al., 2020; Wu et al., 2006). The binding of classical recombination factors such as RAD51 to single-stranded telomeric DNA in POT1-deficient cells possibly triggers HDR at telomeres (Glousker et al., 2020).

Single-stranded DNA from damaged or stalled replication forks or other telomeric structures such as R-loops can also be the substrates for ATR signaling activation. Depletion of the shelterin subunit TRF1 leads to replication stress at telomeres, resulting in the activation of ATR signaling (Sfeir et al., 2009). It suggests the role of TRF1 protein in promoting efficient telomere replication, thereby preventing ATR activation.

Concisely, the shelterin protein complex provides the main solution for the end protection problem by sequestering the DSB-resembling chromosome ends, thereby suppressing inappropriate activation of DDR pathways. Critically short telomeres that fail to recruit enough shelterin proteins trigger the de-repression of DDR, leading to cell cycle arrest.

1.1.3. Telomere replication

1.1.3.1. The end-replication problem and telomere shortening

Telomeres shorten with each cell division due to incomplete replication of chromosome ends. This is because DNA polymerase activity requires free 3'-OH ends, and thus, they can only synthesize new DNA strands from 5' to 3' direction. It is initiated with the synthesis of short RNA primers by primase enzyme to provide 3'-OH ends, followed by DNA strand extension by DNA polymerase α and δ [reviewed in (MacNeill, 2012; Prakash and Borgstahl, 2012)]. On telomeric G-rich strands oriented 5' to 3', DNA synthesis can only happen discontinuously with the generation of many short DNA fragments named Okazaki. The primers are then removed and filled by DNA polymerases using 3'-OH ends from the neighboring fragments [reviewed in (MacNeill, 2012)]. However, due to the unavailability of a 3'-OH group, after removal of the distal-most primer, a short 3' overhang is formed. Meanwhile in the case of telomeric C-rich strands oriented 3' to 5', DNA synthesis happens in a continuous manner, catalyzed by DNA polymerase ε to generate a blunt end, which is processed in the later stage to form a 3' overhang (Soudet et al., 2014; Wu et al., 2012).

Apollo nuclease is recruited to the newly generated blunt end by TRF2 to form a short 3' overhang, which is then bound by POT1 shelterin subunit to inhibit further Apollo nuclease activity (Wu et al., 2012). POT1 protein also binds the 3' overhang generated by lagging strand synthesis for the same purpose. It is followed by extensive 5' resection by exonuclease 1 at both ends to generate transient long 3' overhangs, which are then filled by CST complex (CTC1-STN1-TEN1) and DNA polymerase α-primase, leaving both lagging and leading ends with 3' overhangs (Dai et al., 2010; Wu et al., 2012). The chromatid resulted from lagging strand synthesis keeps the original length, while the other one is shortened.

The progressive shortening of telomeres provides a mechanism to limit cell proliferation. At critically short telomeres, DNA damage signalling is activated, leading to p53 activation and permanent cell cycle arrest termed replicative senescence (Kaul et al., 2012). If both p53 and Rb (retinoblastoma) proteins are suppressed, cells bypass senescence and continue dividing, causing further telomere shortening, which eventually initiates a terminal response termed replicative crisis. Such cells exhibit telomere fusion, genome instability, autophagy hyperactivation and subsequently cell death [reviewed in (Arnoult and Karlseder, 2015)] (Nassour et al., 2019). Stem cells and cancer cells activate telomere maintenance mechanisms depending on the telomerase enzyme or alternative lengthening of telomeres pathway to escape the proliferation limit (Bryan et al., 1995; Bryan and Cech, 1999).

1.1.3.2. Replication stress at telomeres

The telomeric repetitive sequence and its ability to form special structures are obstacles for DNA replication machinery. The 5'-TTAGGG-3' repeats and its GC-rich nature pose a risk for replisome slippage (de Lange et al., 1990). In addition, as lagging strand synthesis is discontinuous, the parental G-rich strand is partially single-stranded during replication which may allow formation of G-quadruplexes (G4) structures, which can impede the progression of the replication fork (Granotier et al., 2005; Lerner and Sale, 2019). Another interfering factor is the transcription at telomeres leading to the generation of long non-coding telomeric repeat-containing RNA (TERRA). Collision of transcription machinery and replisome during DNA strand unwinding and machinery progression can interrupt DNA replication [reviewed in (Bermejo et al., 2012)]. Also, nascent TERRA and R-loops – the structure formed when TERRA hybridizes with the telomeric C-rich strand leading to G-rich strand displacement, need to be removed (Arora et al., 2014; Balk et al., 2013; Luke et al., 2008; Petti et al., 2019). TERRA overexpression leading to increased level of telomeric R-loops causes telomere fragility indicating replication stress at telomeres (Feretzaki et al., 2020). At the displaced G-rich strand, G4 structures can be formed, generating additional obstacles for telomeric DNA replication (Duquette et al., 2004). T-loop structures at chromosome ends also need to be dismantled by RTEL1 to facilitate the access of the replication machinery to telomeres during S phase. T-loops that fail to be unwound are excised by a structure-specific nuclease SLX4, leading to telomere shortening (Sarek et al., 2015; Vannier et al., 2012). Besides, shelterin protein levels at replicating telomeres must be fine-tuned because despite the fact that their tight binding to telomeres might affect replication fork progression, they are involved in promoting telomeric DNA replication (Ohki and Ishikawa, 2004; Sfeir et al., 2009). Furthermore, telomeric replication is mainly unidirectional, thus once the fork is collapsed, there is no convergent fork coming from the other side to rescue.

Several factors have been shown to enable replication fork progression, mostly via removing obstacles such as R-loops, G4s, t-loops and relieving topological stress. The shelterin protein TRF1 recruits BLM helicase to unwind G4 structures (Sfeir et al., 2009; Zimmermann et al., 2014), and counteracts R-loop formation facilitated by TRF2 protein (Lee et al., 2018). TRF1 also recruits TFIIH complex, which suppresses telomere fragility and replication defects (Yang et al., 2022). Furthermore, it was proposed that TRF1 works together with fork protection protein TIMELESS to stabilize telomeric replisome (Leman et al., 2012). In addition, TRF1 mediates the binding of DNA topoisomerase II α to telomeres to remove topological stress during the progression of replication fork (Stagno d´Alcontres et al., 2014). Also, TRF2-bound RTEL1 protein resolves t-loop and G4 structures at telomeres (Vannier et al., 2013, 2012). Recently, comprehensive proteomic study of the telomeric replisome identified many factors that specifically facilitate telomere replication (Lin et al., 2021).

1.1.4. Telomere maintenance

Telomere shortening following each cell cycle ultimately generates critically short telomeres with insufficient shelterin protein binding, leading to the activation of ATM and ATR signalling pathways and consequently, cellular replicative senescence or autophagic cell death (Maciejowski & de Lange, 2017; Nassour et al., 2019; Yu et al., 1990). To circumvent this problem, proliferating cells such as stem cells, germline cells and cancer cells elongate telomeres via either telomerase enzyme activation or in the case of cancer cells, the alternative lengthening of telomeres (ALT).

Telomerase was first detected in the model organism *Tetrahymena thermophila*, and was characterized as a reverse transcriptase with an RNA moiety that serves as a template for DNA repeat synthesis (Greider and Blackburn, 1989, 1987, 1985). The catalytic core TERT was subsequently identified in *Euplotes*, *S. cerevsiae*, *S. pombe* and humans (Lingner et al., 1997; Nakamura et al., 1997). In humans, the telomerase RNA subunit (hTR) specifies 5'-TTAGGG-3' repeats. Telomerase is primarily recruited to telomeres via the TEL (TPP1 glutamate- and leucine-rich) patch of TPP1 (Abreu et al., 2010; Nandakumar et al., 2012). In the majority of human tissues, telomerase is suppressed by epigenetic silencing of hTR and hTERT transcription [reviewed in (Cong et al., 2002)]. This enforces telomere shortening and replicative senescence after a certain number of cell cycles, thereby setting cellular proliferative limit and preventing carcinogenesis. 85% to 90% of cancers bypass this by re-activating telomerase expression and activity mainly via mutations in hTERT promoter, which allow the de-repression of hTERT transcription (Borah et al., 2015; Horn et al., 2013; Huang et al., 2013; Killela et al., 2013; Shay and Bacchetti, 1997; Weinhold et al., 2014).

The ALT is a homology-directed recombination-based pathway used for telomere maintenance in 10 – 15% cancer types, especially in aggressive tumors with mesenchymal cell origin (Bryan et al., 1995; Dunham et al., 2000; Heaphy et al., 2011b; Henson et al., 2005). In ALT cells, recombination intermediates can be either processed by BLM-TOP3A-RMI protein complexes leading to telomere extension without any crossover events, or dissolved by SLX4-SLX1-ERCC4 protein complexes in which there is no telomere extension and telomeric DNA exchange might happen (Svendsen et al., 2009; Wu & Hickson, 2003). This results in distinctively heterogenous telomere length and sister chromatid exchange at telomeres, which are two hallmarks of ALT-positive cells (Bryan et al., 1995; Londoño-Vallejo et al., 2004). Another ALT-specific molecular intermediate is C-circles – the single-stranded C-rich extra-chromosomal telomeric repeats formed as a by-product of recombination (Henson et al., 2009). ALT pathway occurs at ALT-associated PML (promyelocytic leukaemia) bodies (APB), in which telomeres are clustered and processed (Yeager et al., 1999; Zhang et al., 2019).

Although the precise molecular mechanism of ALT is unclear, it has been proposed that alteration of chromatin organization might underly ALT activation. Mutations in genes encoding ATRX (α-thalassemia/mental retardation X-linked) and its partner DAXX (death-domain-associated protein) are frequently identified in ALT-positive tumor cells (Heaphy et al.,

2011a; Schwartzentruber et al., 2012). Loss of ATRX and DAXX alters H3.3 histone deposition, which might affect telomeric heterochromatin conformation and promote telomere recombination (Lewis et al., 2010). ATRX also plays a role in replication progression and telomere cohesion, suggesting an explanation for the function of ATRX deficiency in ALT activity (Pickett and Reddel, 2015). Although mutations of these factors are associated with increased genomic instability and telomere length, they are insufficient to activate ALT (Lovejoy et al., 2012). Other factors that function in ALT regulation is histone chaperons ASF1a and ASF1b. The co-depletion of these factors induces ALT phenotypes including telomeric recombination, telomere length heterogeneity, accumulation of extrachromosomal TTAGGG repeats and the formation of APB (O'Sullivan et al., 2014). In addition, the long-noncoding RNA TERRA also plays a key role in triggering and/or sustaining ALT activity. The CpG islands within subtelomeric TERRA promoters are less methylated in ALT cells, resulting in an increase in TERRA transcription (Arora et al., 2014; Episkopou et al., 2014). In the absence of telomerase, TERRA has been shown to promote telomere maintenance based on recombination, thereby delaying replicative senescence and protecting genomic stability (details discussed below).

1.2. TERRA and R-loops

1.2.1. The telomeric repeat-containing long non-coding RNA TERRA

1.2.1.1. Transcription of TERRA

Heterochromatic features have been reported at subtelomeric and telomeric regions including DNA methylation, hypoacetylation of histone H3 and H4, trimethylation of histone H4 lysine 20 (H4K20me3), trimethylation of histone H3 lysine 9 and 27 (H3K9me3 and H3K27me3) and the binding of HP1α (heterochromatin protein 1) (Blasco, 2007; Tardat and Déjardin, 2018). Consistently, the telomere position effect has been described in yeast, drosophila and human, in which the expression of reporter genes was reversibly suppressed upon being placed near telomeric repeats (Baur et al., 2001; Gottschling et al., 1990; Hazelrigg et al., 1984). Thus, telomeres were believed to have no transcription until the discovery of the long non-coding telomeric repeat containing RNA (TERRA) (Azzalin et al., 2007).

TERRA transcription is catalyzed by RNA polymerase II enzyme, starting from promoters within the subtelomeric regions and progressing into the telomeric repetitive regions using C-rich strand as the template (Azzalin et al., 2007; Feretzaki et al., 2019; Nergadze et al., 2009; Porro et al., 2014a; Schoeftner and Blasco, 2008). Thus, TERRA contains chromosome-specific subtelomeric sequence followed by 5’-UUAGGG-3’ repeats (Feretzaki et al., 2019; Porro et al., 2010). There are no transcription termination sites. The variable length of subtelomeric tract being transcribed into TERRA and the variable number of 5’-UUAGGG-3’ repeats result in the heterogeneity of TERRA length ranging from 100 to 10000 bases with an average length of 1000 bases (Azzalin et al., 2007; Porro et al., 2010; Statello et al., 2021). Analysis of TERRA subtelomeric region reveals no post-transcriptional splicing events (Porro et al., 2014a). Similar to mRNAs transcribed by RNA polymerase II, TERRA molecules are 5’-capped with 7-methylguanosine functioning in protecting RNA molecules from 5’-3’ exonucleases (Porro et al., 2010; Shatkin, 1976). Less than 10% of TERRA are polyadenylated (poly(A)), making them more stable than the non-poly(A) one (Porro et al., 2010). The half-life of the former is around 8 hours, whereas the latter has 3-hour half-life (Porro et al., 2010). A recent study suggests that TERRA polyadenylation preferably happens at TERRA transcribed from specific telomeres (Savoca et al., 2023). Also, while polyadenylation is the main factor determining the stability of poly(A)-positive TERRA, RNA-binding protein RALY stabilizes poly(A)-negative TERRA (Savoca et al., 2023). In terms of localization, at least 90% of TERRA molecules localize in the nucleus, either being in nucleoplasm or telomere-bound (Porro et al., 2010). The majority of telomere-bound TERRA is poly(A)-negative, while poly(A)-positive TERRA stays mainly in the nucleoplasm (Porro et al., 2010). N^6-methyladenosine (m^6A) – another TERRA post-transcriptional modification positioning in their subtelomeric region, has been characterized recently (Chen et al., 2022). It is catalyzed by METTL3 methyltransferase and protected by YTHDC1 reader, contributing to TERRA stability (Chen et al., 2022).

TERRA transcription is regulated by many transcription factors including CTCF and cohesin subunit RAD21, which bind telomeres and maintain TERRA transcription (Deng et al., 2012;

Feretzaki et al., 2019), as well as epigenetic modifications. A subset of human subtelomeric regions contain CpG islands within TERRA promoters, which are methylated *de novo* by DNA methyltransferase DNMT1 and DNMT3B during development, thereby inhibiting the expression of a fraction of TERRA (Feretzaki et al., 2019; Nergadze et al., 2009; Porro et al., 2014a; Yehezkel et al., 2008). Heterochromatin-establishing and binding factors such as H3K9 methyltransferase SUV39H1 and HP1α also suppress TERRA transcription (Arnoult et al., 2012). Longer telomeres contain higher density of H3K9me3 and HP1α protein, and thus, have less TERRA transcription (Arnoult et al., 2012). Besides, depletion of TRF2 shelterin subunit results in elevated level of TERRA, suggesting the suppressive role of TRF2 in TERRA transcription (Nassour et al., 2023; Porro et al., 2014a). TERRA in TRF2-depleted cells binds and recruits SUV39H1 to telomeres leading to H3K9 methylation, thereby maintaining telomere chromatin compaction and sustaining telomere fusion (Arnoult et al., 2012).

Cellular level of TERRA is subjected to cell cycle regulation. RT-qPCR analysis of different TERRA species in synchronized Hela cells reveals that TERRA level peaks in early G1 phase. As cells progress through G1, S and G2, TERRA level gradually decreases and reaches the lowest point in late S/G2 phase. It is then followed by a progressive increase until the cells return to G1 phase (Porro et al., 2010). Whether this is regulated transcriptionally or post-transcriptionally is unclear.

1.2.1.2. Functions of TERRA

TERRA plays an important role in telomere maintenance in both ALT cells (this will be discussed in the next section) and in telomerase-positive cells where TERRA contributes to regulation of telomerase activity. *In vitro* experiments show that TERRA can inhibit telomerase via direct interaction with the catalytic component hTERT and complementary base-pairing with the RNA component hTR (Redon et al., 2010). Telomere extension by telomerase mainly happens during late S-phase when TERRA level is lowest (Porro et al., 2010; Tomlinson et al., 2006). In addition, the balance in the levels of TERRA and hnRNPA1 protein (heterogenous nuclear ribonucleoprotein A1) might facilitate telomerase access to telomeres. hnRNPA1 is a TERRA-binding protein which is also detected at telomeres and can inhibit telomerase activity *in vitro* (Redon et al., 2013). It is possible that when TERRA level exceeds hnRNPA1 binding capacity, TERRA binds telomerase and represses its activity (Redon et al., 2013). However, during S phase when hnRNPA1 level is in equilibrium with TERRA levels, telomerase is released from TERRA binding, being able to bind and catalyse telomere extension (Redon et al., 2013).

The variable balance between TERRA and hnRNPA1 levels during cell cycle and the RPA-displacing activity of hnRNPA1 have been proposed to regulate an RPA-to-POT1 switch after S phase (Flynn et al., 2011). RPA is a non-sequence specific ssDNA binding protein functioning in DNA replication and ATR signalling activation (Zou and Elledge, 2003). RPA binds telomeric single-stranded DNA during S phase to facilitate telomere maintenance. In late S phase when hnRNPA1 is released due to the downregulation of TERRA, RPA is stripped out from telomeres by hnRNPA1. The increase in TERRA level afterwards leads to re-association of TERRA and hnRNPA1, which liberates the G-rich telomeric overhang for POT1 binding (Flynn et al., 2011). The role of POT1 in counteracting telomerase activity has been shown *in vitro* and *in vivo* (Kelleher et al., 2005; Loayza and de Lange, 2003). Thus, fine-tuning POT1 association with telomeres during cell cycle might be an indirect way of TERRA to repress telomerase activity.

1.2.2. R-loops

1.2.2.1. R-loop formation and the impact of R-loops on genomic integrity

R-loops are three-stranded structures consisting of an invading RNA base-pairing with its complementary strand to form a DNA-RNA hybrid, and a displaced single-stranded DNA. These structures can range from 100 bp to more than 2 kb long [reviewed in (García-Muse and Aguilera, 2019)]. They have been detected throughout the genome, preferably in genomic region with high GC content and GC skew in which the displaced DNA strand can presumably form G4 structures and stabilize the DNA-RNA hybrid (Duquette et al., 2004; Miglietta et al., 2020). R-loops were thought to mainly form *in cis* during transcription due to the complementarity between RNA and their template DNA strand (Crossley et al., 2019; Lafuente-Barquero et al., 2020; Reaban et al., 1994; Yu et al., 2003). However, studies in yeasts and plants shows that RNA molecules can invade genomic loci distant from their transcription sites, leading to R-loop formation *in trans* (Ariel et al., 2020; Wahba et al., 2013). Apart from being the by-product of transcription, R-loops serve as important intermediates of specific cellular processes such as replication of mitochondrial DNA and Ig class switching in B cells (Xu and Clayton, 1996; Yu et al., 2003). Besides, R-loops have been demonstrated to be involved in regulation of gene expression [reviewed in (García-Muse and Aguilera, 2019)]. R-loops formed at CpG islands can inhibit DNA methylation, thereby promoting transcription. In addition, localization of R-loops at promoters can either favour or impede the binding of transcription activators or repressors, contributing to transcription activation or silencing. When being enriched at G-rich termination elements, R-loops facilitate RNA polymerase pausing, leading to efficient transcription termination. Apart from interfering with the process of transcription, studies have indicated a connection between R-loops, DNA breaks and DNA damage response.

R-loops can be the source of DNA damage and genomic instability by being obstacles to transcription elongation and the DNA replication machinery (Domínguez-Sánchez et al., 2011; Gan et al., 2011; Huertas and Aguilera, 2003; Wellinger et al., 2006). Also, the displaced single-stranded DNA is susceptible to mutagenesis. On the other hand, it has been demonstrated using many R-loop detection methods in different models that DNA damage, especially DSBs induced by various DNA damaging agents including radiation, targeted oxidative stress and nucleases, causes R-loop accumulation in *cis* [reviewed in (Marnef and Legube, 2021)]. There are several hypotheses on how R-loops are formed. One model hypothesizes that DSBs initiate *de novo* transcription leading to R-loop generation. *In vitro* data suggests that DNA ends can recruit RNA polymerase II (RNAPII) in an MRN complex-dependent manner (Michelini et al., 2017; Sharma et al., 2021). Also, RNAPII and the pre-initiation complex are recruited to DSBs *in vivo* (Pessina et al., 2019). In addition, super-resolution and live-cell imaging shows colocalization of RNAPII and nascent transcripts with DSB sites (Vítor et al., 2019). However, this model conflicts with the transcriptional suppression known to be induced by DSBs. Also, studies have shown that damage-induced R-loops mostly form in *cis* to DSBs at loci priorly occupied by RNAPII [reviewed in (Marnef and Legube, 2021)]. Another hypothesis is that DSBs

can cause transcriptional repression, which promotes R-loop formation at the same loci. It has been demonstrated that when the transition from initiation to elongation and progression within genes of RNAPII is impaired, R-loops are generated (Jonkers and Lis, 2015; Sanz et al., 2016). DRIP-seq (DNA-RNA IP combined with sequencing) data shows that R-loops are formed in *cis* to DSBs induced at loci occupied by RNAPII priorly, but not at intergenic loci (Cohen et al., 2018; Edwards et al., 2020). Also, R-loops accumulate at DNA breaks induced by oxidative stress only within transcribed loci (Teng et al., 2018). In addition to two well-studied models, it has been suggested that chromatin conformation changes around DSBs allow pre-existing RNA to re-anneal to the template DNA (Chedin and Benham, 2020; Salas-Armenteros et al., 2017). Besides, resection generating ssDNA during DNA damage repair can facilitate the binding of RNA to form R-loops (D'Alessandro et al., 2018). R-loops can form in *cis* or in *trans* by RNA transcribed from remote homologous loci, for example TERRA forming R-loops in *trans* at telomeres (Feretzaki et al., 2020). Although studies about DNA breaks inducing R-loop formation are mainly conducted with DSBs, R-loop generation can also be promoted by SSBs *in vitro* (Roy et al., 2010).

R-loops not only induce DNA damage, but also interfere with the DNA damage response. R-loops have been demonstrated to affect resection at DNA double strand breaks, to generate a long 3' ssDNA tail which can invade the homologous DNA strand during HR (Sun et al., 1991; White and Haber, 1990). R-loops might act as an obstacle to the canonical resection as they prevent the activities of EXO1 exonuclease and BLM helicase *in vitro* – the two enzymes required for resection (Daley et al., 2020). In addition, depletion of R-loop removal factor RNaseH coincides with a decrease in resection, while RNaseH overexpression consistently promotes resection (Ohle et al., 2016). However, in certain contexts in which canonical R-loop removal pathways are inefficient, or at genomic loci that are prone to stable R-loop formation, the excessive accumulation of DSB-induced R-loops promotes non-canonical and extensive resection via the endonuclease activity of XPG and XPF enzymes [reviewed in (Marnef and Legube, 2021)]. Beside resection, conflicting evidence has shown that R-loops also contribute to the regulation of RAD51 nucleofilament reassembly. Most reports suggest the negative effect of R-loops as many R-loop removal factors are required for correct RAD51 focus formation (Cohen et al., 2018; Dang and Morales, 2020; Jang et al., 2020; Li et al., 2016; Marin-Vicente et al., 2015; Ohle et al., 2016; Yu et al., 2020). However, a few other studies highlight the opposite since depletion of factors involved in DSB-induced R-loop formation and stabilization reduces RAD51 focus formation (Lu et al., 2018; Zhang et al., 2020). Another way for R-loops to exert influence on the DNA damage response is via their RNA moiety, which can serve as a template or primer for DNA polymerases (Itoh and Tomizawa, 1980; Keskin et al., 2014; Meers et al., 2020, 2016; Stuckey et al., 2015). Furthermore, R-loops can act as a recruitment platform recognized by many DNA damage repair factors. One example is the R-loop-induced recruitment of CSB and RAD52 proteins to DSBs induced by reactive oxygen species at ALT telomeres, which in turn recruit POLD3 to promote BIR (break-induced replication) (Tan et al., 2020). Altogether, it suggests the complicated interplay among R-loop formation, DNA breaks and DNA damage response regulation.

1.2.2.2. R-loops at telomeres

Telomeric R-loops form when TERRA invades and base-pairs with the C-rich telomeric strand leading to the displacement of the G-rich strand. TERRA and R-loops play an essential role in telomere maintenance, especially in ALT cancer cells. Compared to telomerase-positive cells, ALT cells contain less compacted chromatin and elevated telomeric transcription, resulting in higher levels of TERRA and R-loops (Arora et al., 2014; Episkopou et al., 2014). This is probably required to generate a fine-tuned level of replication stress needed to trigger recombination-dependent telomere elongation (Arora et al., 2014; Flynn et al., 2011; Lu and Pickett, 2022; Silva et al., 2019). Also, loss of chromatin remodeler ATRX, which happens very often in ALT cells, compromises the cell cycle regulation of TERRA level, thereby sustaining TERRA and telomeric R-loop levels throughout S-phase and G2, contributing to elevated replication stress in ALT cells (Flynn et al., 2011). Manipulation of TERRA transcription or stability in ALT cells affects R-loop balance, leading to the impairment of ALT activity. TERRA depletion using RNA-targeting Cas9 system causes decreases in ALT phenotypes including PML bodies and telomere clustering leading to reduced telomere lengthening (Guh et al., 2022). Similar observations have been reported using TALEs (Transcription Activator-Like Effectors) fused with transcription repressors targeting subtelomeric regions. TERRA transcription from certain chromosomes is inhibited, thereby constraining R-loop formation. This decreases replication stress and DNA damage markers, and impairs ALT activity and telomere maintenance (Silva et al., 2021). Consistently, the expression of TALEs fused with transcription activators results in increases in TERRA level, DNA damage signaling at telomeres and ALT phenotypes. Interestingly, TERRA overexpression, despite leading to an elevation in telomere synthesis (detected via EdU incorporation at telomeres), causes an increase in telomere-free ends (Silva et al., 2022). These studies indicate that TERRA and R-loops have to be precisely kept at certain levels to maintain telomere elongation in ALT cells.

Due to the important role of R-loops in recombination-dependent telomere maintenance, R-loop levels at telomeres are tightly regulated in ALT cells. One of the factors that regulates TERRA level in ALT cells is RNaseH1 – a member of the RNaseH ribonuclease enzyme family that degrades the RNA component of R-loops (Cerritelli and Crouch, 2009). RNaseH1 enzyme is detected at telomeres in ALT cancer cells. Overexpression or depletion of RNaseH1 leads to dysregulation of telomeric R-loops, interfering with telomere maintenance. RNaseH1-deficient cells show high replicative stress at telomeres, increased telomeric leading strand fragility and C-circles, and rapid telomere loss (Arora et al., 2014; Olson et al., 2006). Overexpression of RNaseH1 also leads to telomere loss, probably because R-loop levels are insufficient to sustain homology-directed recombination required for telomere elongation (Arora et al., 2014). FANCM (Fanconi anemia-associated ATPase/translocase) has also been shown to control TERRA and R-loop levels at telomeres in ALT cells (Hodson et al., 2022; Silva et al., 2019). FANCM is a branchpoint translocase which binds R-loop sites and rewinds the DNA, thereby indirectly removing the RNA (Hodson et al., 2022). FANCM deficiency results in accumulation of R-loops, increases in DNA damage signalling and ALT activity, and

subsequently a decrease in ALT cell viability (Silva et al., 2019). Similarly, depletion of NONO or SFPQ proteins, which function in RNA biogenesis, increases R-loop levels, telomere fragility and some ALT features, which is partially rescued by RNaseH1 overexpression (Petti et al., 2019).

The level of telomeric R-loops is also kept under control by several factors in telomerase-positive cells, thereby maintaining telomere stability. TRF2 protein has been demonstrated by *in vitro* studies to bind TERRA and promote its invasion into telomeric dsDNA leading to R-loop formation, which is counteracted by TRF1 protein (Lee et al., 2018). Depletion of TRF1 leads to an increase in telomeric R-loops in a TRF2-dependent manner, which subsequently causes telomere loss (Lee et al., 2018). POT1 deletion in human cells also increases R-loop level, which correlates with the rise of several ALT features including C-circle accumulation, formation of APBs, activation of telomeric recombination and telomere elongation (Glousker et al., 2020). Another factor that may contribute to R-loop regulation is UPF1 protein – an ATP-driven 5'-3' helicase involved in nonsense-mediated mRNA decay pathway. Loss of UPF1 promotes TERRA association with telomeres, causing DNA damage signaling activation and incomplete leading strand replication at telomeres (Azzalin et al., 2007; Chawla et al., 2011).

The relationship between TERRA expression, R-loop level and telomere length is clinically demonstrated by analyzing primary cells from patients suffering from the rare autosomal recessive syndrome ICF (Immunodeficiency, centromere instability and facial anomalies) (Ehrlich et al., 2006). ICF patient cells contain elevated TERRA transcription correlating with very short telomere length (Yehezkel et al., 2008). The most common mutations in ICF patients are found in the gene encoding the *de novo* DNA methyltransferase enzyme DNMT3B, presumably resulting in hypomethylation of subtelomeres, explaining the upregulation of TERRA (Ehrlich et al., 2006; Yehezkel et al., 2008). However, DNMT3B depletion is not sufficient to increase TERRA transcription, TERRA is upregulated only upon its co-depletion with DNMT1 – another DNA methyltransferase enzyme (Nergadze et al., 2009). Studies in ICF patient samples show that the cell cycle regulation of TERRA is lost, resulting in elevated TERRA and R-loop levels throughout the cell cycle, leading to DNA damage signalling activation at telomeres (Sagie et al., 2017). It has been proposed that R-loops affect the progression of the replication machinery at telomeres, causing the short telomere phenotype and premature replicative senescence symptoms of ICF patients.

1.3. Oxidative stress

Oxidative stress is a consequence of the imbalance between the cellular levels of reactive oxygen species (ROS) and antioxidant defenses, contributing to the initiation and progression of numerous human diseases including age-related diseases and cancer. Intrinsic ROS is primarily generated during inflammatory responses to pathogen invasion, and also products of oxidative phosphorylation at mitochondria. Thus, for most of the diseases, elevated ROS levels come from ROS leakage caused by chronic inflammation and mitochondrial dysfunction, thereby disrupting the cellular redox balance. In addition, a wide range of environmental exposures such as UV light, chemicals, ionizing radiation and heavy metals can induce ROS (Bouvard et al., 2009; Lonkar and Dedon, 2011). Once being triggered, oxidative stress exerts detrimental effects on various cellular components including DNA, signified by increased levels of oxidized bases and single-stranded breaks (SSBs) generated via direct backbone cleavage (Bandyopadhyay et al., 1999; Barzilai and Yamamoto, 2004).

Oxidative lesions are primarily repaired by the base-excision repair (BER) pathway (Figure 2). The first step in BER consists of removal of the damaged base by DNA glycosylases resulting in abasic sites, which are cleaved by APE1 endonuclease to generate 3'-OH and 5'-sugar phosphate (5'-dRP) termini if the glycosylases are monofunctional (Srivastava et al., 1998). DNA polymerase β (Pol β) then removes the 5'-dRP using its lyase activity. If the glycosylases are bifunctional, they catalyse both oxidized base removal and DNA backbone cleavage, leaving either a blocking unsaturated aldehyde or phosphate group at the 3' end of the break (Srivastava et al., 1998). The former is removed by APE1 to create a 3'-OH substrate for Pol β, while PNKP (polynucleotide kinase 3' phosphatase) cleaves the later. In short patch BER, Pol β inserts the missing base, and the nick is sealed by DNA ligase III (Krokan and Bjoras, 2013; Wallace, 2014). If the 5'-dRP is modified and resistant to Pol β processing, long-patch BER is initiated, during which a polymerase (β, ε or δ) inserts several nucleotides to create a displaced DNA flap that is subsequently cleaved by FEN I and the resultant nick is ligated by DNA ligase I (Krokan and Bjoras, 2013; Wallace, 2014). In addition to these core components, there are a number of other proteins being employed to accelerate BER including PARP1 (poly(ADP)-ribose polymerase 1) and scaffold protein XRCC1 (Caldecott et al., 1994; Dantzer et al., 1999; Ronson et al., 2018; Schreiber et al., 2002). PARP1 is a DNA break sensor which is activated by and associated with damage sites resulting in the post-

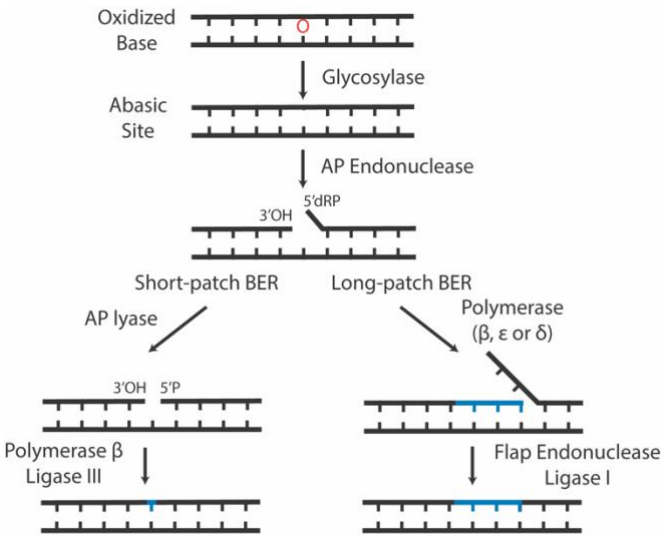

Figure 2: Scheme of the base-excision repair (BER) pathway

translational modification of itself and other proteins with ADP-ribose polymerization (de Murcia and de Murcia, 1994; Hanzlikova et al., 2018). One of its targets is XRCC1, which acts as a scaffold protein for BER proteins including Pol β and PNKP (El-Khamisy et al., 2003). Failure of oxidative lesion and SSB repair can potentially generate DSBs, which are repaired by either NHEJ or HR depending on the cell cycle stage and chromatin conformation (Ceccaldi et al., 2016). Apart from DNA repair pathways, DNA oxidative damage can be prevented by cellular antioxidant enzymes includes catalase, glutathione peroxidases and peroxiredoxins (Perkins et al., 2015).

The G-rich nature of TTAGGG repeats renders telomeres prone to oxidative damage, presumably because guanine has lower redox potential than other natural bases, and thus is more liable to be oxidized to generate 8-oxoguanine (8-oxoG) (Henle et al., 1999; Oikawa et al., 2001, Luo et al., 2001). Besides, similar to other genomic loci, ROS can directly cleave the telomeric DNA backbone, together with DNA processing during oxidative lesion repair, leading to SSB accumulation. When cells are exposed to oxidants, the levels of oxidized bases and SSBs at telomeres are higher than in genomic bulk DNA and microsatellite repeats (Petersen et al., 1998; Wang et al., 2010).

Numerous studies have reported an association between oxidative stress, an increased telomere shortening rate and cellular replicative senescence. Recent population studies demonstrate the correlation between oxidative stress and shorter telomere length measured in white blood cells (Reichert and Stier, 2017). Also, mild oxidative stress induced by culturing cells in 20% oxygen or exposure to low concentration of H_2O_2 accelerates telomere shortening (Coluzzi et al., 2014; Forsyth et al., 2003; Richter and Zglinicki, 2007; Wang et al., 2010). One possible explanation for the negative effect of ROS on telomere length is that 8-oxoG can interfere with telomerase activity. Although 8-oxodGTP is a telomerase substrate, once incorporated into telomere ends, it becomes a chain terminator (Aeby et al., 2016). Furthermore, 8-oxoG present at telomeric sequences also inhibits telomerase activity depending on their positions, proven by studies showing that the oligonucleotide 5'-TTA-8-oxoG-3' cannot be extended by telomerase, while the 5'-TTAGG-8-oxoG-3' substrate can be elongated (Aeby et al., 2016). Apart from 8-oxoG, other oxidative lesions such as hydantoin, thymine glycol and 5-hydroxycytosine can also impede telomere replication (Henderson et al., 2003; McNulty et al., 1998). Besides, SSBs and oxidative lesions can lead to replication fork collapse and DNA truncation, contributing to telomere loss and cellular senescence. Another way of oxidative stress to promote cellular senescence is via the accumulation of the oxidative lesion 8-oxoG, which can induce DDR, telomere fragility and dysfunction by itself, and consequently cellular senescence in the absence of telomere shortening (Barnes et al., 2022).

It has been shown *in vitro* that TRF1 and TRF2 binding to telomeric DNA oligonucleotides is disrupted by the presence of 8-oxoG lesions and other BER intermediates such as abasic sites or single nucleotide gaps within telomeric repeats (Opresko et al., 2005). Besides, oxidative damage can cause changes in telomeric sequence, which might also disrupt shelterin protein binding. This is because DNA polymerases preferentially incorporate A opposite 8-oxoG

instead of C, thereby causing mismatch mutations and changes in telomeric sequences (Beard et al., 2010; David et al., 2007). Consistently, GTAGGG and TGAGGG repeats resulting from the mis-incorporation of 8-oxoG opposite A in 3'-AATCCC-5' repeats are reported to be the most common telomeric repeat variants (Lee et al., 2013). Taken together, oxidative stress promotes oxidized base and SSB generation, thereby interfering with the replication fork, telomerase activity and shelterin protein binding to telomeres, leading to telomere shortening and dysfunction, and eventually cell senescence, apoptosis or malignant transformation.

Several BER factors have been reported to function at telomeres. 8-oxoG opposite to C is recognized and removed by OGG1 glycosylase, which is shown to accumulate at telomeres when oxidative damage is induced (Fouquerel et al., 2019). *Ogg1* knockout in mouse embryonic fibroblasts induces telomere shortening when the cells are cultured at 20% oxygen, (Wang et al., 2010). Another DNA glycosylase involved in the BER pathway at telomeres is NEIL3, which has DNA glycosylase activity toward several oxidized derivatives of thymine and guanine but not 8-oxoG (Krokan and Bjoras, 2013; Wallace, 2014). Interestingly, *in vitro* NEIL3 can act on the telomeric G4 structure and single-stranded DNA, although the mechanism of how NEIL3 deals with the absence of a templating base remains unclear (Zhou et al., 2013). Besides, biochemical studies have demonstrated that Pol β physically interacts with TRF2, and TRF2 stimulates Pol β strand extension and displacement *in vitro* (Fotiadou et al., 2004), together supporting the hypothesis that BER pathway functions at telomeres.

Apart from BER, there are other mechanisms protecting telomeres from oxidative DNA damage. Several nucleotide excision repair (NER) proteins have been shown to contribute to oxidative damage repair at telomere. XPB- and XPD-deficient cells have elevated telomere loss following H_2O_2 treatment (Gopalakrishnan et al., 2010). Furthermore, the mismatch repair (MMR) pathway might alleviate oxidative lesions as loss of MMR protein MSH2 and MLH1 results in increases in both basal and H_2O_2-induced 8-oxoG levels (Colussi et al., 2002). Antioxidant enzymes also protect telomeres against oxidative damage. PRDX1 is an antioxidant enzyme reducing H_2O_2 to H_2O, thereby alleviating cellular ROS burden (Perkins et al., 2015). The association of PRDX1 with telomeres under oxidative stress condition has been reported (Aeby et al., 2016). MTH1 enzyme is involved in free oxidized dNTP hydrolysis to prevent their incorporation into the genome by DNA polymerases (Rudd et al., 2016). MTH1-deficient cells display telomere shortening due to telomerase inhibition when cultured in hyperoxia, and the situation is exacerbated by the co-depletion of MTH1 and PRDX1 (Ahmed and Lingner, 2018). Altogether, this suggests that MTH1 and PRDX1 enzymes cooperatively protect telomeres against oxidative stress. Another protein – NEK7 kinase, also contributes to maintain telomere integrity upon oxidative damage via TRF1 stabilization (Tan et al., 2017).

1.4. The quantitative telomeric chromatin isolation protocol (QTIP)

Telomere function relies on its constituents including telomeric proteins, telomeric DNA and the long non-coding RNA TERRA, which varies during aging, tumorigenesis and in telomere syndromes. In terms of the protein component, in addition to shelterin protein complex, an increasingly large number of less abundant proteins have been identified. However, it is still a challenge to thoroughly characterize telomeric proteome. Our lab has developed a Quantitative Telomeric chromatin Isolation Protocol (QTIP), which allows us to study the telomeric protein composition in a comprehensive manner and answer fundamental questions regarding telomere biology and function (Grolimund et al., 2013; Majerská et al., 2017). The protocol involves purification of crosslinked telomeric chromatin by immunoprecipitation using antibodies against TRF1 and TRF2 – the two abundant shelterin subunits (Grolimund et al., 2013; Majerská et al., 2017). To optimize the purity of the purified telomeric chromatin, QTIP can be performed with an additional purification step using anti-FLAG antibody in cells containing endogenously FLAG-tagged TRF1 and TRF2 proteins, which we refer as 2-step QTIP (Glousker et al., 2020). QTIP can be combined with other methods such as iPOND (isolation of Proteins On Nascent DNA) to specifically purify telomeric chromatin during replication (Dungrawala and Cortez, 2015; Lin et al., 2021).

The purified telomeric chromatin is then analyzed by Mass Spectrometry (MS) in either label-free manner or with labelling, which allows us to combine and compare different samples at one run. Samples containing telomeric chromatin at different states are distinguished by either SILAC (Stable Isotope Labeling by/with Amino acids in Cell culture) or TMT (Tandem Mass Tag) labelling. With SILAC, cells are cultured in medium containing either light isotopes (Arg (R0) and Lys (K0)) or heavy isotopes ([$^{13}C_6$ $^{15}N_4$]Arg (R10) and [$^{13}C_6$ $^{15}N_2$]Lys (K8)) (Ong and Mann, 2006). On the other hand, TMT labelling is based on isobaric mass tags which have identical overall mass but vary in the distribution of heavy isotopes around their structures (Hogrebe et al., 2018; O'Connell et al., 2018; Rauniyar and Yates, 2014). TMT tags are composed of a mass reporter for the differentiation of different tags, linked to a mass balancer for the normalization of the total mass, and an amine-reactive group (Rauniyar and Yates, 2014). SILAC labelling allows us to compare two different samples, while TMT labelling can be used to differentiate a larger set of samples.

By using QTIP, our lab identified novel telomeric factors such as SMCHD1, which is required for the activation of NHEJ at unprotected telomeres (Grolimund et al., 2013; Tang et al., 2014). SMCHD1 depletion led to defect in ATM signaling pathway, thereby preventing telomere fusion in TRF2-depleted cells (Vančevska et al., 2020). THOC protein complex was also identified as telomere-binding factors by QTIP, functioning in R-loop regulation at telomeres (Fernandes and Lingner, 2023; Grolimund et al., 2013). To assess POT1 function, our 2-step QTIP was performed in POT1-deleted cells and we unravelled the role of POT1 in the repression of telomeric homologous recombination, thereby preventing telomere instability (Glousker et al., 2020). In addition, by combining QTIP and iPOND, our lab revealed the

dynamic of telomeric proteome during replication with histone H1 being enriched and POT1 being depleted from the replication fork (Lin et al., 2021).

1.5. Aim of the thesis

Telomeres are interesting loci to study DNA damage induced by oxidative stress. Their 5'-TTAGGG-3' repetitive sequence is highly susceptible to oxidation, making telomeres a hotspot for oxidative damage. Furthermore, the distinct structures at telomeres including G4, R-loops and 3' single-stranded overhangs can potentially interfere with DDR processes. Also, the suppressive effects of shelterin proteins on DDR factors potentially pose obstacles to the repair of damaged telomeric DNA. Thus, we wanted to comprehensively identify and study the molecular changes in telomeric chromatin composition upon oxidative stress induction in order to gain a better understanding about how telomeres are protected from oxidative damage and how they are repaired.

We first examined the nucleic acid composition. Our results show an accumulation of SSBs induced by oxidative stress, upregulation of TERRA transcription and R-loop formation. Also, we observed the generation of internal loops at damaged telomeres. In terms of the protein composition, we demonstrate dissociation of TRF1 protein from damaged telomeres. In addition, we employed two-step QTIP combined with Mass Spectrometry (MS) to quantitatively determine the changes in the telomeric proteome upon oxidative stress induction. The MS data showed the enrichment of DDR factors, antioxidant enzymes, chromatin remodelers and protein post translational modifiers at damaged telomeres. Overall, our data show that oxidative stress leads to drastic alterations of telomeric chromatin composition to facilitate DNA damage repair at telomeres.

Chapter 2. Changes in telomeric chromatin composition upon oxidative stress

2.1. Changes in nucleic acid composition

2.1.1. Accumulation of DNA single-stranded breaks (SSBs)

To study the molecular mechanisms of how telomeres respond to oxidative damage, we induced cellular oxidative stress by treating HEK293E cells with 0.1 mg/ml menadione for 2 hours, which increases mitochondrial membrane permeability leading to elevated levels of intrinsic reactive oxygen species (ROS) (Loor et al., 2010). Genomic DNA was then isolated and digested with frequent cutter restriction enzymes which do not have recognition sites within the 5'-TTAGGG-3' telomeric repeats. The digested DNA was analyzed using alkaline denaturing gels which separate the two DNA strands, thereby allowing us to detect DNA backbone cleavage events. The gels were then hybridized with radiolabeled DNA probes specific for the telomeric G-rich or C-rich strand. Upon oxidative stress induction, we observed a shift in the signal intensity curve of the menadione-treated sample compared to the untreated one, indicating an accumulation of short single-stranded DNA fragments caused by ROS-induced SSB generation in both strands (Figures 3A and 3B). We then measured the SSB levels at telomeres based on the decrease in telomeric DNA fragment length, revealing that DNA damage occurred at similar levels between two telomeric strands (Figure 3C). We also examined double-stranded breaks (DSB) at telomeres upon menadione treatment. For this, the same digested DNA was separated using native gel electrophoresis, which was then hybridized with a telomere-specific probe. The signal intensity profiles of two samples overlapped (Figure 3D), indicating that there was no detectable accumulation of telomeric DNA DSB caused by oxidative stress.

To confirm that the SSB accumulation was due to oxidative stress induced by elevated ROS levels, we treated the cells with 5mM of the glutathione precursor N-acetyl-L-cysteine (NAC), which scavenges ROS (Dekhuijzen, 2004), for half an hour before adding menadione. NAC abolished the shift which we previously observed in the signal intensity curve of the menadione-treated sample (Figures 3A and 3B). Correspondingly, there was almost no difference in the average telomeric DNA fragment length between the menadione-treated and untreated cells (Figure 3C). This indicates that the accumulation of SSBs at telomeres upon menadione treatment was caused by oxidative stress, which could be prevented by the antioxidant NAC.

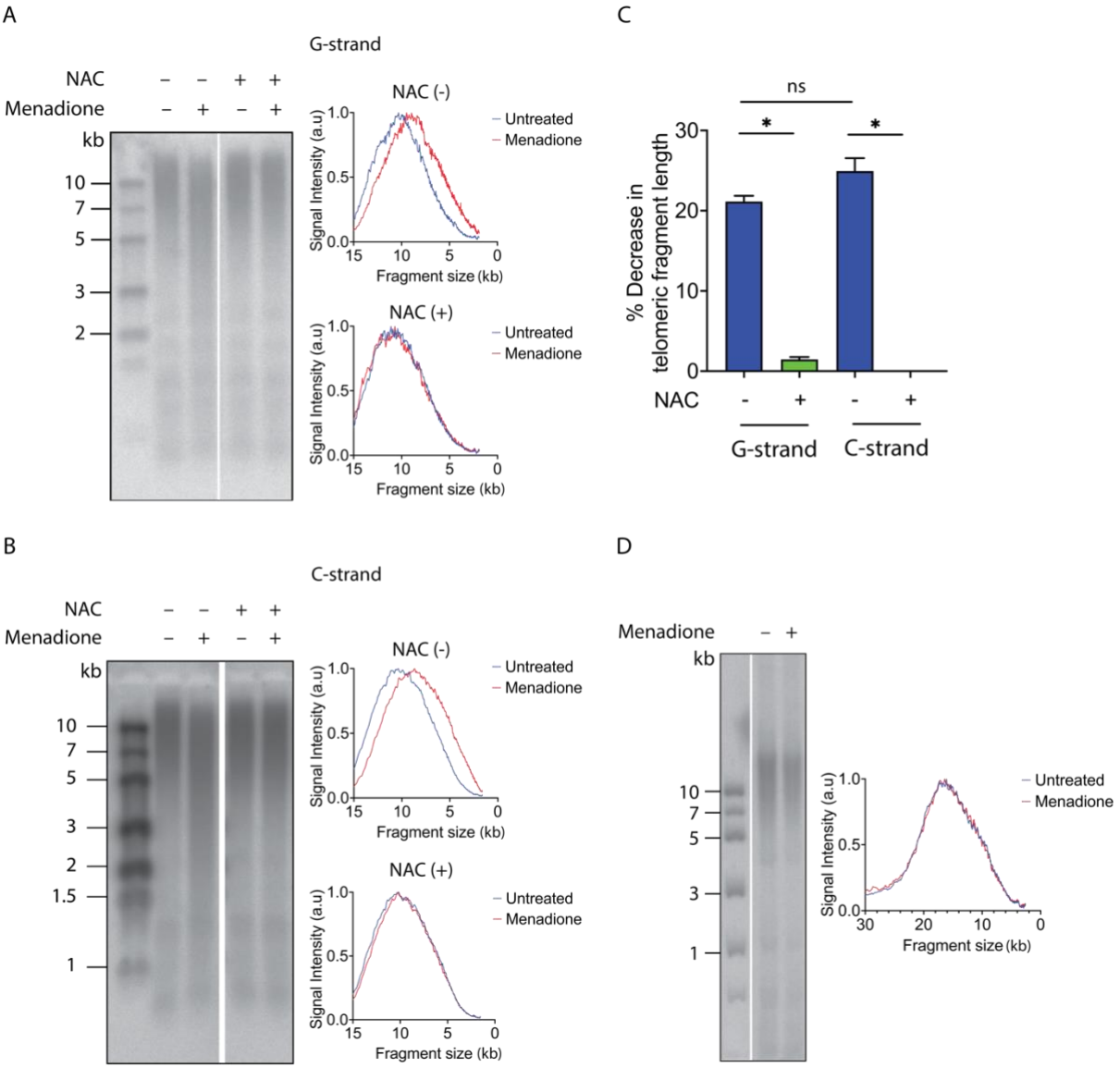

Figure 3: Accumulation of DNA single-stranded breaks (SSBs) at telomeres upon menadione treatment. **(A, B)** Alkaline gel electrophoresis to detect telomeric SSB accumulation at G-rich **(A)** and C-rich **(B)** strands upon menadione treatment, with or without prior treatment with NAC. The signal intensity curves were also shown here. **(C)** The percentage decrease in telomeric fragment length of the menadione-treated sample compared to the untreated one, which represents DNA damage level. Quantification was done using the alkaline gels in **(A)** and **(B)**. (*) $p < 0.05$, ns – not significant. Data represents mean ± SD. n = 3. **(D)** Native gel electrophoresis to detect DSBs after menadione treatment. The signal intensity curves were also shown here.

2.1.2. Increases in telomeric TERRA and R-loop levels

Since it has been shown genome-wide that DNA damage promotes R-loop formation (reviewed in (Marnef and Legube, 2021), (Roy et al., 2010)), we decided to assess the presence of R-loops at telomeres upon oxidative stress induction. We performed DNA:RNA immunoprecipitation (DRIP) in which the structure-specific antibody S9.6 was employed to precipitate R-loops from total nucleic acid (Boguslawski et al., 1986). Precipitated nucleic acid was blotted onto a membrane, followed by hybridization with a C-rich telomere-specific probe. As a control for specificity, isolated nucleic acid was treated *in vitro* with RNaseH prior to immunoprecipitation. RNaseH specifically hydrolyses the RNA component of R-loops. Abolishment of the signal to background level upon RNaseH treatment confirmed the specificity of this assay for telomeric R-loop detection. We discovered that oxidative damage led to an increase in R-loop level at telomeres (Figure 4A and 4B). To measure R-loops located at particular telomeres, we used the same nucleic acid precipitated by DRIP as a sample for qPCR using subtelomere-specific primers binding to sequences in close proximity to the telomeric 5'-TTAGGG-3' repeats. Telomeric R-loop level increased at all tested chromosome ends upon menadione treatment (Figure 4C). The increase in R-loop formation could happen in *cis* during TERRA transcription, or in *trans* due to TERRA invasion post-transcriptionally, or both.

We next examined the levels of TERRA transcribed from different chromosomes with RT-qPCR using primers specific for subtelomeric sequences. GAPDH was used as a reference gene for normalization. We observed that upon oxidative stress induction by menadione, there was an upregulation in TERRA expression from a subset of chromosome ends but not all (Figure 4D), in contrast to R-loops which increased at all tested telomeres (Figure 4C). This suggested that the elevation in R-loop level was not solely in *cis* due to the upregulation in TERRA transcription but that TERRA was recruited in *trans* to oxidatively damaged telomeres. To substantiate this finding, we blocked transcription by treating the cells with 5 µg/ml actinomycin D for half an hour prior to menadione, and studied R-loop level. Successful inhibition of transcription would decrease R-loop level directly via the downregulation of co-transcriptional R-loop formation, or indirectly via the reduction of RNA level. Actinomycin D treatment alone reduced R-loop levels (Figures 4E and 4F), indicating that transcription was effectively suppressed. Interestingly, menadione treatment led to elevated R-loop formation at telomeres regardless of actinomycin D (Figures 4E and 4F), confirming the in-*trans* recruitment of TERRA to damaged telomeres upon oxidative stress induction.

Finally, to assess the dynamics of R-loop formation induced by ROS, we treated the cells with menadione and conducted DRIP at different time points. As shown in Figures 4G and 4H, we observed an increase in R-loop level after half an hour, reaching a plateau after 2 hours of menadione treatment. Overall, our data indicates that oxidative stress upregulates TERRA transcription at a subset of chromosome ends, leading to an elevation in the level of R-loops. In addition, TERRA was recruited to oxidatively damaged telomeres, resulting in an increase in R-loop formation also in *trans.*

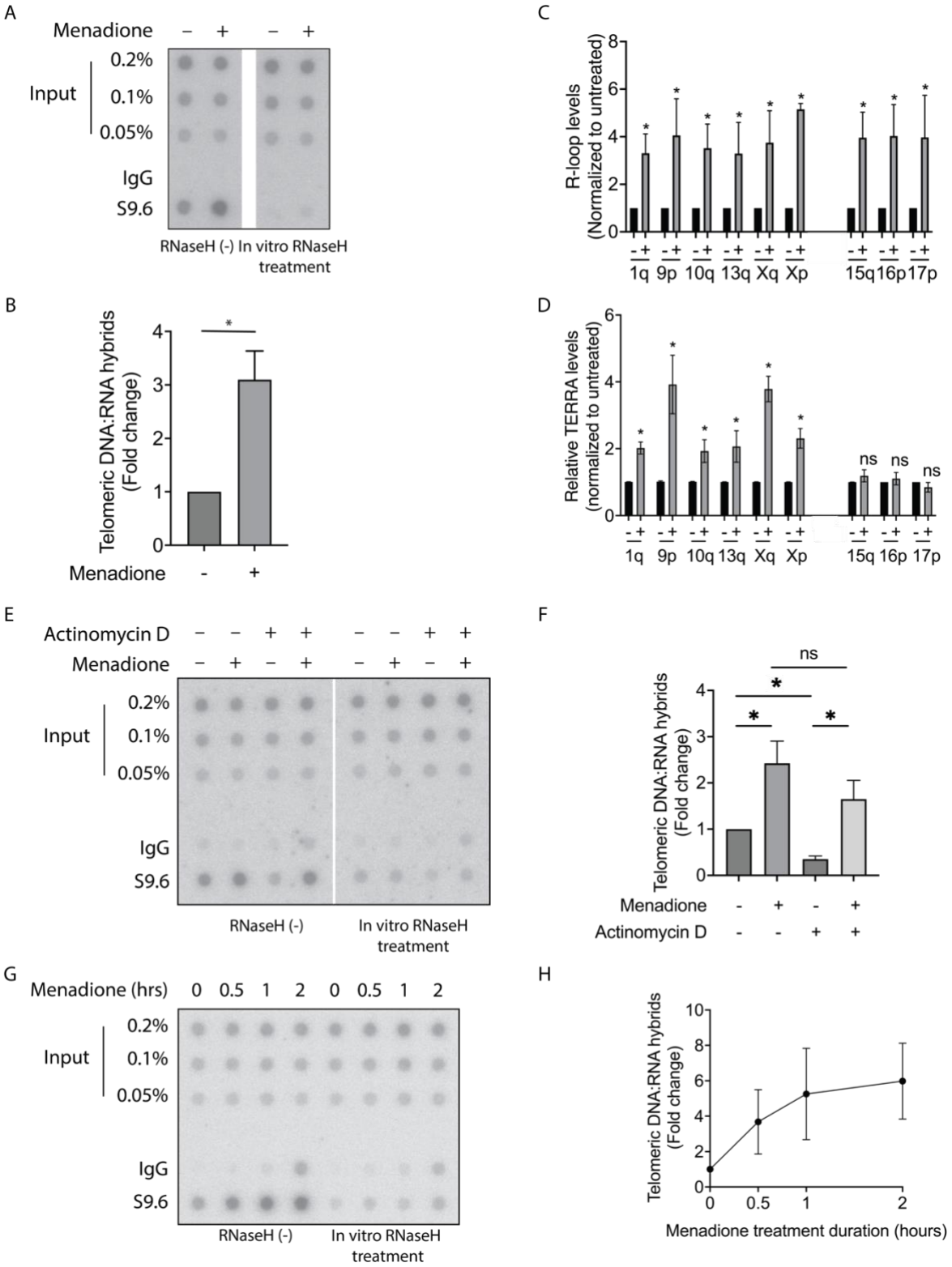
A
Menadione − + − +
Input
0.2%
0.1%
0.05%
IgG
S9.6
RNaseH (-) In vitro RNaseH treatment
B
Telomeric DNA:RNA hybrids (Fold change)
Menadione - +
C
R-loop levels (Normalized to untreated)
1q 9p 10q 13q Xq Xp 15q 16p 17p
D
Relative TERRA levels (normalized to untreated)
ns
1q 9p 10q 13q Xq Xp 15q 16p 17p
E
Actinomycin D − − + + − − + +
Menadione − + − + − + − +
Input
0.2%
0.1%
0.05%
IgG
S9.6
RNaseH (-)
In vitro RNaseH treatment
F
Telomeric DNA:RNA hybrids (Fold change)
ns
Menadione - + - +
Actinomycin D - - + +
G
Menadione (hrs) 0 0.5 1 2 0 0.5 1 2
Input
0.2%
0.1%
0.05%
IgG
S9.6
RNaseH (-)
In vitro RNaseH treatment
H
Telomeric DNA:RNA hybrids (Fold change)
Menadione treatment duration (hours)

Figure 4: Upregulation of TERRA transcription and TERRA recruitment to damaged telomeres upon oxidative stress. **(A)** DRIP-dot blot assay for total DNA:RNA hybrid detection at telomeres upon 2 hours of menadione treatment using S9.6 antibody. *In vitro* digestion with RNaseH prior to IP served as a control for antibody specificity. Immunoprecipitated and input samples were blotted onto a membrane followed by hybridization with a telomere-specific probe for telomeric DNA detection. **(B)** Quantification of telomeric DNA signal in **(A)** as fold change over untreated sample. **(C)** DRIP-qPCR to detect DNA:RNA hybrids at specific chromosome ends upon 2 hours of menadione treatment. qPCR was performed using primers binding to chromosome-specific subtelomeric sequences. Data was shown as fold change over untreated sample. **(D)** RT-qPCR to detect TERRA transcribed from specific chromosome ends upon treating the cells with menadione for 2 hours. qPCR was performed using primers binding to chromosome-specific subtelomeric sequences. Data was shown as fold change over untreated sample. **(E)** DRIP-dot blot assay for total DNA:RNA hybrid detection at telomeres upon 30 minutes of actinomycin D followed by 2 hours of menadione treatment. **(F)** Quantification of telomeric DNA signal in **(E)** as fold change over untreated sample. **(G)** DRIP-dot blot assay for total DNA:RNA hybrid detection at telomeres over a time course of menadione treatment. **(H)** Quantification of telomeric DNA signal in **(G)** as fold change over untreated sample.
(*) $p < 0.05$, ns – not significant. Data represents mean ± SD. n = 3

2.1.3. Accumulation of internal loop (i-loop) structures at telomeres

(In collaboration with Ylli Doksani lab, IFOM ETS – The AIRC Institute of Molecular Oncology, Milan, Italy)

Internal loops (i-loops) are structures generated at telomeres when the internal regions of telomeric DNA cross (Mazzucco et al., 2020). I-loops range from 0.2 to 25 kb, with a median size of 1.6 kb (Mazzucco et al., 2020). Damaged telomeres containing nicks and single-stranded gaps induced by DNase I treatment tend to form i-loops (Mazzucco et al., 2020). It is presumably because single-stranded DNA gaps can undergo base-pairing if they are on opposite strands, while if the gaps are on the same strand, they can promote an exchange of the complementary strand (Figure 5A) (Mazzucco et al., 2020). As oxidative stress induced by menadione led to the accumulation of SSBs at telomeres (Figure 3), we suspected the presence of i-loop structures under the same treatment condition. We first examined the enrichment of unusual telomeric DNA structures by 2-dimensional (2D) gel electrophoresis. The first dimension was performed at low voltage in a low-percentage agarose gel to separate DNA according to their sizes. The second dimension was run at high voltage in a high-percentage agarose gel supplemented with Ethidium Bromide, the mobility of DNA molecules was largely influenced by their structure and thus, allowing us to distinguish between linear and non-linear DNA. Genomic DNA was isolated and digested with frequent cutters which do not have recognition sites within telomeric sequences. The digested DNA was then analysed in a 2D gel, which was blotted onto a membrane and hybridized with a telomere-specific probe. While telomeric DNA from the untreated sample migrated linearly with almost no arc visible, damaged telomeric DNA isolated from the menadione-treated sample showed a strong accumulation of a slow-migrating arc (arrows in Figure 5B). It has been visualized by Electron Microscopy (EM) that the arc, although still contains substantial amounts of linear structures, is rich in i-loops, t-loops, circles, and at lower frequencies X-shaped and Y-shaped structures (Mazzucco et al., 2020).

Having established that oxidative damage induced the enrichment of the slow-migrating arc shown in the 2D gel, which contains unusual DNA structures at telomeres, we aimed to investigate if this was associated with the accumulation of telomeric i-loops. We enriched telomeric DNA from total genomic DNA using a two-step procedure (Mazzucco et al., 2022). Genomic DNA was digested with frequent cutter restriction enzymes which do not have recognition sites within the telomeric TTAGGG repeats. The digested DNA was then separated by sucrose gradient for the first step, or agarose gel for the second step, and the high molecular weight fraction containing intact telomeric DNA was collected (Mazzucco et al., 2022). The enrichment efficiency was assessed by dot blot assay based on telomeric DNA signal per ng of DNA being blotted (Mazzucco et al., 2022). The two-step procedure resulted in more than 1000-fold enrichment of telomeric DNA (Figures 5C and 5D). The enriched sample was then analyzed by EM for the presence of i-loops. The cells were treated with psoralen followed by exposure to 356-nm UV *in vivo*, which causes inter-strand crosslinks to preserve DNA secondary structures. In two independent replicates, menadione treatment resulted in a twofold increase in i-loops with around 10% of analyzed telomeric DNA molecules

containing the structures (Figure 5E and 5F). Consistent with previously published data, menadione-induced i-loops mostly occurred in proximity of single-stranded damage (Figure 5F). Overall, our data showed that i-loop formation was induced at telomeres following oxidative damage. These structures can be excised to generate extrachromosomal telomeric circles, which could potentially leads to telomere erosion (Mazzucco et al., 2020).

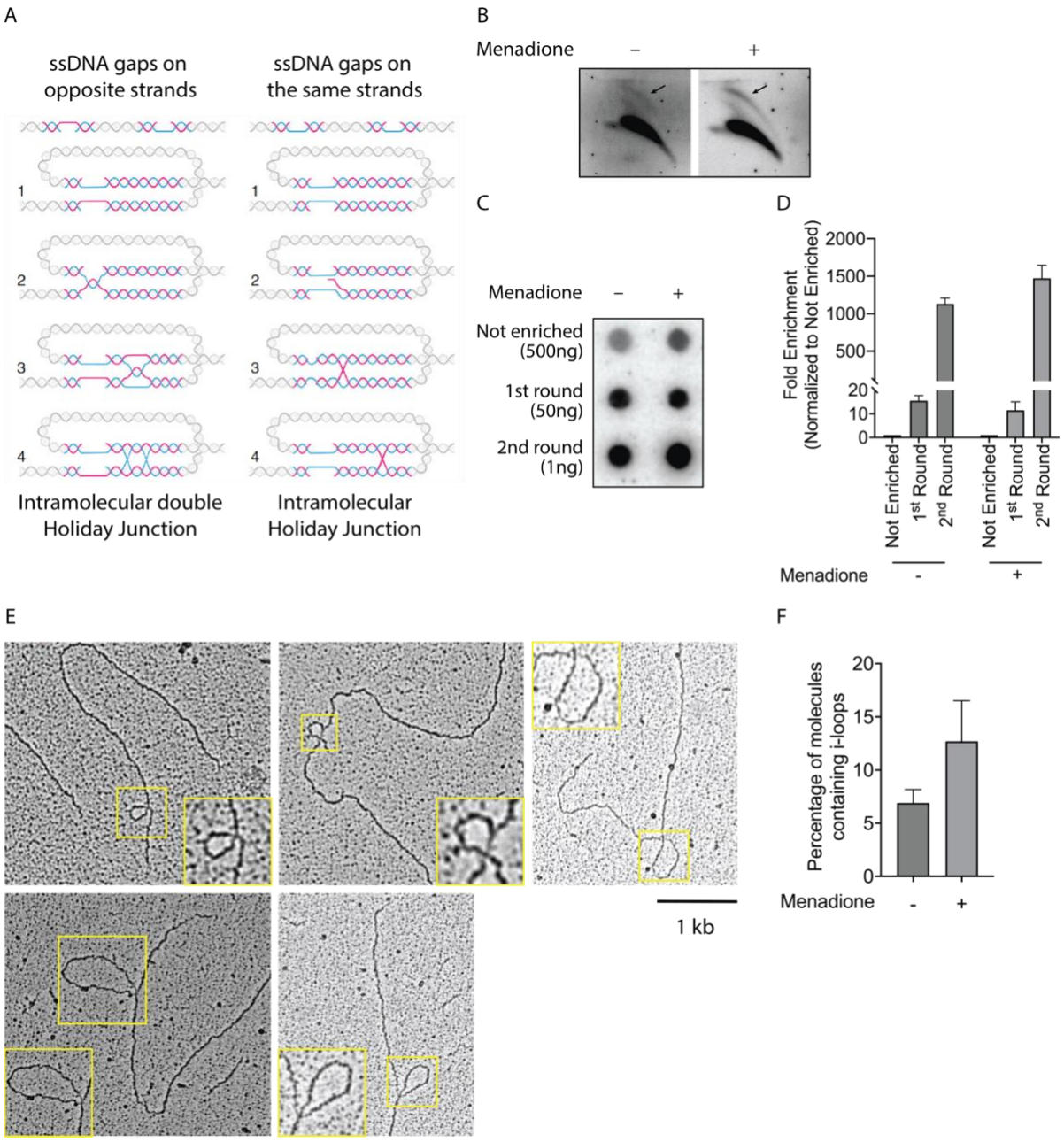

Figure 5: Accumulation of internal loop (i-loop) structures at telomeres upon oxidative stress. **(A)** Hypothetical models for i-loop structures induced by ssDNA gaps on telomeric strands (Adapted from Mazzucco et al., 2020). **(B)** 2D gel showing the accumulation of a slow-migrating arc (arrows) containing unusual DNA structures following menadione treatment **(C)** Dot blot showing the enrichment of telomeric repeats. The indicated amounts of DNA from each round of enrichment were blotted onto a membrane, which was then hybridized with a telomere-specific probe. **(D)** Quantification of the telomeric DNA signal per ng relative to the not-enriched DNA. **(E)** Examples of telomeric DNA molecules with i-loops observed in the menadione-treated samples. Telomere-enriched DNA from **(C)** was analysed by EM. **(F)** Percentages of molecules containing i-loops is reported based on the EM analysis in **(E)**.
Data represents mean ± SD. n = 2. EM analysis was done by Dr. Giulia Mazzucco - IFOM

2.2. Changes in protein composition

2.2.1. Dissociation of TRF1 proteins from damaged telomeres

Since it had been shown *in vitro* that oxidative lesions can disrupt the binding of TRF1 and TRF2 proteins to telomeric DNA oligonucleotide substrates (Opresko et al., 2005), we assessed in cells the levels of TRF1 protein at telomeres upon menadione treatment via chromatin immunoprecipitation (ChIP). Precipitated telomeric DNA was measured by dot blot hybridization with a telomere-specific probe. The telomeric DNA signal obtained from the menadione-treated cells was significantly lower than that from the untreated cells, indicating that there was less TRF1 protein binding to oxidatively damaged telomeres (Figures 6A and 6B). Pretreating the cells with the antioxidant NAC prior to menadione rescued the phenotype, confirming that the reduced binding occurred in an oxidative-stress-dependent manner (Figures 6A and 6B). To substantiate our observation, we isolated chromatin fractions and measured TRF1 protein levels. We observed that there was markedly less TRF1 protein binding to chromatin under oxidative stress condition (Figure 6C). Meanwhile, the TRF1 signal in the whole cell lysate was comparable between the two samples (Figure 6C), indicating that the reduction in telomeric TRF1 protein was not due to a decrease in the total TRF1 protein level, but more likely because of changes in TRF1 localization. We then conducted subcellular fractionation and examined TRF1 protein levels across different fractions. Histone H3, HSP90 and SP1 proteins were used as specific markers for chromatin-bound, cytoplasmic and nucleoplasmic fractions respectively. hnRNPA1 protein was present both at chromatin and in nucleoplasm. Under untreated condition, TRF1 mainly localized in nucleoplasm (N) and at chromatin (Ch), while upon oxidative stress induction, TRF1 translocated into a pellet extract fraction (PE), which was the insoluble fraction remaining after chromatin-bound proteins were extracted, and normally contains cytoskeletal proteins (Figure 6D). We speculate that upon oxidative stress, TRF1 translocated into stress granules or that TRF1 aggregated and therefore became less soluble. In addition, we studied the kinetics of TRF1 dissociation from telomeres in a time course of menadione treatment. ChIP data showed that TRF1 was evicted from telomeres only after half an hour and the signal continued to diminish during the two hours treatment (Figures 6E and 6F). To corroborate these findings, we employed live-cell imaging. We used Hela cells containing endogenously Halo-tagged TRF1 generated by our lab. The cells were incubated with a cell-permeable fluorescent ligand which could form covalent bonds with the Halo tag. Images were captured after half-an-hour, one- and two-hours of treatment with menadione. The TRF1 signal at telomeres was strongly reduced over time under menadione treatment, whereas it remained relatively constant in the untreated sample. Therefore, this experiment confirms that TRF1 dissociates from telomeres upon menadione treatment.

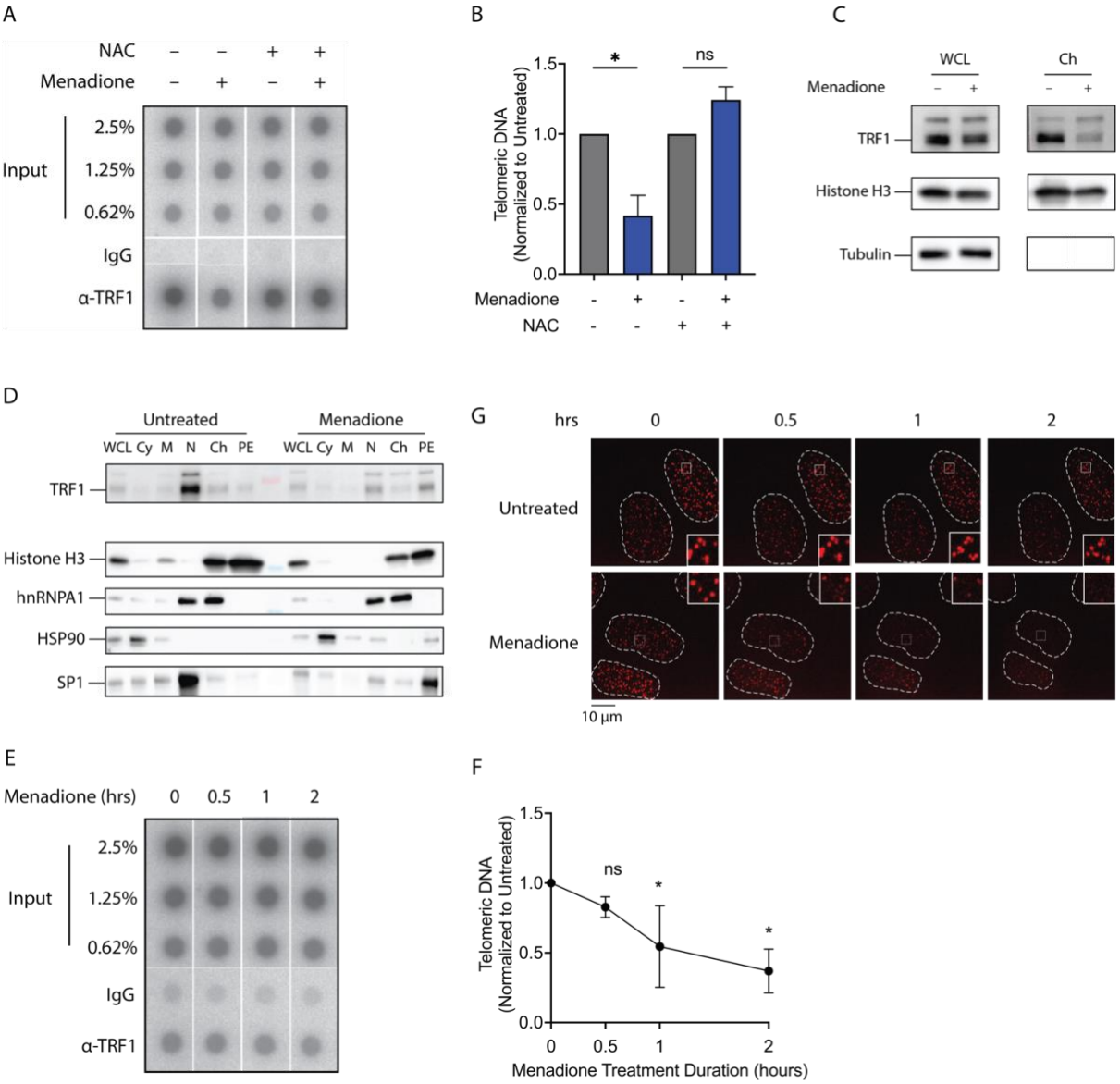
A
NAC – – + +
Menadione – + – +
Input
2.5%
1.25%
0.62%
IgG
α-TRF1
B
Telomeric DNA (Normalized to Untreated)
1.5
1.0
0.5
0.0
*
ns
Menadione - + - +
NAC - - + +
C
WCL
Ch
Menadione – + – +
TRF1
Histone H3
Tubulin
D
Untreated
Menadione
WCL Cy M N Ch PE WCL Cy M N Ch PE
TRF1
Histone H3
hnRNPA1
HSP90
SP1
G
hrs 0 0.5 1 2
Untreated
Menadione
10 µm
E
Menadione (hrs) 0 0.5 1 2
Input
2.5%
1.25%
0.62%
IgG
α-TRF1
F
Telomeric DNA (Normalized to Untreated)
1.5
1.0
0.5
0.0
ns
*
*
0 0.5 1 2
Menadione Treatment Duration (hours)

Figure 6: TRF1 dissociation from oxidatively damaged telomeres. **(A)** TRF1 protein dissociated from telomeres upon menadione treatment in a ROS-dependent manner. ChIP using antibody against TRF1 protein following 2 hours of menadione treatment with or without treating the cells with NAC priorly was performed. Immunoprecipitated DNA was blotted onto a membrane which was then hybridized with a telomere-specific probe. **(B)** Quantification of telomeric DNA signal in **(A)** as fold change over untreated sample. **(C)** Total (WCL) and chromatin-bound (Ch) levels of TRF1 by Western Blot using an antibody against FLAG tag. Since the cells contain endogenously FLAG-tagged TRF1 and TRF2, the upper band in the blot corresponds to TRF2 protein. Histone H3 served as the loading control. **(D)** TRF1 protein levels in different subcellular fractions (WCL: Whole Cell Lysate, Cy: Cytoplasm, M: Membrane, N: Nucleoplasm, Ch: Chromatin-bound, PE: Pellet Extract). Histone H3, hnRNPA1, HSP90 and SP1 proteins served as specific markers for subcellular fractions. **(E)** TRF1 protein level at telomeres over a time course of menadione treatment measured by TRF1 ChIP-dot blot. **(F)** Quantification of telomeric DNA signal in **(E)** as fold change over untreated sample. **(G)** Live-cell imaging of Halo-tagged TRF1 over 2 hours of menadione treatment. The nuclei were outlined with dashed lines. White squares show 5X zoom-in.
(*) $p < 0.05$, ns – not significant. Data represents mean ± SD. n = 3

We then embarked on investigating the molecular mechanisms underlying TRF1 dissociation from damaged telomeres. Since post-translational modifications (PTM) can change protein-to-DNA binding capacity, and also stimulate protein translocation, we decided to examine potential TRF1 PTMs, which could change protein molecular weight (MW) and lead to mobility shift. We immunoprecipitated TRF1 protein, which was then fractionated the by PAGE to analyze TRF1 protein distribution in an MW-dependent manner. We used HEK293E cells containing endogenously FLAG-tagged TRF1, and conducted FLAG immunoprecipitation (IP) as it provided higher purity than IP using antibodies directed against TRF1. Western blot was also conducted using anti-FLAG antibody. As we only detected TRF1 signal in the whole cell lysate (WCL), nucleoplasm, chromatin-bound and pellet extract fractions (Figure 6D), we used them as the input for IP. Western blot showed smeary signal at high MW position specifically in the WCL and pellet extract IP samples from menadione-treated cells (Figure 7A), suggesting that menadione treatment might induce TRF1 protein modifications possibly leading to their translocation from nucleoplasm and chromatin into pellet extract fraction.

We then used the same IP samples for western blot using antibodies against ubiquitin and small ubiquitin-like modifier (SUMO) proteins. We observed global increases in the total level of ubiquitination and SUMOylation in response to oxidative stress, as the ubiquitin and SUMO western blot signals were higher in the WCL and pellet extract input samples from menadione-treated cells compared to the untreated one (Figures 7B and 7C). It is probably because during oxidative stress, many proteins become misfolded and damaged, making them targets for ubiquitin conjugation and proteasome-mediated degradation. However, there was no ubiquitin and SUMO signal being detected in the IP samples (Figures 7B and 7C), indicating that TRF1 protein was not a substrate for ubiquitination and SUMOylation under oxidative stress condition.

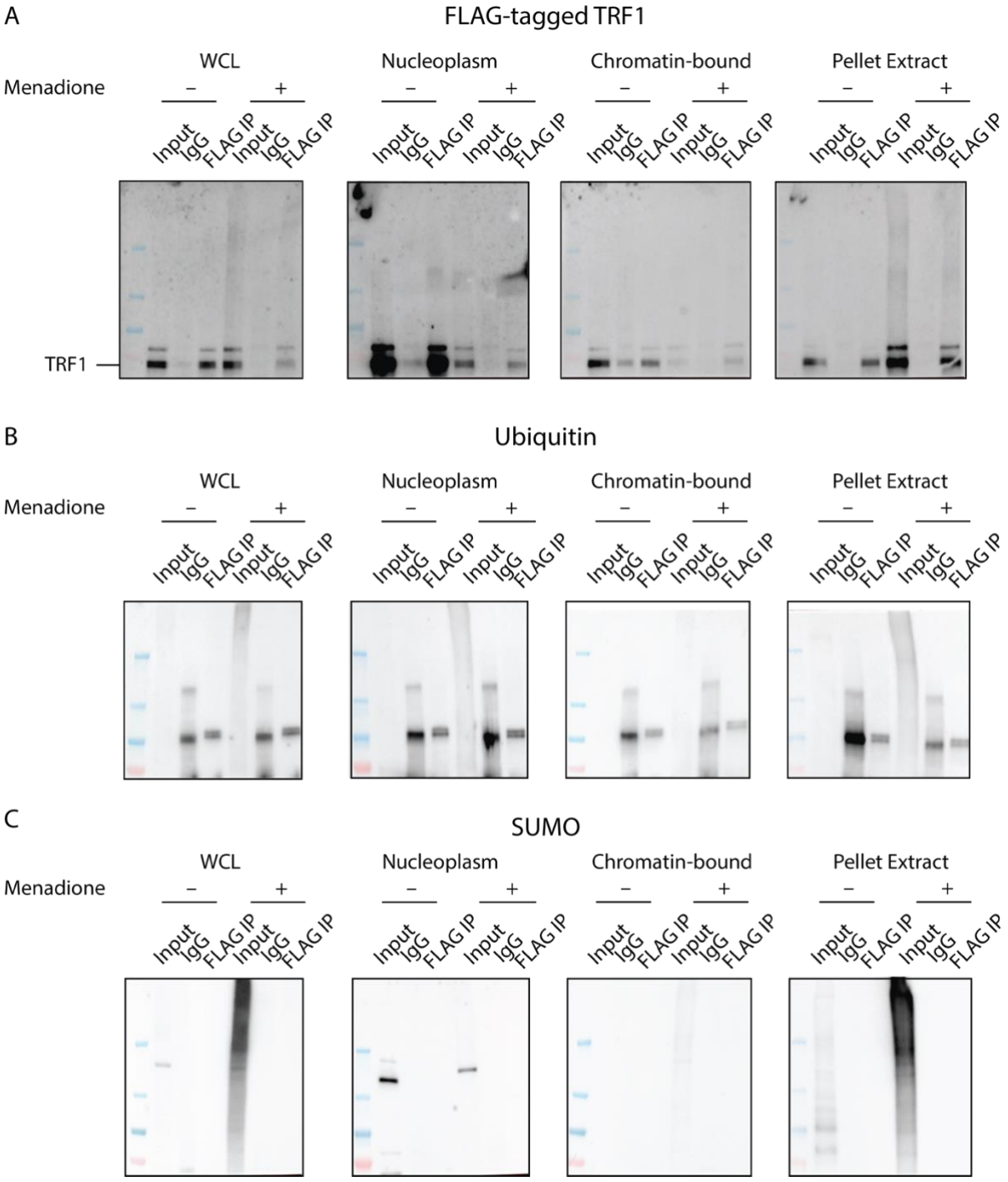

Figure 7: TRF1 dissociation from telomeres following oxidative stress induction is not due to TRF1 ubiquitination nor SUMOylation. **(A)** FLAG-tagged TRF1 immunoprecipitation upon menadione treatment using antibody against FLAG. IgG was used as a negative control. 10% of Input and 20% of IP samples were used for Western Blot with antibody against FLAG. **(B)** The same samples as in **(A)** were used for Western Blot with antibody against Ubiquitin. **(C)** The same samples as in **(A)** were used for Western Blot with antibody against SUMO

Another PTM that potentially leads to a smeary pattern at high MW positions is poly(ADP-ribose) (PAR) polymerization (PARylation). It has been shown that the PARylation of TRF1 by tankyrase (TNKS) – a telomeric PAR polymerase, releases TRF1 from telomeres, leading to the ubiquitination and subsequent degradation of unbound TRF1 (Smith et al., 1998; Smith and de Lange, 2000). Also, TNKS is recruited to telomeric damage sites, and the impairment of TNKS recruitment or function sensitizes cells to telomeric DNA damage (Yang et al., 2017). Thus, we decided to inhibit TNKS using a potent TNKS inhibitor (TNKSi) (Haikarainen et al., 2013), and examined its effect on DNA damage and TRF1 protein level at telomeres upon menadione treatment. As TNKS self-regulates its cellular protein levels via auto-PARylation causing its degradation (Yeh et al., 2006), successful inhibition of TNKS PARylation activity resulted in an increase in total TNKS protein level (Figure 8A). We then checked DNA damage at telomeres mediated by menadione with or without TNKSi. We observed that the same level of SSBs was generated in both conditions (Figures 8B and 8C). Also, TRF1 dissociated similarly from oxidatively damaged telomeres regardless of TNKS inhibition (Figures 8D and 8E). This indicates that TNKS does not play a role in regulation of telomeric DDR and TRF1 binding to telomeres under oxidative stress condition.

We then assessed the role of another PAR polymerase PARP1, which recognizes DNA breaks and orchestrates DDR activity via stimulating the PARylation and activation of PARP1 itself and other proteins (de Murcia and de Murcia, 1994; Hanzlikova et al., 2018). We inhibited PARP1 using a well-established PARP1 inhibitor talazoparib. As expected, there was a marked decrease in total PAR level, confirming the potency of talazoparib (Figure 8E). Also, we validated the role of PARP1 in protecting telomeres from oxidative damage, as PARP1 inhibition exacerbated ROS-induced SSB accumulation (Figures 8F and 8G). However, upon menadione treatment, TRF1 protein was released from telomeres to the same extent in spite of talazoparib, indicating that PARP1 does not control TRF1 dissociation from damaged telomeres (Figures 8H and 8I).

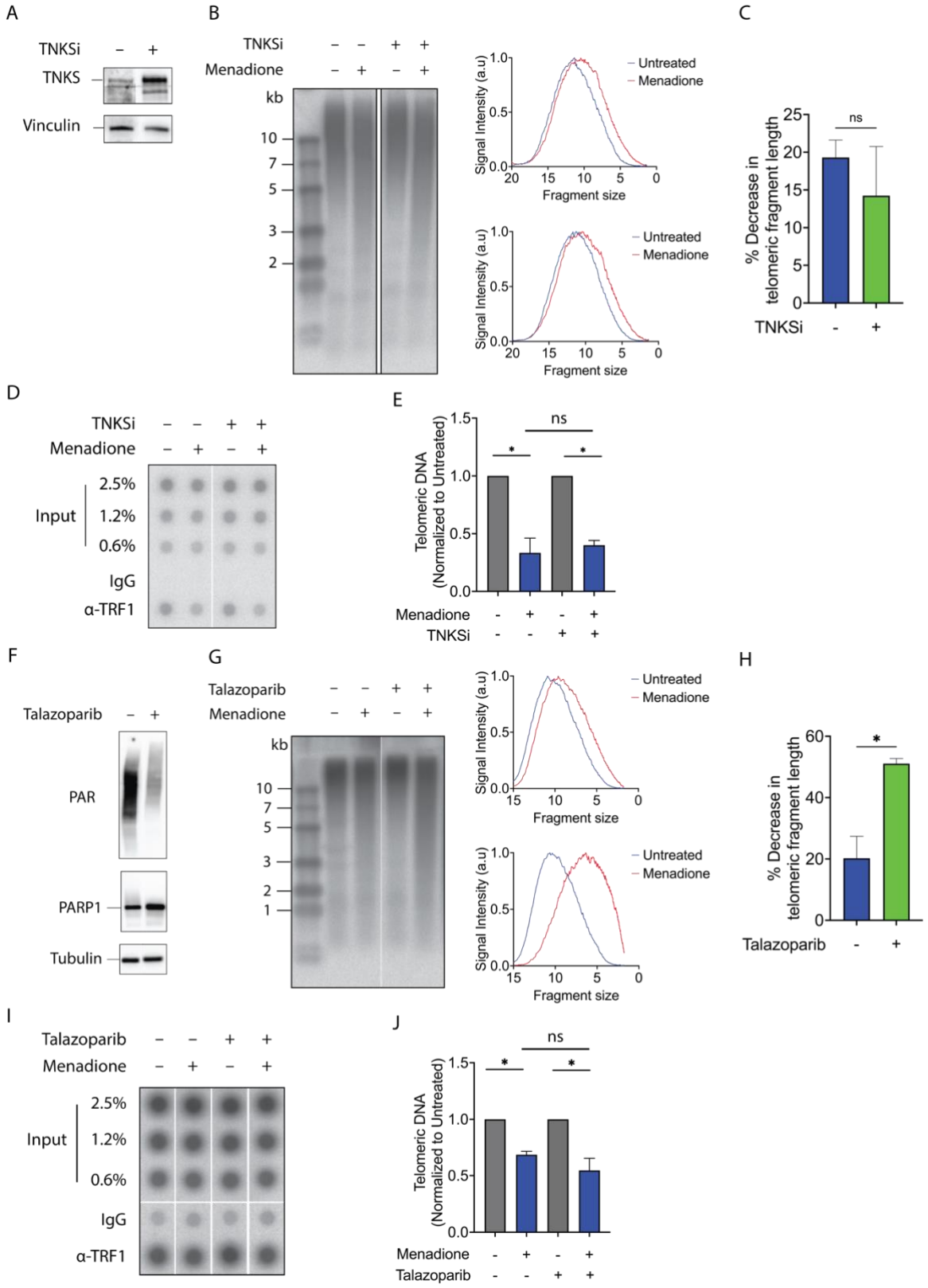
A
TNKSi – +
TNKS
Vinculin
B
TNKSi – – + +
Menadione – + – +
kb
10
7
5
3
2
Signal Intensity (a.u)
Fragment size
Untreated
Menadione
C
% Decrease in telomeric fragment length
ns
TNKSi - +
D
TNKSi – – + +
Menadione – + – +
Input
2.5%
1.2%
0.6%
IgG
α-TRF1
E
Telomeric DNA (Normalized to Untreated)
ns
*
*
Menadione - + - +
TNKSi - - + +
F
Talazoparib – +
PAR
PARP1
Tubulin
G
Talazoparib – – + +
Menadione – + – +
kb
10
7
5
3
2
1
Signal Intensity (a.u)
Fragment size
Untreated
Menadione
H
% Decrease in telomeric fragment length
*
Talazoparib - +
I
Talazoparib – – + +
Menadione – + – +
Input
2.5%
1.2%
0.6%
IgG
α-TRF1
J
Telomeric DNA (Normalized to Untreated)
ns
*
*
Menadione - + - +
Talazoparib - - + +

Figure 8: TRF1 dissociation from telomeres following oxidative stress induction is not due to TRF1 PARylation. **(A)** Western Blot of TNKS expression following TNKSi treatment. Vinculin served as the loading control. **(B)** Alkaline gel electrophoresis to detect telomeric SSBs upon menadione treatment with or without TNKSi. The signal intensity curves were also shown here. **(C)** The percentage decrease in telomeric fragment length of the menadione-treated sample compared to the untreated one, which represents the levels of DNA damage. Quantification was done using the alkaline gel in **(B)**. **(D)** TRF1 protein level at telomeres following menadione treatment with or without TNKSi. ChIP was done using antibody against TRF1 protein. Immunoprecipitated DNA was blotted onto a membrane which was then hybridized with a telomere-specific probe. (**E**) Quantification of telomeric DNA signal in **(D)** as fold change over untreated sample. **(F)** Western Blot of total PAR level following talazoparib treatment. Tubulin served as the loading control. **(G)** Alkaline gel electrophoresis to detect telomeric SSBs upon menadione treatment with or without talazoparib. The signal intensity curves are also shown here. **(H)** The percentage decrease in telomeric fragment length of the menadione-treated sample compared to the untreated one, which represents the levels of DNA damage. Quantification was done using the alkaline gel in **(G)**. **(I)** TRF1 protein level at telomeres following menadione treatment with or without talazoparib. ChIP was done using antibody against TRF1 protein. Immunoprecipitated DNA was blotted onto a membrane which was then hybridized with a telomere-specific probe. **(J)** Quantification of telomeric DNA signal in **(I)** as fold change over untreated sample.
(*) $p < 0.05$, ns – not significant. Data represents mean ± SD. n = 3

2.2.2. Substantial changes in the whole telomeric proteome induced by oxidative stress

(In collaboration with the Proteomics Core Facility, EPFL and the Protein Analysis Facility, University of Lausanne, Lausanne, Switzerland)

Due to changes that we observed in the telomeric nucleic acid composition and the dissociation of TRF1 protein from telomeres upon oxidative stress, we expected that oxidative stress would trigger substantial changes in the whole telomeric proteome composition. To determine in a comprehensive manner the changes of the telomeric proteome under oxidative stress, we employed two-step QTIP (Glousker et al., 2020) to isolate telomeric chromatin in the presence or absence of menadione, which was then analyzed by Mass Spectrometry (MS) (Figure 9A). Since QTIP experiments require large number of cells, we used HEK293E cells that are grown in suspension and that expressed endogenously FLAG-tagged TRF1 and TRF2 proteins (Lin et al., 2021). To ascertain that menadione inflicts damage as effectively in large-scale culture, we first assessed the level of telomeric SSBs induced by menadione in QTIP samples using alkaline denaturing gel electrophoresis. As expected, we observed a shift in the signal intensity curve of the menadione-treated sample compared to the untreated one, indicating an accumulation of SSBs (Figure 9B). Quantitative estimation showed that menadione induced similar levels of SSBs at telomeres between large and small-scale cell culture (Figure 9C). Then, the crosslinked and sonicated telomeric chromatin was purified by anti-FLAG sepharose beads targeting the FLAG epitopes of TRF1 and TRF2 proteins. Immunoprecipitated chromatin was eluted with excessive amount of FLAG peptides, and then re-precipitated using antibodies against TRF1 and TRF2 proteins (Glousker et al., 2020) (Figure 9A). To evaluate the enrichment and recovery of telomeric chromatin, we performed dot blot hybridization with probes specific for telomeric DNA or Alu element, which represents non-telomeric DNA (Figure 9D). With two purification steps, telomeric DNA was enriched over Alu more than 2000 folds for both untreated and menadione-treated samples (Figure 9E). This purification factor indicates that the telomeric chromatin was of high purity. In terms of recovery, we achieved around 5% recovery of telomeric DNA for the untreated sample, while it was around 2% recovery for the menadione-treated one. The difference is due to the dissociation of TRF1 protein from damaged telomeres described above (Figure 9E), which requires normalization during data analysis.

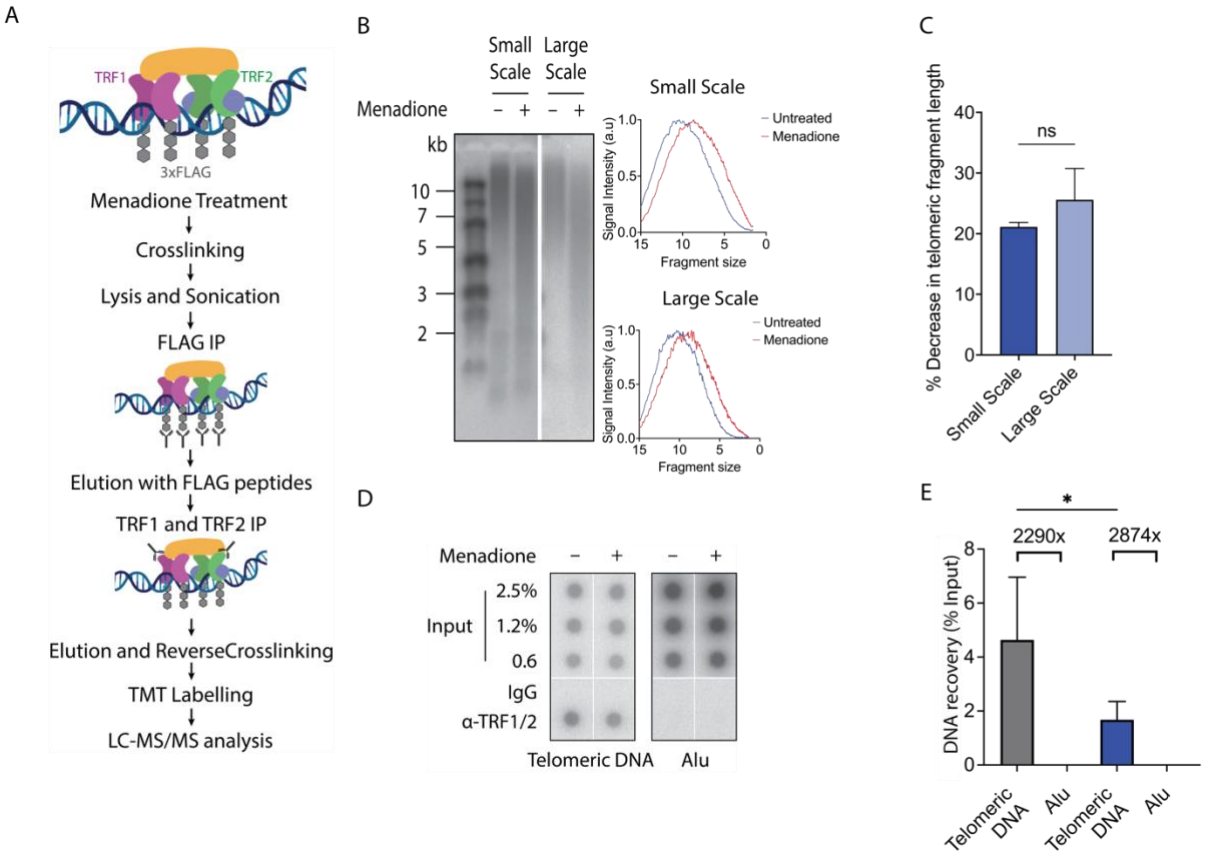

Figure 9: Precipitation of telomeric chromatin with high purity using the two-step QTIP. **(A)** Scheme of the two-step QTIP. **(B)** Alkaline gel electrophoresis to compare the level of SSB accumulation induced by menadione treatment in small-scale versus large-scale cell culture. The signal intensity curves are also shown here. **(C)** The percentage decrease in telomeric fragment length of the menadione-treated sample compared to the untreated one, which represents the levels of DNA damage. Quantification was done using the alkaline gel in **(B). (D)** Precipitated DNA by two-step QTIP was blotted onto a membrane, which was hybridized with a telomere-specific probe to measure the efficiency, or an Alu element-specific probe to measure the specificity of telomere chromatin enrichment. **(E)** Quantification of DNA signal in **(D)** with the numbers indicating the fold enrichment of precipitated telomeric DNA over Alu repeat DNA.
(*) $p < 0.05$, ns – not significant. Data represent mean ± SD. n = 3

We performed four biological replicates, with non-specific IgG pulldown being included as a negative control. By applying TMT isobaric labelling in which peptides from each sample were tagged with a unique reporter ion, we managed to mix and run replicates together, thereby minimizing the variation among different MS runs. After digestion, labeling and pooling, peptides in each mix were fractionated according to their isoelectric points to maximize separation and increase the depth of protein identification. Comparison between the QTIP sample and IgG negative control confirmed that the two-step approach produced telomeric chromatin with very high purity. Indeed, we detected more than 2000 proteins specifically enriched in the QTIP sample compared to the IgG control. We consistently identified in the QTIP sample peptides corresponding to shelterin proteins, while none of them was present in the IgG control (Figure 10A). In addition, we identified many proteins that have been reported to be telomere-associated, including telomere end processing enzymes Apollo, Mre11 and RAD50, components of the THO complex, SMCHD1, SAMHD1 and the scarce t-loop unwinding helicase RTEL1 (Fernandes and Lingner, 2023; Grolimund et al., 2013; Majerska et al., 2018) (Figure 10A). When comparing between untreated and menadione-treated samples, due to the difference in the levels of telomeric chromatin recovery, we normalized all protein intensities to TRF1 and TRF2 so that after normalization, the TRF1 and TRF2 intensities between the untreated and treated samples became equal within each replicate (Figure 10B). Normalized MS data showed that other shelterin proteins POT1, TPP1 and Rap1 seemed unchanged, while TIN2 decreased slightly at telomeres upon oxidative stress. POT1 and TPP1 ChIP data validated this finding (Figures 10C and 10D). The normalized MS data also indicated that upon oxidative stress induction, more than 1600 proteins were significantly enriched at damaged telomeres, including DDR factors, antioxidant enzymes, chromatin remodelers and post translational modification enzymes (Figure 10B, this will be discussed in more detail in the next figure). However, we believe that these enrichments need to be experimentally validated. It is because a certain number of proteins could be precipitated as efficiently in both untreated and menadione-treated samples despite the difference in telomeric chromatin recovery. Thus, the normalization to TRF1 and TRF2 intensities would lead to overestimation of the signal of the proteins of interest in the menadione-treated sample.

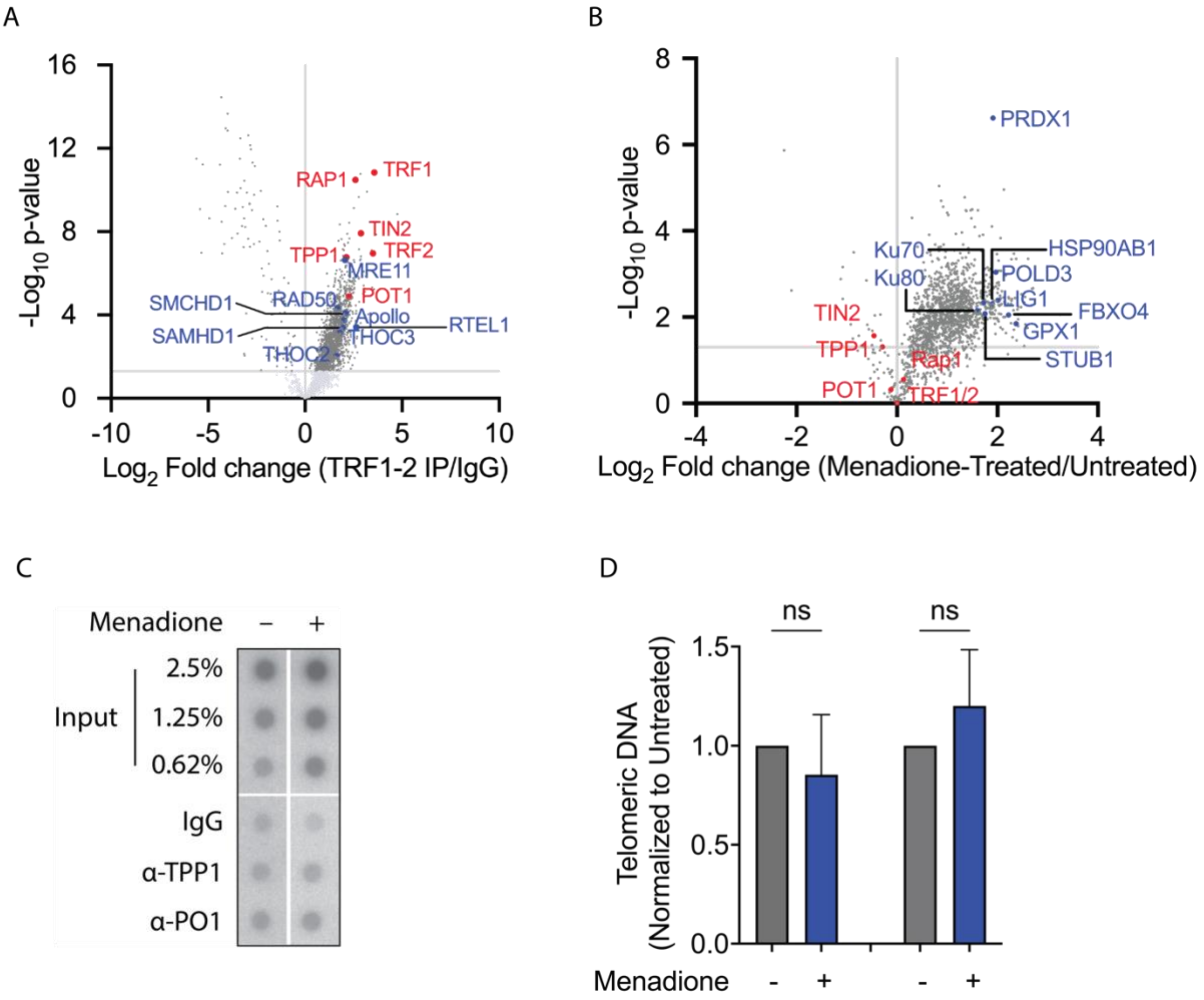

Figure 9: Two-step QTIP to discover remodeling of the telomeric proteome upon oxidative stress. **(A)** Scatter plot representing immunoprecipitation specificity (TRF1-2 IP/IgG). Shelterin proteins were colored in red while other telomeric proteins that had been previously reported were colored in blue. **(B)** Scatter plot showing the comparison in the protein intensities between the untreated and menadione-treated samples. The Mass Spectrometry data was normalized to TRF1/2 signal. Shelterin proteins were colored in red while proteins highly enriched in the menadione-treated sample were colored in blue. **(C)** TPP1 and POT1 ChIP-dot blot following menadione treatment. **(D)** Quantification of telomeric DNA in **(C).**
(*) $p < 0.05$, ns – not significant. Data represents mean ± SD. n = 3

We identified proteins functioning in major DDR pathways including base excision repair (BER), nucleotide excision repair (NER), mismatch repair (MMR), non-homologous end joining and homologous recombination repair pathways (Figure 11A). Since SSBs and probably oxidized nucleotides accumulated at telomeres upon oxidative stress (Figure 3), the activation and thus recruitment of factors functioning in single-stranded DDR pathways to damaged telomeres is inevitable. Furthermore, the enrichment of DSB repair factors was also observed. In addition, histone modification enzymes were also recruited to telomeres under oxidative stress (Figure 11B) probably through the activation of DDR pathways or in a telomere-specific manner via TERRA for example, as is the case for KDM1A/LSD1 (Porro et al., 2014b). This possibly leads to chromatin architectural alteration, thereby facilitating the recruitment of DNA repair proteins to damage sites. Histone modifiers such as KDM1A might also affect other enzyme activities (Porro et al., 2014b). Moreover, as expected, there were many antioxidant enzymes present at telomeres upon menadione treatment including PRDX1 (Peroxiredoxin 1) (Figure 11C), which has been shown to be associated with and have protective function against oxidative damage at telomeres before (Aeby et al., 2016; Ahmed & Lingner, 2018; Ahmed & Lingner, 2020). The recruitment of antioxidant enzymes may remove ROS in the microenvironment around telomeres, thereby alleviating potential protein and DNA damage. In addition, several heat shock proteins (HSP) were also detected at damaged telomeres (Figure 11C), probably to refold telomeric proteins, thereby maintaining telomeric function and integrity. We also noticed the enrichment of a large number of post-translational modification enzymes including kinases, ubiquitin ligases and SUMO ligases (Figure 11D). They might participate in regulating other protein activities via phosphorylation for example, or stability via ubiquitination and SUMOylation. Interestingly, some of them have been reported to modify TRF1 protein, which proposes a mechanism of how TRF1 dissociates from damaged telomeres.

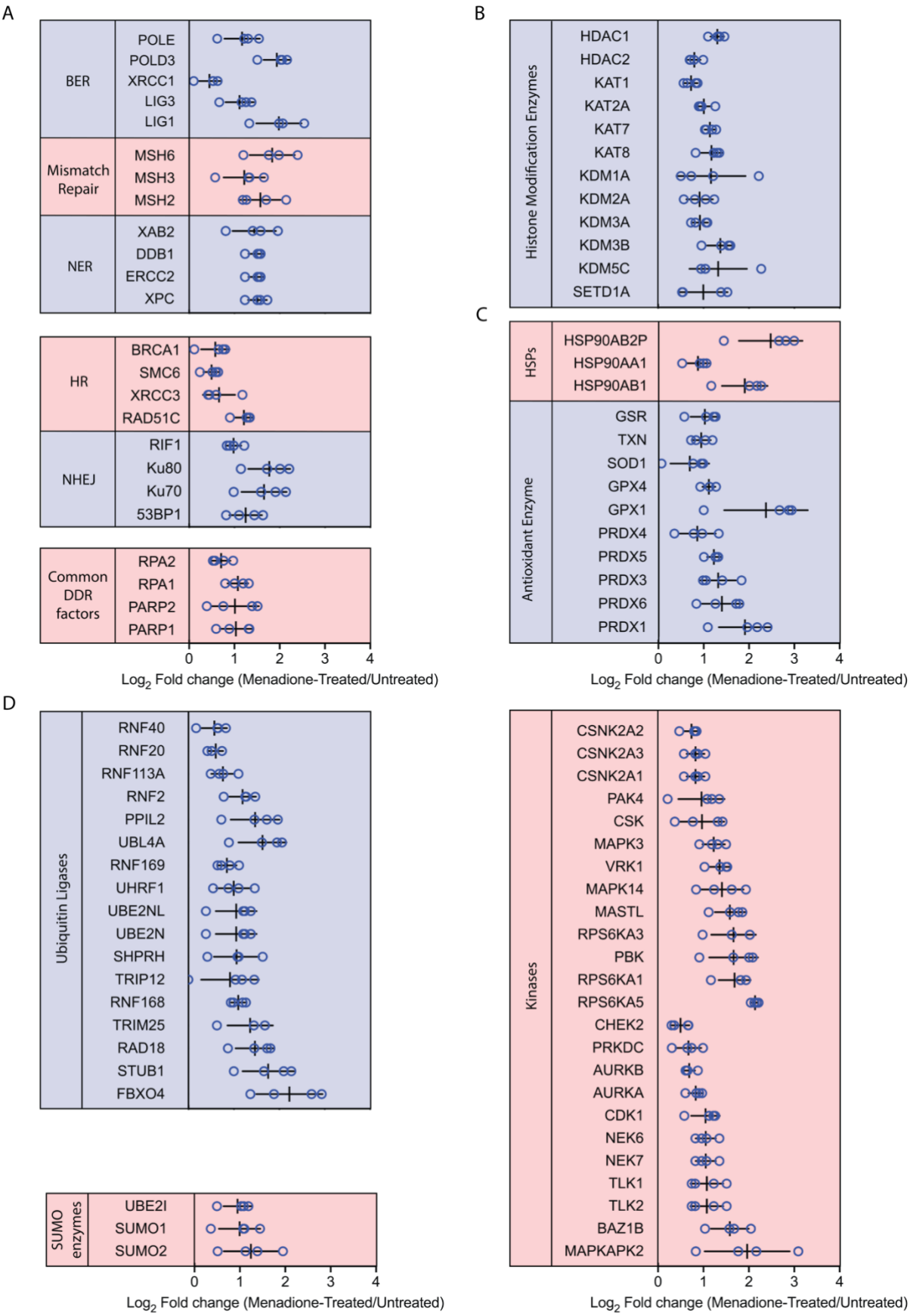

Figure 11: The enrichment of DDR factors **(A)**, chromatin remodelers **(B)**, antioxidant enzymes and HSPs **(C)** and post translational modification enzymes **(D)** upon oxidative stress induction.

Chapter 3. Discussion

Telomeric DNA is particularly susceptible to oxidative damage due to the repression of DNA damage repair pathways at intact telomeres, triple-G-containing 5'-TTAGGG-3' repetitive sequences, which are highly prone to oxidation, and 3' overhangs, which cannot be repaired by the base excision repair (BER) pathway due to the lack of complementary strands. In the t-loop structures, the 3' overhangs are base-paired. However, the displaced G-rich strand would be single-stranded and thus, not in an appropriate configuration for BER pathway. Here, we induced oxidative stress by menadione treatment which disrupts mitochondrial integrity and triggers elevation of intrinsic ROS level (Loor et al., 2010). This might mimic aging process during which defective mitochondrial function generates ROS [reviewed in (López-Otín et al., 2013)]. Oxidative stress leads to the accumulation of SSBs equally at both the G- and C-rich telomeric DNA strands (Figures 3A, 3B and 3C). SSBs can be generated due to the processing of oxidized nucleotides during DDR, or because of direct backbone cleavage by ROS. Importantly, addition of the antioxidant NAC before menadione treatment suppressed telomeric damage (Figures 3A, 3B and 3C) demonstrating that menadione elicited its effects via ROS. In addition, DSBs can accumulate due to replication stress induced by oxidative lesions, or if two SSBs lying in opposite strands are sufficiently close such that the force generated by hydrogen bonds is inadequate to keep two strands together. Thus, we also examined DSBs present at telomeres. However, in contrast to SSBs, we did not detect a marked increase in DSBs upon menadione treatment (Figure 3D). This can be due to the low frequency of stochastic events in which SSBs are at close proximity in opposite DNA strands, and to the fact that SSBs converted into DSBs during replication only occurs in dividing cells, which merely take up 20% - 30% of the cell population. Furthermore, DSB break repair at telomeres may have been very fast, thus preventing its detection.

Many studies have reported the crosstalk between R-loop formation, DNA damage and cellular oxidative stress. In the review by Marnef & Legube (2021), many mechanisms of how DSBs induce R-loop formation are proposed. Also, *in vitro* data show that nicks in non-template strand favor R-loop formation (Roy et al., 2010). In addition, under hydroxyurea (HU) treatment, R-loop level increases in S/G2-phase cells genome-wide, which can be rescued by NAC treatment or PRDX2 depletion, confirming that it is ROS-dependent (Andrs et al., 2023). Here we show that R-loop level at telomeres increase under oxidative stress and it is due to the upregulation in both TERRA transcription and TERRA recruitment in *trans* to damaged telomeres (Figure 4). The molecular mechanism behind TERRA recruitment can be due to changes in chromosome conformation that facilitate TERRA invasion and binding. Presumably, several proteins govern this process. The RAD51 protein is a prime candidate as it has been demonstrated to promote TERRA-mediated R-loop formation post-transcriptionally (Feretzaki et al., 2020). In addition, R-loops at telomeres may trigger the formation of G-quadruplex (G4) structures in the displaced G-rich DNA strand. G-quadruplexes in turn may stabilize TERRA R-loops in a positive-feedback mechanism upon ROS induction (Tan et al., 2020). At damaged telomeres, R-loops might facilitate HR activity functioning in DSB repair, probably via providing

a recruitment platform for DNA recombination proteins. It has been shown in ALT-positive U2OS cells that ROS-induced R-loops promote the binding of CSB and RAD52 proteins to telomeres, which in turns recruit RAD51 and POLD3 proteins to trigger transcription-coupled homologous recombination and break-induced replication (Tan et al., 2020; Teng et al., 2018). Although DSB accumulation under our treatment condition is probably at a low level (Figure 3D), they need to be repaired promptly to prevent detrimental consequences such as telomere loss. R-loops might play an essential role in this process. Despite its contribution to DNA repair, high levels of unresolved R-loop and G4 structures might worsen the DNA damage situation, and thus, they should be properly dissolved in a timely manner by BLM helicase for example (Tan et al., 2020).

We also examined the levels of lncRNA TERRA transcribed from nine different chromosome ends under oxidative stress condition. Six of them showed marked increases (1q, 9p, 10q, 13q, XqYq and XpYp) while three of them were unchanged (15q, 16p and 17p) (Figure 4D). This could be due to the variation in TERRA transcriptional regulation among different chromosomes, leading to the upregulation of TERRA transcription at one subset of telomeres but not the other. TERRA transcription is governed by chromosome-specific subtelomeric sequences, which contain TERRA promoters with CpG islands and binding motifs for transcription factors (Azzalin et al., 2007; Feretzaki et al., 2019). Studies have shown that not all subtelomeric sequences have CpG islands, and CG content varies within the ones that have CpG islands (Feretzaki et al., 2019). When comparing our data with the published study, we found that there was no correlation between the presence of CpG islands and the upregulation of TERRA transcription. Furthermore, bioinformatic analysis of the sequence upstream of TERRA transcription start sites reveals that different chromosome ends have different prevalence of binding motifs recognized by transcriptional regulatory factors (Feretzaki et al., 2019). However, there is no enrichment of any particular binding motif in the upregulated TERRA promoters. Apart from upregulated transcription, elevated TERRA levels can be explained by an increase in TERRA stability. A recent study identified that METTL3 methyltransferase installs N^6-Methyladenosine (m^6A) modification at TERRA subtelomeric sequences, which stabilizes TERRA (Chen et al., 2022). The TERRA m^6A is recognized and protected by YTHDC1 proteins (Chen et al., 2022). Our QTIP data shows that both METTL3 and YTHDC1 proteins are enriched at oxidatively damaged telomeres, indicating that there could be an upregulation in TERRA methylation, leading to increased TERRA stabilization and thus, TERRA level. However, since TERRA m^6A modification has not been shown to be chromosome-specific, it does not explain why the increases in TERRA level only happen at certain telomeres. Another factor determining TERRA stability is polyadenylation, which was recently shown to be telomere-specific (Savoca et al., 2023). Oxidative stress might change the polyadenylation pattern of certain TERRA species, leading to increased TERRA stability and TERRA levels.

In terms of telomeric protein composition, we observed the dissociation of TRF1 from telomeres upon oxidative damage induction (Figure 6), supported by a previous study showing that oxidative lesions can disrupt the binding of TRF1 and TRF2 proteins to telomeric DNA

oligonucleotide substrates *in vitro* (Opresko et al., 2005). We discovered that TRF2 protein was also released from damaged telomeres under our treatment condition, but to a lesser extent than TRF1 (data not shown). However, a study from Barnes et al. suggests that there is no loss of TRF1 and TRF2 at telomeres upon local oxidative damage induction at telomeres (Barnes et al., 2022). The study used a system of FAPs (fluorogen-activating peptides) fused with TRF1 protein (FAP-TRF1), which binds specifically to telomeres. FAPs have high affinity to MG2I, which generates singlet oxygen upon FAP binding and excitation by far-red light. Thus, by confining the presence of FAPs and MG2I at telomeres, they managed to induce oxidative stress locally (Barnes et al., 2022; Fouquerel et al., 2019). The fact that they did not observe TRF1 and TRF2 dissociation from damaged telomeres could be because they used a different oxidative damage inducing system to produce short half-life ROS and the induction only lasted for 5 minutes. This is probably insufficient to inflict effects on TRF1 and TRF2 binding to telomeres. In addition, while menadione mediates the accumulation of SSBs at telomeres (Figure 3), the FAP-TRF1 system induces mostly 8oxoG lesions with almost no SSBs (Fouquerel et al., 2019). The difference in oxidative lesions being induced by two systems could explain the discrepancy in our observations. We also examined the telomeric levels of other shelterin protein components TPP1 and POT1 by ChIP, and observed that there was no significant change following menadione treatment (Figures 9H and 9I). Although it has been shown that double knockout of TRF1 and TRF2 removes other shelterin components and generates shelterin-free telomeres (Sfeir and de Lange, 2012), in our case, there are around 50% of TRF1 and TRF2 proteins remaining at damaged telomeres (Figure 6B), which could be sufficient to maintain the binding of other shelterin proteins. Another possibility is that due to technical limitation of ChIP experiment, the potential alterations in telomeric levels of TPP1 and POT1 proteins cannot be detected.

There are many possible molecular mechanisms behind TRF1 dissociation from damaged telomeres. *In vitro* studies have shown that TRF1 protein cannot bind to DNA:RNA hybrid substrates (Lee et al., 2018). Thus, the increase in R-loop level at telomeres under oxidative stress (Figure 4) potentially prevents TRF1 binding to damaged telomeres. In addition, TRF1 protein physically associates with TERRA sequence both *in vitro* and *in vivo* (Deng et al., 2009; Lee et al., 2018; Scheibe et al., 2013). We observed increases in TERRA transcribed from certain chromosome ends following menadione treatment (Figure 4), which can associate with free TRF1 protein and make them unavailable for telomere binding. Furthermore, TRF1 dissociation from damaged telomeres can be induced by post-translational modifications. It has been reported that TRF1 phosphorylation by CDK1 prevents TRF1 from associating with telomeric DNA (McKerlie and Zhu, 2011). We observed an enrichment of CDK1 at telomeres in response to oxidative stress by QTIP (Figure 10D), which might result in TRF1 phosphorylation and TRF1 release from telomeres. Another kinase Nek7 is recruited to oxidatively damaged telomeres leading to TRF1 phosphorylation, which inhibits the interaction of TRF1 with the E3 ligase subunit Fbx4, thereby maintaining TRF1 stability (Tan et al., 2017). Consistently, we also observed the recruitment of Nek7 to telomeres following menadione treatment (Figure 10D). Although having not been tested, TRF1 phosphorylation

by Nek7 might affect the telomere-binding affinity of TRF1 protein. Finally, TRF1 protein might be oxidatively damaged and thus, can no longer bind telomeric DNA sequence. The effect of TRF1 dissociation on DDR at telomeres following oxidative stress induction is unclear. However, considering the suppressive effect of shelterin protein complexes on DDR activation [reviewed in (de Lange, 2005)], the loss of shelterin protein components at damaged telomeres might change telomeric chromatin conformation to be more accessible for DDR factors.

Having discovered many significant changes in telomeric chromatin following menadione treatment, we proceeded to study the whole telomeric proteome in response to oxidative stress in a comprehensive manner. We implemented here the two-step QTIP to obtain telomeric chromatin with high purity, which was then analyzed by Mass Spectrometry with TMT labelling to quantitatively compare the telomeric proteome changes under oxidative damage. In all four replicates, we consistently identified shelterin proteins and other telomere-associated proteins such as THO protein complex, SMCHD1, SAMHD1 and RTEL1 (Grolimund et al., 2013). When comparing between telomeric chromatin from untreated and menadione-treated cells, we identified more than 1600 proteins significantly enriched at damaged telomeres, including DDR factors functioning in all major repair pathways, antioxidant enzymes, chromatin remodelers and post-translational modification enzymes (Figure 11). SSBs and oxidized nucleotides accumulated at telomeres following menadione treatment, explaining the recruitment of single-stranded DNA repair factors. Previous studies have demonstrated the presence of BER factors PARP1 and XRCC1 proteins at telomeres upon oxidative stress induction, consistent with our QTIP data (Fouquerel et al., 2019). Furthermore, we identified several nucleotide excision repair (NER) factors being recruited to telomeres following menadione treatment. NER has also been shown to function in oxidative damage repair at telomeres (Gopalakrishnan et al., 2010). In addition, mismatch repair (MMR) factor MSH2 was recruited to damaged telomere, which might contribute to the resolution of oxidative lesions as it has been shown that depletion of MSH2 and MLH1 leads to increases in both basal and H_2O_2-induced 8-oxoG levels (Colussi et al., 2002). Apart from single-stranded DDR factors, we also had DSB repair factors being recruited to telomeres following oxidative stress induction, suggesting the presence of DSBs at telomeres, although it was insufficient to be detected by native gel electrophoresis (Figure 3). Although being at a low level, DSBs need to be repaired promptly to prevent detrimental consequences such as telomere loss. In addition, the accumulation of HR factors might reflect the presence of ssDNA gaps that we observed via EM analysis (Figure 5E).

We identified many histone modification enzymes recruited to telomeres under oxidative stress (Figures 11B and 11D). Previous studies have demonstrated the importance of histone post-translational modifications in regulating recruitment of DDR factors to facilitate repair response. One example is the ubiquitination of H2A and H2AX by RNF168, which promotes the binding of 53BP1 to DSB sites to activate the NHEJ pathway (Mattiroli et al., 2012). In addition, histone modifications might modulate chromatin conformation and accessibility for

DDR factors. Also, remodelling enzymes might affect activity of other proteins as in the case of KDM1A which can stimulate MRE11 nuclease activity *in vitro* (Porro et al., 2014b). We also noticed the enrichment of antioxidant enzymes including PRDX1 (Figure 11C), which is recruited to telomeres following oxidative stress induction and protects telomeres from oxidative damage (Aeby et al., 2016; Ahmed & Lingner, 2018; Ahmed & Lingner, 2020). The presence of antioxidant enzymes would reduce ROS in the microenvironment around telomeres, thereby preventing protein and DNA damage from occurring. Furthermore, heat shock proteins (HSP) were also at telomeres upon oxidative stress (Figure 11C), presumably to refold damaged telomeric proteins, thereby maintaining telomeric function and integrity. Another group of proteins being enriched at damaged telomeres is protein post-translational modification enzymes including kinases, ubiquitin ligases and SUMO ligases (Figure 11D). They might regulate other protein activity via phosphorylation, or stability via ubiquitination and SUMOylation. Overall, telomeric proteome analysis under oxidative stress provides a comprehensive snapshot of proteins that reflect the pathways and mechanisms engaged during telomere processing and repair.

Our findings provide novel insights into the mechanism of telomere protection against oxidative stress, which can be translated into clinical applications. Cancer cells are more susceptible to oxidative stress than non-cancer cells [reviewed in (Sabharwal and Schumacker, 2014)], providing great potential to specifically target cancer using ROS-inducing interventions. It has been reported that the accumulation of oxidative damage at telomeres is associated with the activation of DNA damage signalling, telomerase activity inhibition and accelerated telomere shortening, resulting in premature cellular senescence (Aeby et al., 2016; Barnes et al., 2022; Fouquerel et al., 2019). Thus, by understanding the molecular mechanisms that safeguard telomeric DNA from oxidative damage, we can amplify the level of DNA lesions at telomeres, thereby triggering senescence or autophagy in cancer cells. In addition, oxidative stress is elevated during aging due to endogenous metabolism and inflammation, as well as exogenous environmental sources (Gan et al., 2018; Osterod et al., 2001). Knowledge of how oxidative damage alters telomeres and how they are processed is important to protect telomeres from oxidative stress, and thus, promote healthy aging.

While our study provides valuable information about the impact of oxidative stress on telomeres, it has certain limitations. One of them is that we employed menadione as a unique tool to induce oxidative DNA damage at telomeres in an unspecific manner. As menadione treatment caused mitochondria damage, it served our purpose of mimicking the physiological condition in which defective mitochondria release excessive ROS, resulting in cellular oxidative stress. However, we need to distinguish the effect of oxidative stress on telomeres from oxidative stress – independent consequences induced by mitochondrial dysfunction for example. For this, we can use antioxidants such as NAC to prevent oxidative stress and examine the rescue effect on interested phenotypes. Furthermore, we might induce oxidative stress using other methods such as H_2O_2 treatment to confirm if similar phenotypes can be observed. In addition, as oxidative stress broadly affects many aspects of cell physiology, this

method poses difficulties to disentangle between the direct and indirect effects of ROS on telomeric chromatin composition and structure. We believe that both direct and indirect impacts are of biological relevance and of interest for further study. However, if there is a need to differentiate them, we can employ the system developed by the Opresko lab to generate oxidative damage at telomeres in a more targeted manner (Fouquerel et al., 2019). Another limitation is that TRF1 dissociation from damaged telomeres caused lower telomeric chromatin purification efficiency of the menadione-treated sample. This can be compensated by protein intensity normalization during data processing. Also, since there is no detectable change in telomere length upon menadione treatment, PiCH (proteomics of isolated chromatin segments) protocol in which telomere-specific oligonucleotides are used to pull down telomeric chromatin could be an appropriate alternative (Déjardin and Kingston, 2009).

Chapter 4. Conclusion and Future Perspectives

Overall, we observe the accumulation of SSBs at telomeres upon oxidative stress induction. Also, telomeric R-loop level increases in response to oxidative stress due to the upregulation of TERRA transcription and TERRA recruitment to damaged telomeres. We also discover the generation of internal loops at telomeric damage sites, probably due to the presence of single-stranded DNA gaps, which can undergo base-pairing if they are on opposite strands, while if the gaps are on the same strand, they can promote an exchange of the complementary strand (Mazzucco et al., 2020). Furthermore, TRF1 protein dissociates from damaged telomeres. There are several hypothetical mechanisms behind the dissociation. As TRF1 protein cannot bind to DNA:RNA hybrids, the increase in telomeric R-loop in response to oxidative stress might prevent TRF1 from binding to telomeres. In addition, upregulated TERRA level might sequester free TRF1 protein, thereby reducing the level of telomere-bound TRF1. Lastly, oxidative lesions in telomeric DNA and TRF1 protein might reduce their binding affinity. We also look at changes in the whole telomeric chromatin upon oxidative stress induction by QTIP combined with Mass Spectrometry analysis, and discover the enrichment of DDR factors functioning in major repair pathways, antioxidant enzymes, heat-shock proteins, chromatin remodelers and post-translational modification enzymes at damaged telomeres. They might work collaboratively to promote DDR at telomeres and protect telomeres from oxidative damage.

Our findings open many questions for future study. We would like to first understand the roles of R-loops at damaged telomeres. We can modulate R-loop level by RNaseH1 overexpression or knockdown and study the effect on DNA damage accumulation and repair at telomeres upon oxidative stress induction. Also, since RAD51 promotes TERRA R-loops in *trans* post-transcriptionally, we would like to study the putative involvement of RAD51 in TERRA recruitment to telomeres that were damaged by ROS by depleting RAD51 with siRNAs and measuring R-loop levels following menadione treatment. In addition, the molecular mechanisms behind TRF1 dissociation from damaged telomeres are unclear. This could be due to TRF1 post-translational modifications induced by oxidative stress, which can be discovered by Mass Spectrometry analysis of immunoprecipitated TRF1. Also, the effect of DNA:RNA hybrids on the binding of TRF1 to telomeres can be examined *in vitro* by Electrophoretic Mobility Shift Assay (EMSA), and *in vivo* by modulating R-loop level and examining TRF1 protein level at damaged telomeres. Furthermore, the hypothesis that TERRA might sequester free TRF1 protein, thereby reducing the level of telomere-bound TRF1, can be verified by measuring the binding of TRF1 and TERRA molecules upon menadione treatment by TRF1 RNA IP. Once we unravel the mechanism of TRF1 dissociation from damaged telomeres, we can rescue the phenotype and study the effect on DDR at telomeres. Lastly, it is important to understand the roles of antioxidant enzymes, chromatin remodelers and repair factors recruited to telomeres under oxidative stress. This can be done by depleting the factors and studying the effect on DNA damage accumulation and repair at telomeres.

Materials and Methods

Supplementary table 1. Antibodies

Application	Antibody target	Supplier: catalog number	Dilution/Amount
Western Blot	FLAG	Sigma: A8592	1:2000
	Histone H3	Abcam: ab1791	1:10000
	hnRNPA1	Santa Cruz: sc-32301	1:1000
	HSP90	Abcam: ab13492	1:1000
	SP1	Sigma: 17-601	1:1000
	SUMO	Abcam: ab3742	1:1000
	Ubiquitin	Enzo Life Science: BML-PW8810	1:1000
	PAR	Enzo Life Sciences: ALX-804-220-R100	
	Tankyrase	Abcam: ab227469	1:3000
	Vinculin	Abcam: ab129002	1:10000
	PARP1	Abcam: ab194586	1:2000
	Mouse IgG (H+L) HRP-conjugated	Promega: W4021	1:10,000
	Rabbit IgG (H+L) HRP-conjugated	Promega: W4011	1:10,000
DRIP	DNA:RNA hybrid	Kerafast: ENH001	0.1 µg/µg nucleic acid
ChIP	TRF1	Home-made	Appropriate amount according to titration
	TRF2		
	TPP1		
	POT1		
QTIP	FLAG	Millipore: A2220 (beads)	Appropriate amount according to titration
	TRF1/TRF2	Home-made sepharose beads crosslinked to antibodies	
IP	FLAG	Millipore: A2220 (beads)	10 µl/100 µg protein

Supplementary Table 2. Primers for DRIP-qPCR

Target loci	Oligonucleotide Sequences (5’-3’)
1q Fwd	TAGTGTGGAAAGCGGGAAAC
1q Rev	TGCAGTTGAACCCTGCAATA
9p Fwd	GAGATTCTCCCAAGGCAAGG
9p Rev	ACATGAGGAATGTGGGTGTTAT
10q Fwd	GCATTCCTAATGCACACATGAC
10q Rev	TACCCGAACCTGAACCCTAA
13q Fwd	GCACTTGAACCCTGCAATACAG
13q Rev	CCTGCGCACCGAGATTCT
XqYq Fwd	AGCGTCGGAACGCAAAT
XqYq Rev	TGGGTATCATGTGTGCATTAGG
XpYp Fwd	CCACAACCCCACCAGAAAGA
XpYp Rev	GCGCGTCCGGAGTTTG
15q Fwd	TGCAACCGGGAAAGATTTTATT
15q Rev	GCGTGGCTTTGGGACAACT
16p Fwd	GCCTGGCTTTGGGACAACT
16p Rev	TGCAACCGGGAAAGATTTTATT
17p Fwd	CTTATCCACTTCTGTCCCAAGG
17p Rev	CCCAAAGTACACAAAGCAATCC

Supplementary Table 3. Primers for RT-qPCR

Target loci	Oligonucleotide Sequences (5’-3’)
1q Fwd	TAGTGTGGAAAGCGGGAAAC
1q Rev	TGCAGTTGAACCCTGCAATA
9p Fwd	TCCCTATAATCCGCCACTACT
9p Rev	ACATTGCAGGGTCCTCTTG
10q Fwd	GCCTTGCCTTGGGAGAATCT
10q Rev	AAAGCGGGAAACGAAAAGC
13q Fwd	GCACTTGAACCCTGCAATACAG
13q Rev	CCTGCGCACCGAGATTCT
XqYq Fwd	TCCTAATGCACACATGATACCC
XqYq Rev	CCCTAAGCACATGAGGAATGT
XpYp Fwd	GAGTGAAAGAACGAAGCTTCC
XpYp Rev	CCCTCTGAAAGTGGACCTAT
15q Fwd	TGCAACCGGGAAAGATTTTATT
15q Rev	GCGTGGCTTTGGGACAACT
16p Fwd	GCCTGGCTTTGGGACAACT
16p Rev	TGCAACCGGGAAAGATTTTATT
17p Fwd	GGGACAGAAGTGGATAAGCTGATC
17p Rev	GATCCCACTGTTTTTATTACTGTTCCT

Cell culture

Suspension HEK293E cells were cultured in EX-CELL 293 Serum-Free Medium (Merck) supplemented with 4 mM GlutaMAX. Hela cells were maintained in Dulbecco's modified Eagle's medium (DMEM) (Gibco) supplemented with 100 U/ml of penicillin/streptomycin and 10% fetal bovine serum (FBS). Cells were maintained in a controlled humidified atmosphere with 5% (v/v) CO_2, at 37°C, with constant agitation in the cases of suspension HEK293E cells. The generation of HEK293E cells containing endogenously FLAG-tagged TRF1 and TRF2 were previously described (citation). Hela cells containing endogenously Halo-tagged TRF1 protein was generated by Dr. Eftychia Kyriacou – a postdoc in our laboratory.

Oxidative stress induction

Cells were treated with 0.1 mg/ml menadione for 2 hours with or without prior treatment with one of the following drugs: 5 nM N-Acetyl Cysteine (NAC) (Sigma-Aldrich) for 30 mins, 10 µM TNKS inhibitor (ChemBridge Corporation, Ref No: 6661308) for 16 hrs or 1 µM Talazoparib for 16 hrs. In the time course experiments, cells were treated with 0.1 mg/ml menadione for 30 mins, 1 hr or 2 hrs. After the treatment, cells were washed with cold 1X PBS three times before proceeding to any experiment.

DNA isolation

Each pellet containing 3 x 10^6 cells was lysed with 1 ml of TENS buffer (10 mM Tris-HCl pH 7.5, 10 mM EDTA, 100 mM NaCl, 1% SDS) supplemented with 100 µg/ml Proteinase K overnight at 37°C. The lysate was added onto a 15-ml MaXtract High Density tube (Qiagen), followed by 1 volume of Phenol-Chloroform-Isoamyl (25:24:1) (Biosolve) (PCI) pre-warmed to room temperature. The tube was mixed on a wheel for 10 mins, and then centrifuged for 5 mins at 1500g. Then, 1 volume of PCI was added, and the tube was again mixed in a wheel for 10 mins and centrifuged for 5 mins at 1500g. The top layer was transferred to a new 15-ml tube, DNA was precipitated with 2 volumes of Isopropanol and 1/10 volume of Sodium Acetate (3M, pH 5.3). The DNA was collected by cold centrifugation at 10000g for 30 mins, and then washed twice with 70% Ethanol. After letting the DNA dry for a few minutes, the DNA was dissolved in 200 µl of 10 mM Tris-HCl pH 7.5 overnight in cold room. The next day, the DNA was treated with 100ng/µl RNAse A (Millipore) for 30 min at 37°C, followed by 100ng/µl proteinase K treatment for 1 hr at 50°C. The DNA was then cleaned with PCI as described above, and dissolved in 100 µl of 10 mM Tris-HCl pH 7.5 overnight in cold room. DNA concentration and purity was measured by NanoDrop Spectrophotometer (Thermo Fisher Scientific). The DNA was then used for alkaline, native or 2-dimension (2D) gel electrophoresis.

Gel electrophoresis

6 µg of genomic DNA was digested with HinfI and RsaI (10 U each) (NEB) in a 50-µl reaction containing 1X CutSmart buffer (NEB) overnight at 37°C. For single-stranded break analysis, 2 µg of digested DNA was separated by gel electrophoresis in 0.8% alkaline sepharose gel containing 50 mM NaOH and 1 mM EDTA at 2 V/cm for 16 h. The gel was then neutralized with

neutralization buffer (0.5 M Tris-HCl at pH 7.5, 1.5 M NaCl) for 1 hr and dried on for 2.5 hrs at 55°C in a gel drier. For double-stranded breaks analysis, we used native gel electrophoresis in which 2 µg of digested DNA was separated in 0.8% sepharose gel made in 1X TBE and dried as described above. The dried gel was treated with first with denaturation buffer (0.5 M NaOH, 1.5 M NaCl) for 1 hr, followed by 1 hr of neutralization buffer. In both cases of alkaline and native gels, the gel was pre-hybridized with Church buffer (0.5 M $NaHPO_4$, 1 mM EDTA, pH 8.0, 1% (w/v) BSA, 7% SDS) for at least 1 h, followed by overnight incubation with telomere-specific probes at 50°C. After hybridization, the gel was washed once with 4X SSC, twice with 4X SSC + 0.1% SDS, twice with 2X SSC + 0.1% SDS and then once with 4X SSC for at least 30 mins each at 50°C, and then exposed to a phosphor screen overnight. The screen was then scanned using a Typhoon phosphorimager (GE). Average telomeric DNA fragment length was estimated based on densitometry using AIDA software. The quantification of DNA damage (both SSBs and DSBs) was represented by the percentage decrease in telomere length of treated samples compared to untreated samples.

2-dimension (2D) gel electrophoresis

20 µg of genomic DNA was digested with MboI and AluI (50 U each) (NEB) in a 200-µl reaction containing 1X CutSmart buffer (NEB) overnight at 37°C, and then precipitated with 1 volume of Isopropanol and 1/10 volume of sodium acetate (3M, pH 5.3). The digested DNA was then collected by cold centrifugation at 16000g for 30 mins, and then washed twice with 70% Ethanol. After letting the DNA dry for a few minutes, the DNA was dissolved in 20 µl of TE buffer (1 mM EDTA pH 8.0, 10 mM Tris pH 8.0) over the day at 37°C with gentle shaking. The first dimension was run in 0.4% agarose gel made in 0.5X TBE without ethidium bromide (EtBr) for 16 hrs at 1V/cm. The gel was then stained with 0.3 µg/ml EtBr in 0.5X TBE and the gel lane was excised above 1kb for the second dimension, which was run in 0.7% agarose gel made in 0.5X TBE supplemented with 0.3 µg/ml ethidium bromide for 12 hrs at 4V/ml in cold room. The gel was then used for Southern Blotting. If necessary, psoralen crosslinking was reversed by exposing the gel to 254-nm UV for 10 mins in a Stratagene UV Crosslinker.

For Southern Blotting, the gel was first incubated with HCl 0.25N with gentle shaking for 30 mins twice for depurination, followed by denaturing solution (0.5M NaOH, 1.5M NaCl) for 30 mins twice, and then neutralizing solution (0.5M Tris-HCl pH 7.5, 3M NaCl). The DNA was then transferred by capillarity overnight in SSC 20X onto a Hybond-XL membrane (Amersham). DNA was then crosslinked to the membrane with a Stratagene UV Crosslinker using 254-nm UV light. The membrane was pre-hybridized with Church buffer (see compositions above) for at least 1 h, followed by an overnight incubation with a telomere-specific probe at 65°C. After hybridization, the membrane was washed three times with wash buffer (40 mM sodium phosphate buffer pH 7.2, 1 mM EDTA pH 8, 1% SDS) for at least 30 mins per wash at 65°C, and then exposed to a phosphor screen. The screen was then scanned using a Typhoon phosphorimager (GE).

Chromatin Immunoprecipitation (ChIP)

10 x 10^6 cells were crosslinked with 1 ml of 1% methanol-dree formaldehyde (Thermo Fisher Scientific) diluted in 1X PBS for 15 mins at room temperature on a rotating wheel. Formaldehyde was quenched by adding Tris pH 8.0 to the final concentration of 200 mM, followed by 10 mins incubation on a wheel at room temperature. Cells were then collected by centrifugation and washed with ice-cold PBS three times. The sample could be stored -80°C or used immediately for ChIP.

Cells were lysed with 1 ml of lysis buffer (1% SDS, 50 mM Tris-HCl pH 8, 10 mM EDTA pH 8) supplemented with protease inhibitor cocktail (cOmplete, Roche) for 10 mins at room temperature, and then centrifuged at 3220g for 5 mins to collect chromatin sample, which was then wash with LB3 buffer (10 mM Tris pH 8.0, 200 mM NaCl, 1 mM EDTA, 0.5 mM EGTA, 0.1% Na-Deoxycholate, 0.25% sodium lauroyl sarkosinate) supplemented with protease inhibitor cocktail once and resuspended in 1 ml of LB3 buffer. The chromatin sample was then transferred to sonication vials with AFA fiber (Covaris) and fragmented using a Focused-Ultrasonicator (E220, Covaris) (10% duty factor, 140 W power, 200 cycles per burst, for 20 min) to achieve fragments between 200 – 500 bp. Sonicated chromatin was centrifuged at 21000g for 15 mins and the supernatant was collected. An amount equal to 20 µg of DNA (measured by NanoDrop Spectrophotometer) was used for one immunoprecipitation (IP) with an appropriate amount (decided based on titration) of indicated antibodies (TRF1, TRF2, POT1 and TPP1 antibodies was raised in-house, IgG control was from Santa Cruz) and 20 µl of protein G sepharose beads. The mixture was topped up to 1ml per IP with IP buffer (50 mM Tris-HCl pH 8.0, 600 mM NaCl, 10 mM EDTA pH 8.0, 0.75% Triton X-100) supplemented with protease inhibitor cocktail, and then rotated in cold room on a wheel overnight. An amount equal to 2 µg of DNA from each sample was kept as Input.

The beads were collected by cold centrifugation at 400g for 2 mins the next day, and washed in cold room for 5 mins per wash once with Wash 1 buffer (0.1% SDS, 1% Triton, 2 mM EDTA pH 8.0, 20 mM Tris pH 8.0, 300 mM NaCl), once with Wash 2 buffer (0.1 % SDS, 1% Triton, 2 mM EDTA pH 8.0, 20 mM Tris pH 8.0, 500 mM NaCl), once with Wash 3 buffer (250 mM LiCl, 1% NP-40, 1% Na-deoxycholate, 1 mM EDTA pH 8.0, 10 mM Tris pH 8.0) and once with TE buffer. Input samples and the beads were resuspended in reverse-crosslink buffer (0.1% SDS, 0.1 M sodium bicarbonate, 0.5 mM EDTA pH 8.0, 20 mM Tris pH 8.0) supplemented with 10 µg/ml DNase-free Rnase (Roche) at 65°C on a rotating wheel overnight. DNA was isolated using QIAquick PCR Purification kit (Qiagen) and eluted in 200 µl H_2O. Samples were then analyzed by dotblot.

DNA-RNA Immunoprecipitation (DRIP)

10 x 10^6 cells were resuspended in 175 µl of ice-cold RLN buffer (50 mM Tris-HCl pH 8.0, 140 mM NaCl, 1.5 mM $MgCl_2$, 0.5% NP-40, 1 mM dithiothreitol (DTT), and 100 U/ml RNasin Plus (Promega)), kept on ice for 5 mins and then centrifuged at 4°C for 2 min at 300 g. The nuclei pellet was collected, warmed up to room temperature, lysed with 500 µl RA1 buffer

(NucleoSpin RNA purification kit, Macherey-Nagel) supplemented with 1% β-mercaptoethanol, and then homogenized by passing through a 0.9 x 40 mm needle 10 times. The lysate was then loaded onto a 2 ml Phase Lock Gel heavy (5PRIME) tube, mixed with 250 µl H_2O and 750 µl phenol-chloroform-isoamylalcohol (25:24:1) (Biosolve) pre-warmed to room temperature, followed by centrifugation at room temperature at 13,000 g for 5 min. The upper phase containing nucleic acids was collected into a new eppendorf tube. Nucleic acids were precipitated by adding 750 µl of cold isopropanol and 50 mM NaCl, and incubating on ice for 30 min. Nucleic acids were then collected by centrifugation at 4°C for 30 min at 10,000 g, followed by two washes with cold 70% ethanol. After drying, nucleic acids were resuspended in 130 µl of H_2O overnight in the cold room. The nucleic acid sample was sonicated using a Focused-Ultrasonicator (E220, Covaris) (10% duty factor, 140 W power, 200 cycles per burst, for 150 s, with an AFA intensifier), to achieve 100-300 bp DNA fragments. The sample concentration was measured using a NanoDrop Spectrophotometer (Thermo Fisher Scientific). 120 µg of nucleic acids were digested with 10 U RNaseH (Roche) to be used as a negative control, or H_2O, in a total volume of 150 µl containing 1X RNaseH buffer (20 mM HEPES-KOH pH 7.5, 50 mM NaCl, 10 mM $MgCl_2$, 1 mM DTT) for 90 min at 37°C. The digestion reaction was stopped by adding 2 µl of 0.5 M EDTA pH 8.0. Samples were diluted 1:10 in DIP-1 buffer (10 mM HEPES-KOH pH 7.5, 275 mM NaCl, 0.1% Na-deoxycholate, 0.1% SDS, 1% Triton X-100) and pre-cleared with 40 µl of protein G sepharose beads (Cytiva) for 1 h, in the cold room, on a rotating wheel. 60 µg of the diluted nucleic acids was used per immunoprecipitation (IP) using 6 µg of either S9.6 antibody (Kerafast, ENH001) or mouse IgG antibody (Santa Cruz, sc-2025), and 20 µl of protein G sepharose beads (Cytiva). 0.6 µg of nucleic acids of each sample were kept as 1% input. The following day, the sepharose beads were collected by centrifugation at 400 g for 2 min at 4°C, and then washed for 5 min/wash at 4°C on a rotating wheel once with DIP-2 buffer (50 mM HEPES-KOH pH 7.5, 140 mM NaCl, 1 mM EDTA pH 8.0, 1% Triton X-100, 0.1% Na-deoxycholate), once with DIP-3 buffer (50 mM HEPES-KOH pH 7.5, 500 mM NaCl, 1 mM EDTA pH 8.0, 1% Triton-X100, 0.1% Na-deoxycholate), once with DIP-4 buffer (10 mM Tris-HCl pH 8.0, 1 mM EDTA pH 8.0, 250 mM LiCl, 1% NP-40, 1% Na-deoxycholate) and once with TE buffer (10 mM Tris–HCl pH 8.0, 1 mM EDTA pH 8.0). Input and IP samples were resuspended with 100 µl elution buffer (20 mM Tris-HCl pH 8.0, 0.1% SDS, 0.1 M $NaHCO_3$, 0.5 mM EDTA pH 8.0) supplemented with 10 µg/ml DNase-free RNase (Roche) and incubated overnight at 65°C. DNA was purified with the QIAquick PCR Purification kit (Qiagen) and eluted in 200 µl H_2O. Samples were then analyzed by qPCR or dotblot.

Dot blot analysis

A serial dilution of each input sample was performed so that the signal from IP samples lied within the dilution range. Purified DNA was denatured at 95°C for 10 mins and then kept on ice for at least 10 mins. The samples were loaded onto a Hybond-XL membrane (Amersham) using a dotblot apparatus (Bio-Rad), DNA was crosslinked to the membrane with a Stratagene UV Crosslinker using 254-nm UV light. The membrane was denatured in 0.5 M NaOH, 1.5 M

NaCl for 15 mins, followed by 10 mins of neutralization in 0.5 M Tris-Cl pH 7.0, 1.5 M NaCl with constant shaking at room temperature, and then pre-hybridized with Church buffer (0.5 M $NaHPO_4$, 1 mM EDTA, pH 8.0, 1% (w/v) BSA, 7% SDS) for at least 1 h, followed by an overnight incubation with a C-rich telomere-specific probe at 65°C. After hybridization, the membrane was washed three times with wash buffer (1X SSC + 0.1% SDS) for at least 30 mins per wash at 65°C, and then exposed to a phosphor screen. The screen was then scanned using a Typhoon phosphorimager (GE). Dotblot signal was quantified using AIDA software.

qPCR (quantitative Polymerase Chain Reaction) analysis of DRIP samples

Each qPCR reaction contained 1 µl of purified DNA from either IP or diluted input samples, 1 µM forward and reverse primers (Supplementary table 2), 5 µl Power SYBR Green PCR Master Mix (Thermo Fisher Scientific) and H_2O up to a total volume of 10 µl. Each reaction was run in technical triplicate in a 384-well reaction plate. qPCR reactions were carried at 95°C for 10 min, followed by 40 cycles of 95°C for 15 s, and annealing and extension at 60°C for 1 min, using a QuantStudio 7 Flex Real-Time PCR system (Thermo Fisher Scientific). Melting curve analysis was also included. Input samples were diluted in a serial dilution, and then used as standard curves to calculate the corresponding percentage of input of IgG and S9.6 IP samples.

TERRA RT-qPCR (quantitative reverse transcription polymerase chain reaction)

RNA was isolated using the NucleoSpin RNA Isolation kit (Macherey-Nagel) according to the manufacturer's protocol. Three DNase treatments – two on-column and one in-solution – were performed.

The reverse transcription (RT) reaction was performed in 200 µl PCR tubes. All reactions were prepared on ice unless specified otherwise. A 13 µl reaction containing 1 µl TERRA-specific oligo at 1 µM (5'-CCCTAACCCTAACCCTAACCCTAACCCTAA-3'), 1 µl GAPDH specific oligo at 1 µM (5'-GCCCAATACGACCAAATCC-3'), 1 µl dNTP mix at 10 mM (each dNTP) and 3 µg of total RNA was incubated in a PCR thermocycler at 65 °C for 5 min and immediately transferred on ice to denature TERRA. For extension reaction, the following was prepared in a master mix and added into the denatured TERRA mix: 4 µl of 5X First Strand Synthesis Buffer (Invitrogen), 1 µl of 0.1M DTT, 1 µl of RNasein (Promega) and 1 µl of SuperScript III reverse transcriptase (Invitrogen). H_2O was used instead of SuperScript III, as a negative control. Reverse transcription was then carried in a thermocycler at 55°C for 60 min, followed by enzyme inactivation at 70°C for 15 min. The cDNA was diluted to a final volume of 40 µl.

Each qPCR reaction contained 2 µl of cDNA from RT reaction, 1 µM forward and reverse primers (Supplementary table 3), 5 µl Power SYBR Green PCR Master Mix (Thermo Fisher Scientific) and H_2O up to a total volume of 10 µl. Each reaction was run in technical triplicate in a 384-well reaction plate. qPCR reactions were carried at 95°C for 10 min, followed by 40 cycles of 95°C for 15 sec, and annealing and extension at 60°C for 1 min, using a QuantStudio 7 Flex Real-Time PCR system (Thermo Fisher Scientific). Melting curve analysis was also included. Relative expression levels were analyzed by normalization to GAPDH housekeeping gene and compared to the RT negative control samples.

Telomeric DNA enrichment

Around 500 x 10^6 cells were used for each enrichment. For psoralen crosslinking, the cell suspended in 1X cold PBS was poured into a 10-cm dish, which was kept on ice while stirring for the whole crosslinking procedure. The cells were first treated with 30 µg/ml trioxsalen (Sigma) for 5 mins in the dark and then irradiated for 8 mins with 365-nm UV light using a Stratagene UV Crosslinker. The trioxsalen incubation and UV irradiation steps were repeated three more times.

Genomic DNA was then extracted and telomeric DNA was enriched following a published protocol with some modifications (Mazzucco et al., 2022). Typically, nuclei were extracted by incubating the cells with ice-cold RLN buffer for 5 mins followed by a cold centrifugation at 300g for 2 mins to eliminate cytoplastic RNA. The nuclei were then lysed with 40 ml of TNES buffer (10 mM Tris-HCl pH 8.0, 100 mM NaCl, 10 mM EDTA, 0.5% SDS) supplemented with 100 µg/ml proteinase K (Roche) overnight at 37°C. The sample was then mixed with 1 volume of PCI (Biosolve) pre-warmed to room temperature on a rotating wheel for 10 mins, and then centrifuged for 5 mins at 3220g. Then, the top layer was transferred to a new tube and 1 volume of chloroform was added. The tube was again mixed in a wheel for 10 mins and centrifuged for 5 mins at 3220g. The top layer was collected, DNA was precipitated with 1 volumes of Isopropanol and 1/10 volume of Sodium Acetate (3M, pH 5.3). The DNA was collected by cold centrifugation at 3220g for 30 mins, and then washed with 70% Ethanol. After letting the DNA dry for a few minutes, the DNA was dissolved in 200 µl of 10 mM Tris-HCl pH 8 overnight at 4°C. DNA concentration was measured using Qubit Broad Range assay kit (Invitrogen) following the manufacturer's instructions.

2 mg of genomic DNA was digested with HinfI and MspI (500 U each, NEB) in a 20-ml reaction containing 1X CutSmart buffer (NEB) overnight at 37°C. The next day, 250U of each enzyme was added and the reaction was kept for another 2 hours at 37°C. The digested DNA was then precipitated with Isopropanol and Sodium Acetate and resuspended in TE buffer as described above, and then loaded onto a sucrose gradient (10% - 20% - 30%, 8 ml each fraction) and centrifuged in SW32-Ti rotor (Beckman) at 30100 rpm at 4°C 16 hrs. Different volumes (fractions) are separately collected. The high molecular weight (HMW) fraction containing telomeric DNA was concentrated and the buffer was exchanged into TE buffer using Amicon Ultra-15 30kDa MWCO (Millipore). DNA concentration was measured by Qubit Broad Range assay kit (Invitrogen) following the manufacturer's instructions. The DNA was then diluted to 100 µg/ml with 1X CutSmart buffer (NEB) and digested with RsaI, AluI, MboI, HinfI and MspI (50U each, NEB) overnight at 37°C. The next day, 25U of each enzyme was added and the reaction was kept for another 2 hours at 37°C. The digested DNA was then cleaned up with PCI and chloroform, precipitated with Isopropanol and Sodium Acetate as described above, resuspended in 50 µl of TE buffer and then separated in a 0.7% low-melting agarose gel (Lonza) TAE 1X without EtBr at low voltage the minimum time necessary. Fragments migrating above the 1-kb ladder band were extracted from agarose slice using Silica Bead DNA gel extraction kit (Thermo Fisher Scientific) following the manufacturer's instructions except that the beads

were not pipetted once DNA was bound to avoid DNA shearing. The DNA was eluted using TE buffer and quantified using Qubit High Sensitivity assay kit (Invitrogen).

Electron Microscopy (EM) sample preparation and analysis

EM sample preparation and analysis was performed by Dr. Giulia Mazzucco (IFOM) following previously described protocols (Lopes, 2009; Mazzucco et al., 2020).

Telomere-enriched DNA was first spread in the presence of benzalkonium chloride (BAC) using water as hypophase. Formamide was used as a partially denaturing reagent to disentangle DNA molecules. In short, 5 µl of DNA solution corresponding to 5 – 20 ng of telomere-enriched DNA were mixed with 5 µl of formamide (Thermo Scientific) and 0.4 µl of 0.02% BAC (Sigma). After mixing, the drop was spread on a water surface in a 15-cm dish containing 50 ml of distilled water using a freshly-cleaved mica sheet as a ramp. The monomolecular DNA film was then gently touched with carbon-coated EtBr-treated EM grids. The grids with absorbed DNA were immediately stained with 0.2 µg/µl uranyl acetate, washed in EtOH 100% and subjected to platinum rotary shadowing. The detailed procedures of EM grid preparation and platinum rotary shadowing were described in Lopes, 2009. Images were taken using FEI Tecnai12 BioTwin Transmission Electron Microscope using the same setting as in Huda et al., 2023 and Mazzucco et al., 2020.

The analyzed images were obtained in large area acquiring overlapping fields and then stitching them using the digital micrograph software. Images in .dm3 format were analyzed in ImageJ using an ImageJ macro for annotation and storage (as in Mazzucco et al., 2020). The analysis consisted in the annotation of the number of molecules containing i-loops among all the molecules present in the acquired area. The ratio between i-loops containing molecules over all the acquired molecules for each sample was reported and compared between the untreated and menadione-treated samples.

Subcellular fractionation

Subcellular fractionation was performed using Subcellular Protein Fractionation Kit for Cultured Cells (Thermo Fisher Scientific) according to the manufacturer's protocol with some minor modifications. Typically, 10 x 10^6 cells equivalent to 50 µl packed cell volume were incubated with 500 µl of cold CEB containing protease inhibitors for 30 mins in cold room with gentle mixing. The sample was then centrifuged at 500g for 5 minutes, the supernatant was collected as cytoplasmic extract. The pellet was then resuspended with 500 µl of ice-cold MEB containing protease inhibitors, vortexed for 5 secs and incubated at 4°C for 10 mins with gentle mixing, followed by centrifugation at 3000g for 5 mins. The supernatant was collected as membrane extract. Then, 250 µl of ice-cold NEB containing protease inhibitors was added to the pellet, which was then mixed, vortexed for 15 secs and and incubated at 4°C for 30 mins. The sample was then centrifuged at 5000g for 5 mins. The supernatant was collected as nucleoplasmic extract. The pellet was then resuspended in 250 µl of room temperature NEB containing protease inhibitors, $CaCl_2$, micrococcal nuclease, $MgCl_2$ and benzonase endonuclease, homogenized by passing through 0.9 x 40 mm needle 10 times, vortexed for

15 secs and incubated at 37°C for 30 mins. The sample was again vortexed for 15 secs and centrifuge at 16000g for 5 mins, the supernatant was collected as chromatin-bound extract. Finally, the pellet was dissolved in 250 µl of room temperature PEB containing protease inhibitors, vortexed for 15 secs and incubated at room temperature for 30 mins, followed by centrifugation at 16000g for 5 mins. The supernatant was collected as pellet extract. The fractionation efficiency was assessed by western blot based on the presence of subcellular fraction specific markers. We used HSP90 as a marker for cytoplasmic extract, SP1 as a marker for nucleoplasmic extract, Histone H3 as a marker for chromatin-bound extract, and hnRNPA1 as a marker present in both nucleoplasmic and chromatin-bound fractions.

FLAG Immunoprecipitation

Whole cell lysate, nucleoplasmic, chromatin-bound and pellet extracts were used for FLAG Immunoprecipitation (IP). For whole cell lysate sample, 2 x 10^6 cells were lysed with 200 µl of RIPA buffer (50 mM Tris-HCl pH 8.0, 1% NP-40, 0.5% Na-deoxycholate, 0.1% SDS, 150 mM NaCl) supplemented with protease inhibitor cocktail (cOmplete, Roche), 250 U/ml benzonase and 2 mM $MgCl_2$. Chromatin-bound fraction was diluted 1:1 while pellet extract was diluted 1:10 with IP buffer (50 mM Tris HCl, pH 7.4, 150 mM NaCl, 1 mM EDTA, 1% Triton X-100) to reduce the detergent content. 100 µg of protein measured by BCA assay (Thermo Fisher Scientific) from each sample was used per IP. The samples were incubated overnight in cold room with either 40 µl of 50% slurry beads of anti-FLAG M2 Affinity Agarose gel (Sigma) or protein G sepharose beads and mouse IgG control. After 5 washes with IP buffer for 5 mins per wash, precipitated protein was eluted 5 rounds with 40 µl of 100 µg/ml of FLAG peptide in IP buffer at room temperature with constant shaking. The precipitation efficiency was assessed by western blot using anti-FLAG antibody (Supplementary table 1)

Western blotting

0.5 x 10^6 cells were lysed with 50 µl of RIPA buffer (50 mM Tris-HCl pH 8.0, 1% NP-40, 0.5% Na-deoxycholate, 0.1% SDS, 150 mM NaCl) supplemented with 250 U/ml benzonase and 2 mM $MgCl_2$, and then diluted 1:1 with 2X Laemmli buffer. The sample was then boiled at 95°C for 10 mins, followed by separation on a 4 – 15% SDS-PAGE precast gel (Mini-PROTEAN TGX Gels, Bio-Rad). The proteins were then transferred onto 0.2 µm nitrocellulose membrane (Amersham) at 100V for 90 mins or 30V for 16 hrs. The membrane was then blocked with blocking solution (5% BSA (w/v) in 1X PBST (1X PBS + 0.1% Tween-20)) for at least 1 hr, followed by overnight incubation in cold room with primary antibodies against proteins of interest diluted in blocking solution. The membrane was then washed 3 times with PBST for 5 min per wash, and incubated with Horseradish Peroxidase-conjugated secondary antibodies (Supplementary table 1) diluted in blocking solution for 1 hr at room temperature. The membrane was again washed 3 times with PBST for 5 min per wash, and developed using ChemiGlow Chemiluminescence Substrate (Bio Techne). The signal was detected by Fusion FX imaging system (Vilber).

Live-cell Imaging

Hela cells containing endogenously Halo-tagged TRF1 were seeded at a density of 0.3 x 10^6 cells in 2 ml medium in a glass-bottom 35-mm dish two days before. At the day of imaging, complete DMEM and Fluorobrite medium supplemented with 10% fetal bovine serum (FBS) was pre-warmed at 37°C. Labelling medium was prepared by diluting JF-646 HaloTag Ligand in complete DMEM to a final concentration of 0.2 µM. The cells were then incubated with labelling medium for 15 mins in the 37°C incubator, followed by washing once with complete DMEM and twice with Fluorobrite medium. The cells were then placed back in the incubator for at least 15 minutes with Fluorobrite medium with before being transferred to the microscope. Hoechst 33342 (Thermo Fisher Scientific) was added to the final concentration of 5 µg/ml to stain nuclei.

Live imaging was done using Visitron Spinning Disk CSU W1 confocal microscope. The cells were placed in a 37°C chamber with CO_2 supply for the entire imaging process. JF-646 was excited with 640-nm laser (10%, 1s exposure time) while 405-nm laser was used to excite Hoechst 33342 (10%, 100ms exposure time). Pinhole diameter was set at 50 µm. 100X EMCCD camera was used to capture images in Z-stack (20 stacks, 0.3 µm step). For both untreated and menadione-treated samples, the imaging process was automated and images were captured at timepoints 0, 30 mins, 1 hr and 2 hrs. ImageJ was then used for image processing.

Two-step quantitative telomeric chromatin isolation protocol (QTIP)

Telomeric chromatin immunoprecipitation was performed as previously described (Glousker et al., 2020) with slight modifications. 4 x 10^9 cells per condition were harvested, washed twice with cold 1X PBS and crosslinked in 400 ml of 1% formaldehyde and 2 mM EGS for 15 mins at 25°C, which was quenched with 0.2M Tris-HCl pH 8.0 for 10 mins at 25°C. The cells were then lysed with lysis buffer (50 mM Tris-HCl pH 8.0, 1 mM EDTA, 1% SDS) supplemented with protease inhibitor cocktail (cOmplete, Roche) at 10 x 10^6 cells/ml on a rotating wheel for 10 minutes at 25°C. Pellets enriched with chromatin were collected by centrifugation at 4°C for 5 mins at 3220g, washed twice and resuspended at 20 x 10^6 cells/ml with LB3 buffer (10 mM Tris pH 8.0, 200 mM NaCl, 1 mM EDTA, 0.5 mM EGTA, 0.1% Na-Deoxycholate, 0.25% sodium lauroyl sarkosinate) supplemented with cOmplete (Roche). The lysate was aliquoted into 8 50-ml tubes with 25 ml per tube, and then sonicated using a Branson tip sonicator (30% power, 10 secs constant pulse, 20 secs pause for a total sonication time of 20 mins). The sonicated sample was dialyzed against IP buffer (50 mM Tris-HCl pH 8.0, 600 mM NaCl, 10 mM EDTA pH 8.0, 0.75% Triton X-100).

Precipitation procedure was performed at 4°C unless stated otherwise. The first precipitation was done overnight using 1.5 ml of 50% slurry beads of either anti-FLAG M2 Affinity Agarose gel (Sigma) or protein G sepharose beads (Cytiva) crosslinked to mouse IgG. Before precipitation, the beads were blocked with 1 mg/ml yeast tRNA for 1 hr. After being washed 5 x 5 mins with IP buffer, precipitated chromatin was eluted with 100 µg/ml FLAG peptide 5 times, 30 mins each with constant shaking at room temperature. For the second precipitation,

the eluate from FLAG IP was incubated overnight on a rotating wheel with protein G sepharose beads (Cytiva) crosslinked to home-made antibodies against TRF1 and TRF2 overnight, while the one from mouse IgG IP was used for precipitation using sheep IgG beads. 2 ml of 50% slurry beads was again blocked with yeast tRNA and used per IP. The beads were then washed for 5 mins per wash with Wash 1 buffer (0.1% SDS, 1% Triton, 2 mM EDTA pH 8.0, 20 mM Tris pH 8.0, 300 mM NaCl), Wash 2 buffer (0.1 % SDS, 1% Triton, 2 mM EDTA pH 8.0, 20 mM Tris pH 8.0, 500 mM NaCl), Wash 3 buffer (250 mM LiCl, 1% NP-40, 1% Na-deoxycholate, 1 mM EDTA pH 8.0, 10 mM Tris pH 8.0) and TE buffer (10 mM Tris-HCl pH 8.0, 1 mM EDTA pH 8.0). Elution was performed 5 x 15 mins at 37°C with constant shaking using 2.5 bed bead volume of 0.25 M ammonium hydroxide.

The eluate was then concentrated using Amicon Ultra-15 Centrifugal Filter Units 10kDa MWCO (Millipore), and dialyzed against 0.1M Tris-HCl pH 8 using Slide-A-Lyzer™ G2 Dialysis Cassettes, 2K MWCO, 0.5 mL (Thermo Fisher Scientific) at 4°C. Finally, the sample was heated at 65°C overnight for reverse-crosslinking and then treated with Benzonase (250U, Millipore) for 1 hr at 37°C. 2mM $MgCl_2$ was added to facilitate Benzonase activity.

Mass Spectrometry (MS) sample preparation and analysis

Sample processing was performed by Protein Analysis Facility – University of Lausanne. After processing, samples were sent to Proteomics Core Facility – École polytechnique fédérale de Lausanne for LC-MS/MS analysis. Data analysis was performed by Protein Analysis Facility – University of Lausanne.

Protein Digestion

QTIP samples submitted in 150 µl of 0.1 M Tris-HCl pH 8.0 were adjusted to 1% sodium deoxycholate and 10 mM DTT, and then heated at 95°C for 30 mins to denature proteins. Alkylation of reduced cysteines was done by adding ¼ volume of 160 mM chloroacetamide and incubating the samples at room temperature for 45 mins in the dark. EDTA was added to a final concentration of 3 mM. Digestion was performed for 1 hr at 37°C with 1 µg of Trypsin/LysC mix (Promega) followed by a second overnight digestion with the same protease mixture. The digested samples were phase extracted to remove sodium deoxycholate by adding 600 µl of 1% TFA in ethyl acetate, vortex for 2 mins and then centrifugation. The bottom phase containing peptides was collected, diluted 2X with 0.5% formic acid and desalted on strong cation exchange (SCX) cartridges (Thermo Fisher Scientific). The cartridges were washed with 0.5% formic acid and 20% acetonitrile (MeCH), and peptides were eluted in 200 µl of 80% MeCH and 1% ammonia. 10% aliquot of each sample was analyzed label-free by LC-MS for quality control and for estimation of total peptide amount.

TMT labeling

Desalted samples were dried, resuspended in 100 µl water, and dried again to remove excess ammonia. All samples were then resuspended in 15 µl of 50 mM HEPES buffer pH 8.0. Due to the limitation in the number of TMT-plex, the number of samples was reduced by pooling

equally IgG samples of the same condition from 4 replicates before labelling to the final volume of 15 µl. The samples were reacted with 0.4 mg of TMT reagent for 2 hrs at room temperature. Excess reagent was quenched with 4 µl of 5% hydroxylamine for 15 mins. An aliquot from each labelling was analyzed by LC-MS for labelling efficiency control. TMT multiplex samples were then mixed, dried and desalted with SepPak C18 96-well plate (Waters Corps.) to be ready for LC-MS/MS run. There were 2 runs in total. For each run, pooled IgG controls were mixed with QTIP samples from 2 replicates.

Peptide Fractionation

Dried TMT mixes were resuspended in 4M urea containing 0.1% ampholytes pH 3.0 – 10 (GE Healthcare) and fractionated in to 24 fractions by off-gel focusing as previously described (Geiser et al., 2011). The peptide fractions were then desalted on SepPak microC18 96-well plate (Waters Corp.), dried and dissolved in 30 µl of 2% acetonitrile and 0.05% trifluoracetic acid for LC-MS/MS analysis.

MS analysis

The data-dependent LC-MS/MS analysis was carried out on a Orbitrap Exploris mass spectrometer (Thermo Fisher Scientific) interfaced through a nano-electrospray ion source to an Ultimate 3000 RSLC nano UPLC system (Thermo Fisher Scientific). Peptides were separated on a 50-cm long capillary column (75 µm ID, 100 Å, Reprosil Pur 1.9 µm silica beads, Dr. Maisch) over a biphasic gradient at 250 nl/min for a total time of 150 mins. MS^1 acquisitions were performed at a resolution of 240000. Peptides were then fragmented by higher energy collision dissociation (HCD) with collision energy value of 30%. Fragmented ion scans for MS^2 were acquired in the ion trap at low resolution using a maximum injection time of 20 ms.

Raw data processing

Data was analyzed with MaxQuant 1.6.3.4 incorporating with Andromeda search engine (Cox et al., 2011; Cox and Mann, 2008). TMT labeling and cysteine carbamidomethylation were set as fixed modifications while oxidation (M) and acetylation (protein N-term) were selected as variable modifications. Protein identifications were performed against the UniProt human proteome database, version of October 29th, 2017 (2017_10, www.uniprot.org) containing 71803 sequences. The database was completed with sequences of most usual contaminants, benzonase endonuclease, mouse and sheep immunoglobulins. Mass tolerance was 4.5 ppm on precursors (after recalibration) and 20 ppm on HCD fragments. 1% FDR filter was applied for both peptide and protein identifications. For unlabelled samples, iBAQ values generated by MaxQuant in label-free quantitation were used (Schwanhäusser et al., 2011). For TMT analysis, the raw reporter ion intensities generated by MaxQuant and summed for each protein group were used in all following steps of quantitation. Only identified peptide ions with a precursor intensity fraction (PIF parameter) greater than 0.75 were accepted and used for TMT quantitation.

Data clean-up, normalization and statistic tests

The MaxQuant output table “proteinGroups.txt” for the four TMT replicates was processed to first remove proteins matched to the contaminants database as well as proteins identified only by modified peptides and reverse database hits, giving a first unfiltered list of 3280 identified proteins. All intensity values were then log-2 transformed. Signal intensities of internal "standard" proteins trypsin and benzonase were relatively flat, indicating that there was no systematic loss of sample during preparation. Thus, no technical compensation of intensities was applied. The table was next filtered to keep only proteins with minimum of two “razor or unique” peptides. A t-test (p-value filter at 0.05) was performed to compare the the signal intensities of proteins identified in TERF1/2 IPs vs pooled IgG controls to identify proteins significantly enriched in IP samples. 1554 proteins passed the t-test.

Due to TRF1 and TRF2 dissociation from damaged telomeres, the menadione-treated sample had lower precipitation efficiency than the untreated. Thus, normalization was required before performing statistic test between two conditions. Compensation factors for normalization was calculated for each replicate based on the average of TRF1 and TRF2 intensities. The factors were then applied to bring intensity of TRF1 and TRF2 proteins in the menadione-treated sample relatively equal to the values of the untreated one. After normalization, to determine proteins changing between the untreated and menadione-treated conditions, we applied a paired T-test with Benjamini-Hochberg FDR correction (Benjamini and Hochberg, 1995) and threshold of adjusted p-value at 0.05. 1651 proteins passed the t-test.

References

Abreu, E., Aritonovska, E., Reichenbach, P., Cristofari, G., Culp, B., Terns, R.M., Lingner, J., Terns, M.P., 2010. TIN2-Tethered TPP1 Recruits Human Telomerase to Telomeres In Vivo. Mol. Cell. Biol. 30, 2971–2982. https://doi.org/10.1128/MCB.00240-10

Aeby, E., Ahmed, W., Redon, S., Simanis, V., Lingner, J., 2016. Peroxiredoxin 1 Protects Telomeres from Oxidative Damage and Preserves Telomeric DNA for Extension by Telomerase. Cell Rep. 17, 3107–3114. https://doi.org/10.1016/j.celrep.2016.11.071

Ahmed, W., Lingner, J., 2020. PRDX1 Counteracts Catastrophic Telomeric Cleavage Events That Are Triggered by DNA Repair Activities Post Oxidative Damage. Cell Rep. 33, 108347. https://doi.org/10.1016/j.celrep.2020.108347

Ahmed, W., Lingner, J., 2018. PRDX1 and MTH1 cooperate to prevent ROS-mediated inhibition of telomerase. Genes Dev. 32, 658–669. https://doi.org/10.1101/gad.313460.118

Andrs, M., Stoy, H., Boleslavska, B., Chappidi, N., Kanagaraj, R., Nascakova, Z., Menon, S., Rao, S., Oravetzova, A., Dobrovolna, J., Surendranath, K., Lopes, M., Janscak, P., 2023. Excessive reactive oxygen species induce transcription-dependent replication stress. Nat. Commun. 14, 1791. https://doi.org/10.1038/s41467-023-37341-y

Ariel, F., Lucero, L., Christ, A., Mammarella, M.F., Jegu, T., Veluchamy, A., Mariappan, K., Latrasse, D., Blein, T., Liu, C., Benhamed, M., Crespi, M., 2020. R-Loop Mediated trans Action of the APOLO Long Noncoding RNA. Mol. Cell 77, 1055-1065.e4. https://doi.org/10.1016/j.molcel.2019.12.015

Arnoult, N., Karlseder, J., 2015. Complex interactions between the DNA-damage response and mammalian telomeres. Nat. Struct. Amp Mol. Biol. 22, 859.

Arnoult, N., Van Beneden, A., Decottignies, A., 2012. Telomere length regulates TERRA levels through increased trimethylation of telomeric H3K9 and HP1α. Nat. Struct. Mol. Biol. 19, 948–956. https://doi.org/10.1038/nsmb.2364

Arora, R., Lee, Y., Wischnewski, H., Brun, C.M., Schwarz, T., Azzalin, C.M., 2014. RNaseH1 regulates TERRA-telomeric DNA hybrids and telomere maintenance in ALT tumour cells. Nat. Commun. 5, 5220. https://doi.org/10.1038/ncomms6220

Azzalin, C.M., Reichenbach, P., Khoriauli, L., Giulotto, E., Lingner, J., 2007. Telomeric Repeat–Containing RNA and RNA Surveillance Factors at Mammalian Chromosome Ends. Science 318, 798. https://doi.org/10.1126/science.1147182

Balk, B., Maicher, A., Dees, M., Klermund, J., Luke-Glaser, S., Bender, K., Luke, B., 2013. Telomeric RNA-DNA hybrids affect telomere-length dynamics and senescence. Nat. Struct. Mol. Biol. 20, 1199–1205. https://doi.org/10.1038/nsmb.2662

Bandyopadhyay, U., Das, D., Banerjee, R.K., 1999. Reactive oxygen species: Oxidative damage and pathogenesis. Curr. Sci. 77, 658–666.

Banin, S., Moyal, L., Shieh, S.-Y., Taya, Y., Anderson, C.W., Chessa, L., Smorodinsky, N.I., Prives, C., Reiss, Y., Shiloh, Y., Ziv, Y., 1998. Enhanced Phosphorylation of p53 by ATM in Response to DNA Damage. Science 281, 1674–1677. https://doi.org/10.1126/science.281.5383.1674

Barbara, M., 1941. The stability of broken ends of chromosomes in Zea Mays. Genetics 26, 234–282. https://doi.org/10.1093/genetics/26.2.234

Barbara, M., 1939. The Behavior in Successive Nuclear Divisions of a Chromosome Broken at Meiosis. Proc. Natl. Acad. Sci. 25, 405–416. https://doi.org/10.1073/pnas.25.8.405

Barnes, R.P., de Rosa, M., Thosar, S.A., Detwiler, A.C., Roginskaya, V., Van Houten, B., Bruchez, M.P., Stewart-Ornstein, J., Opresko, P.L., 2022. Telomeric 8-oxo-guanine drives rapid premature senescence in the absence of telomere shortening. Nat. Struct. Mol. Biol. 29, 639–652. https://doi.org/10.1038/s41594-022-00790-y

Barzilai, A., Yamamoto, K.-I., 2004. DNA damage responses to oxidative stress. BRIDGE BROKEN ENDS - Cell. Response DNA Breaks Health Dis. 3, 1109–1115. https://doi.org/10.1016/j.dnarep.2004.03.002

Baumann, P., Cech, T.R., 2001. Pot1, the Putative Telomere End-Binding Protein in Fission Yeast and Humans. Science 292, 1171. https://doi.org/10.1126/science.1060036

Baur, J.A., Zou, Y., Shay, J.W., Wright, W.E., 2001. Telomere Position Effect in Human Cells. Science 292, 2075–2077. https://doi.org/10.1126/science.1062329

Beard, W.A., Batra, V.K., Wilson, S.H., 2010. DNA polymerase structure-based insight on the mutagenic properties of 8-oxoguanine. Nucleotide Pool Damage Its Biol. Consequences 703, 18–23. https://doi.org/10.1016/j.mrgentox.2010.07.013

Benjamini, Y., Hochberg, Y., 1995. Controlling the False Discovery Rate: A Practical and Powerful Approach to Multiple Testing. J. R. Stat. Soc. Ser. B Methodol. 57, 289–300.

Bermejo, R., Lai, M.S., Foiani, M., 2012. Preventing Replication Stress to Maintain Genome Stability: Resolving Conflicts between Replication and Transcription. Mol. Cell 45, 710–718. https://doi.org/10.1016/j.molcel.2012.03.001

Bilaud, T., Brun, C., Ancelin, K., Koering, C.E., Laroche, T., Gilson, E., 1997. Telomeric localization of TRF2, a novel human telobox protein. Nat. Genet. 17, 236–239. https://doi.org/10.1038/ng1097-236

Blasco, M.A., 2007. The epigenetic regulation of mammalian telomeres. Nat. Rev. Genet. 8, 299–309. https://doi.org/10.1038/nrg2047

Boguslawski, S.J., Smith, D.E., Michalak, M.A., Mickelson, K.E., Yehle, C.O., Patterson, W.L., Carrico, R.J., 1986. Characterization of monoclonal antibody to DNA · RNA and its application to immunodetection of hybrids. J. Immunol. Methods 89, 123–130. https://doi.org/10.1016/0022-1759(86)90040-2

Borah, S., Xi, L., Zaug, A.J., Powell, N.M., Dancik, G.M., Cohen, S.B., Costello, J.C., Theodorescu, D., Cech, T.R., 2015. TERT promoter mutations and telomerase reactivation in urothelial cancer. Science 347, 1006. https://doi.org/10.1126/science.1260200

Bouvard, V., Baan, R., Straif, K., Grosse, Y., Secretan, B., Ghissassi, F.E., Benbrahim-Tallaa, L., Guha, N., Freeman, C., Galichet, L., Cogliano, V., 2009. A review of human carcinogens—Part B: biological agents. Lancet Oncol. 10, 321–322. https://doi.org/10.1016/S1470-2045(09)70096-8

Broccoli, D., Smogorzewska, A., Chong, L., de Lange, T., 1997. Human telomeres contain two distinct Myb–related proteins, TRF1 and TRF2. Nat. Genet. 17, 231–235. https://doi.org/10.1038/ng1097-231

Bryan, T.M., Cech, T.R., 1999. Telomerase and the maintenance of chromosome ends. Curr. Opin. Cell Biol. 11, 318–324. https://doi.org/10.1016/S0955-0674(99)80043-X

Bryan, T.M., Englezou, A., Gupta, J., Bacchetti, S., Reddel, R.R., 1995. Telomere elongation in immortal human cells without detectable telomerase activity. EMBO J. 14, 4240–4248. https://doi.org/10.1002/j.1460-2075.1995.tb00098.x

Burma, S., Chen, B.P., Murphy, M., Kurimasa, A., Chen, D.J., 2001. ATM Phosphorylates Histone H2AX in Response to DNA Double-strand Breaks*. J. Biol. Chem. 276, 42462–42467. https://doi.org/10.1074/jbc.C100466200

Caldecott, K.W., McKeown, C.K., Tucker, J.D., Ljungquist, S., Thompson, L.H., 1994. An interaction between the mammalian DNA repair protein XRCC1 and DNA ligase III. Mol. Cell. Biol. 14, 68–76. https://doi.org/10.1128/mcb.14.1.68-76.1994

Ceccaldi, R., Rondinelli, B., D'Andrea, A.D., 2016. Repair Pathway Choices and Consequences at the Double-Strand Break. Spec. Issue Qual. Control 26, 52–64. https://doi.org/10.1016/j.tcb.2015.07.009

Celli, G.B., de Lange, T., 2005. DNA processing is not required for ATM-mediated telomere damage response after TRF2 deletion. Nat. Cell Biol. 7, 712–718. https://doi.org/10.1038/ncb1275

Cerritelli, S.M., Crouch, R.J., 2009. Ribonuclease H: the enzymes in eukaryotes. FEBS J. 276, 1494–1505. https://doi.org/10.1111/j.1742-4658.2009.06908.x

Cesare, A.J., Kaul, Z., Cohen, S.B., Napier, C.E., Pickett, H.A., Neumann, A.A., Reddel, R.R., 2009. Spontaneous occurrence of telomeric DNA damage response in the absence of chromosome fusions. Nat. Struct. Amp Mol. Biol. 16, 1244.

Chapman, J.R., Barral, P., Vannier, J.-B., Borel, V., Steger, M., Tomas-Loba, A., Sartori, A.A., Adams, I.R., Batista, F.D., Boulton, S.J., 2013. RIF1 Is Essential for 53BP1-Dependent Nonhomologous End Joining and Suppression of DNA Double-Strand Break Resection. Mol. Cell 49, 858–871. https://doi.org/10.1016/j.molcel.2013.01.002

Chawla, R., Redon, S., Raftopoulou, C., Wischnewski, H., Gagos, S., Azzalin, C.M., 2011. Human UPF1 interacts with TPP1 and telomerase and sustains telomere leading-strand replication. EMBO J. 30, 4047–4058. https://doi.org/10.1038/emboj.2011.280

Chedin, F., Benham, C.J., 2020. Emerging roles for R-loop structures in the management of topological stress. J. Biol. Chem. 295, 4684–4695. https://doi.org/10.1074/jbc.REV119.006364

Chen, L., Zhang, C., Ma, W., Huang, J., Zhao, Y., Liu, H., 2022. METTL3-mediated m6A modification stabilizes TERRA and maintains telomere stability. Nucleic Acids Res. 50, 11619–11634. https://doi.org/10.1093/nar/gkac1027

Chong, L., van Steensel, B., Broccoli, D., Erdjument-Bromage, H., Hanish, J., Tempst, P., de Lange, T., 1995. A Human Telomeric Protein. Science 270, 1663–1667. https://doi.org/10.1126/science.270.5242.1663

Cohen, S., Puget, N., Lin, Y.-L., Clouaire, T., Aguirrebengoa, M., Rocher, V., Pasero, P., Canitrot, Y., Legube, G., 2018. Senataxin resolves RNA:DNA hybrids forming at DNA double-strand breaks to prevent translocations. Nat. Commun. 9, 533. https://doi.org/10.1038/s41467-018-02894-w

Colussi, C., Parlanti, E., Degan, P., Aquilina, G., Barnes, D., Macpherson, P., Karran, P., Crescenzi, M., Dogliotti, E., Bignami, M., 2002. The Mammalian Mismatch Repair Pathway Removes DNA 8-oxodGMP Incorporated from the Oxidized dNTP Pool. Curr. Biol. 12, 912–918. https://doi.org/10.1016/S0960-9822(02)00863-1

Coluzzi, E., Colamartino, M., Cozzi, R., Leone, S., Meneghini, C., O'Callaghan, N., Sgura, A., 2014. Oxidative Stress Induces Persistent Telomeric DNA Damage Responsible for Nuclear Morphology Change in Mammalian Cells. PLOS ONE 9, e110963. https://doi.org/10.1371/journal.pone.0110963

Cong, Wright Woodring E., Shay Jerry W., 2002. Human Telomerase and Its Regulation. Microbiol. Mol. Biol. Rev. 66, 407–425. https://doi.org/10.1128/mmbr.66.3.407-425.2002

Cox, J., Mann, M., 2008. MaxQuant enables high peptide identification rates, individualized p.p.b.-range mass accuracies and proteome-wide protein quantification. Nat. Biotechnol. 26, 1367–1372. https://doi.org/10.1038/nbt.1511

Cox, J., Neuhauser, N., Michalski, A., Scheltema, R.A., Olsen, J.V., Mann, M., 2011. Andromeda: A Peptide Search Engine Integrated into the MaxQuant Environment. J. Proteome Res. 10, 1794–1805. https://doi.org/10.1021/pr101065j

Crossley, M.P., Bocek, M., Cimprich, K.A., 2019. R-Loops as Cellular Regulators and Genomic Threats. Mol. Cell 73, 398–411. https://doi.org/10.1016/j.molcel.2019.01.024

Dai, X., Huang, C., Bhusari, A., Sampathi, S., Schubert, K., Chai, W., 2010. Molecular steps of G-overhang generation at human telomeres and its function in chromosome end protection. EMBO J. 29, 2788–2801. https://doi.org/10.1038/emboj.2010.156

D'Alessandro, G., Whelan, D.R., Howard, S.M., Vitelli, V., Renaudin, X., Adamowicz, M., Iannelli, F., Jones-Weinert, C.W., Lee, M., Matti, V., Lee, W.T.C., Morten, M.J., Venkitaraman, A.R., Cejka, P., Rothenberg, E., d'Adda di Fagagna, F., 2018. BRCA2 controls DNA:RNA hybrid level at DSBs by mediating RNase H2 recruitment. Nat. Commun. 9, 5376. https://doi.org/10.1038/s41467-018-07799-2

Daley, J.M., Tomimatsu, N., Hooks, G., Wang, W., Miller, A.S., Xue, X., Nguyen, K.A., Kaur, H., Williamson, E., Mukherjee, B., Hromas, R., Burma, S., Sung, P., 2020. Specificity of end resection pathways for double-strand break regions containing ribonucleotides and base lesions. Nat. Commun. 11, 3088. https://doi.org/10.1038/s41467-020-16903-4

Dang, T.T., Morales, J.C., 2020. XRN2 Links RNA:DNA Hybrid Resolution to Double Strand Break Repair Pathway Choice. Cancers 12. https://doi.org/10.3390/cancers12071821

Dantzer, F., Schreiber, V., Niedergang, C., Trucco, C., Flatter, E., Rubia, G.D.L., Oliver, J., Rolli, V., Ménissier-de Murcia, J., de Murcia, G., 1999. Involvement of poly(ADP-ribose) polymerase in base excision repair. Biochimie 81, 69–75. https://doi.org/10.1016/S0300-9084(99)80040-6

David, S.S., O'Shea, V.L., Kundu, S., 2007. Base-excision repair of oxidative DNA damage. Nature 447, 941.

de Lange, T., 2018. Shelterin-Mediated Telomere Protection. Annu. Rev. Genet. 52, 223–247. https://doi.org/10.1146/annurev-genet-032918-021921

de Lange, T., 2005. Shelterin: the protein complex that shapes and safeguards human telomeres. Genes Dev. 19, 2100–2110. https://doi.org/10.1101/gad.1346005

de Lange, T., Shiue, L., Myers, R.M., Cox, D.R., Naylor, S.L., Killery, A.M., Varmus, H.E., 1990. Structure and Variability of Human Chromosome Ends. Mol. Cell. Biol. 10, 518–527. https://doi.org/10.1128/mcb.10.2.518-527.1990

de Murcia, G., de Murcia, J.M., 1994. Poly(ADP-ribose) polymerase: a molecular nick-sensor. Trends Biochem. Sci. 19, 172–176. https://doi.org/10.1016/0968-0004(94)90280-1

Déjardin, J., Kingston, R.E., 2009. Purification of Proteins Associated with Specific Genomic Loci. Cell 136, 175–186. https://doi.org/10.1016/j.cell.2008.11.045

Dekhuijzen, 2004. Antioxidant properties of N-acetylcysteine: their relevance in relation to chronic obstructive pulmonary disease. Eur. Respir. J. 23, 629. https://doi.org/10.1183/09031936.04.00016804

Denchi, E.L., de Lange, T., 2007. Protection of telomeres through independent control of ATM and ATR by TRF2 and POT1. Nature 448, 1068.

Deng, Z., Norseen, J., Wiedmer, A., Riethman, H., Lieberman, P.M., 2009. TERRA RNA Binding to TRF2 Facilitates Heterochromatin Formation and ORC Recruitment at Telomeres. Mol. Cell 35, 403–413. https://doi.org/10.1016/j.molcel.2009.06.025

Deng, Z., Wang, Z., Stong, N., Plasschaert, R., Moczan, A., Chen, H.-S., Hu, S., Wikramasinghe, P., Davuluri, R.V., Bartolomei, M.S., Riethman, H., Lieberman, P.M., 2012. A role for CTCF and cohesin in subtelomere chromatin organization, TERRA transcription, and telomere end protection. EMBO J. 31, 4165–4178. https://doi.org/10.1038/emboj.2012.266

Doksani, Y., Wu, J.Y., de Lange, T., Zhuang, X., 2013. Super-Resolution Fluorescence Imaging of Telomeres Reveals TRF2-Dependent T-loop Formation. Cell 155, 345–356. https://doi.org/10.1016/j.cell.2013.09.048

Domínguez-Sánchez, M.S., Barroso, S., Gómez-González, B., Luna, R., Aguilera, A., 2011. Genome Instability and Transcription Elongation Impairment in Human Cells Depleted of THO/TREX. PLOS Genet. 7, e1002386. https://doi.org/10.1371/journal.pgen.1002386

Dungrawala, H., Cortez, D., 2015. Purification of Proteins on Newly Synthesized DNA Using iPOND, in: Hancock, R. (Ed.), The Nucleus. Springer New York, New York, NY, pp. 123–131. https://doi.org/10.1007/978-1-4939-1680-1_10

Dunham, M.A., Neumann, A.A., Fasching, C.L., Reddel, R.R., 2000. Telomere maintenance by recombination in human cells. Nat. Genet. 26, 447–450. https://doi.org/10.1038/82586

Duquette, M.L., Handa, P., Vincent, J.A., Taylor, A.F., Maizels, N., 2004. Intracellular transcription of G-rich DNAs induces formation of G-loops, novel structures containing G4 DNA. Genes Dev. 18, 1618–1629. https://doi.org/10.1101/gad.1200804

Edwards, D.S., Maganti, R., Tanksley, J.P., Luo, J., Park, J.J.H., Balkanska-Sinclair, E., Ling, J., Floyd, S.R., 2020. BRD4 Prevents R-Loop Formation and Transcription-Replication Conflicts by Ensuring Efficient Transcription Elongation. Cell Rep. 32, 108166. https://doi.org/10.1016/j.celrep.2020.108166

Ehrlich, M., Jackson, K., Weemaes, C., 2006. Immunodeficiency, centromeric region instability, facial anomalies syndrome (ICF). Orphanet J. Rare Dis. 1, 2. https://doi.org/10.1186/1750-1172-1-2

El-Khamisy, S.F., Masutani, M., Suzuki, H., Caldecott, K.W., 2003. A requirement for PARP-1 for the assembly or stability of XRCC1 nuclear foci at sites of oxidative DNA damage. Nucleic Acids Res. 31, 5526–5533. https://doi.org/10.1093/nar/gkg761

Episkopou, H., Draskovic, I., Van Beneden, A., Tilman, G., Mattiussi, M., Gobin, M., Arnoult, N., Londoño-Vallejo, A., Decottignies, A., 2014. Alternative Lengthening of Telomeres is characterized by reduced compaction of telomeric chromatin. Nucleic Acids Res. 42, 4391–4405. https://doi.org/10.1093/nar/gku114

Feretzaki, M., Pospisilova, M., Valador Fernandes, R., Lunardi, T., Krejci, L., Lingner, J., 2020. RAD51-dependent recruitment of TERRA lncRNA to telomeres through R-loops. Nature 587, 303–308. https://doi.org/10.1038/s41586-020-2815-6

Feretzaki, M., Renck Nunes, P., Lingner, J., 2019. Expression and differential regulation of human TERRA at several chromosome ends. RNA 25, 1470–1480. https://doi.org/10.1261/rna.072322.119

Fernandes, R.V., Feretzaki, M., Lingner, J., 2021. The makings of TERRA R-loops at chromosome ends. Cell Cycle 20, 1745–1759. https://doi.org/10.1080/15384101.2021.1962638

Fernandes, R.V., Lingner, J., 2023. The THO complex counteracts TERRA R-loop-mediated telomere fragility in telomerase+ cells and telomeric recombination in ALT+ cells. Nucleic Acids Res. gkad448. https://doi.org/10.1093/nar/gkad448

Flynn, R.L., Centore, R.C., O'Sullivan, R.J., Rai, R., Tse, A., Songyang, Z., Chang, S., Karlseder, J., Zou, L., 2011. TERRA and hnRNPA1 orchestrate an RPA-to-POT1 switch on telomeric single-stranded DNA. Nature 471, 532–536. https://doi.org/10.1038/nature09772

Forsyth, N.R., Evans, A.P., Shay, J.W., Wright, W.E., 2003. Developmental differences in the immortalization of lung fibroblasts by telomerase. Aging Cell 2, 235–243. https://doi.org/10.1046/j.1474-9728.2003.00057.x

Fotiadou, P., Henegariu, O., Sweasy, J.B., 2004. DNA Polymerase β Interacts with TRF2 and Induces Telomere Dysfunction in a Murine Mammary Cell Line. Cancer Res. 64, 3830. https://doi.org/10.1158/0008-5472.CAN-04-0136

Fouquerel, E., Barnes, R.P., Uttam, S., Watkins, S.C., Bruchez, M.P., Opresko, P.L., 2019. Targeted and Persistent 8-Oxoguanine Base Damage at Telomeres Promotes Telomere Loss and Crisis. Mol. Cell. https://doi.org/10.1016/j.molcel.2019.04.024

Gan, W., Guan, Z., Liu, J., Gui, T., Shen, K., Manley, J.L., Li, X., 2011. R-loop-mediated genomic instability is caused by impairment of replication fork progression. Genes Dev. 25, 2041–2056. https://doi.org/10.1101/gad.17010011

Gan, W., Liu, X.-L., Yu, T., Zou, Y.-G., Li, T.-T., Wang, S., Deng, J., Wang, L.-L., Cai, J.-P., 2018. Urinary 8-oxo-7, 8-dihydroguanosine as a Potential Biomarker of Aging. Front. Aging Neurosci. 10, 34.

García-Muse, T., Aguilera, A., 2019. R Loops: From Physiological to Pathological Roles. Cell 179, 604–618. https://doi.org/10.1016/j.cell.2019.08.055

Geiser, L., Dayon, L., Vaezzadeh, A.R., Hochstrasser, D.F., 2011. Shotgun Proteomics: A Relative Quantitative Approach Using Off-Gel Electrophoresis and LC-MS/MS, in: Walls, D., Loughran, S.T. (Eds.), Protein Chromatography: Methods and Protocols. Humana Press, Totowa, NJ, pp. 459–472. https://doi.org/10.1007/978-1-60761-913-0_27

Glousker, G., Briod, A.-S., Quadroni, M., Lingner, J., 2020. Human shelterin protein POT1 prevents severe telomere instability induced by homology-directed DNA repair. EMBO J. 39, e104500. https://doi.org/10.15252/embj.2020104500

Gopalakrishnan, K., Low, G.K.M., Ting, A.P.L., Srikanth, P., Slijepcevic, P., Hande, M.P., 2010. Hydrogen peroxide induced genomic instability in nucleotide excision repair-deficient lymphoblastoid cells. Genome Integr. 1, 16. https://doi.org/10.1186/2041-9414-1-16

Gottschling, D.E., Aparicio, O.M., Billington, B.L., Zakian, V.A., 1990. Position effect at S. cerevisiae telomeres: Reversible repression of Pol II transcription. Cell 63, 751–762. https://doi.org/10.1016/0092-8674(90)90141-Z

Granotier, C., Pennarun, G., Riou, L., Hoffschir, F., Gauthier, L.R., De Cian, A., Gomez, D., Mandine, E., Riou, J.-F., Mergny, J.-L., Mailliet, P., Dutrillaux, B., Boussin, F.D., 2005. Preferential binding of a G-quadruplex ligand to human chromosome ends. Nucleic Acids Res. 33, 4182–4190. https://doi.org/10.1093/nar/gki722

Greider, C.W., Blackburn, E.H., 1989. A telomeric sequence in the RNA of Tetrahymena telomerase required for telomere repeat synthesis. Nature 337, 331–337. https://doi.org/10.1038/337331a0

Greider, C.W., Blackburn, E.H., 1987. The telomere terminal transferase of tetrahymena is a ribonucleoprotein enzyme with two kinds of primer specificity. Cell 51, 887–898. https://doi.org/10.1016/0092-8674(87)90576-9

Greider, C.W., Blackburn, E.H., 1985. Identification of a specific telomere terminal transferase activity in tetrahymena extracts. Cell 43, 405–413. https://doi.org/10.1016/0092-8674(85)90170-9

Grolimund, L., Aeby, E., Hamelin, R., Armand, F., Chiappe, D., Moniatte, M., Lingner, J., 2013. A quantitative telomeric chromatin isolation protocol identifies different telomeric states. Nat. Commun. 4, 2848.

Guh, C.-Y., Shen, H.-J., Chen, L.W., Chiu, P.-C., Liao, I.-H., Lo, C.-C., Chen, Y., Hsieh, Y.-H., Chang, T.-C., Yen, C.-P., Chen, Y.-Y., Chen, T.W.-W., Chen, L.-Y., Wu, C.-S., Egly, J.-M., Chu, H.-P.C., 2022. XPF activates break-induced telomere synthesis. Nat. Commun. 13, 5781. https://doi.org/10.1038/s41467-022-33428-0

Haikarainen, T., Koivunen, J., Narwal, M., Venkannagari, H., Obaji, E., Joensuu, P., Pihlajaniemi, T., Lehtiö, L., 2013. para-Substituted 2-Phenyl-3,4-dihydroquinazolin-4-ones As Potent and Selective Tankyrase Inhibitors. ChemMedChem 8, 1978–1985. https://doi.org/10.1002/cmdc.201300337

Hanzlikova, H., Kalasova, I., Demin, A.A., Pennicott, L.E., Cihlarova, Z., Caldecott, K.W., 2018. The Importance of Poly(ADP-Ribose) Polymerase as a Sensor of Unligated Okazaki Fragments during DNA Replication. Mol. Cell 71, 319-331.e3. https://doi.org/10.1016/j.molcel.2018.06.004

Hastie, N.D., Dempster, M., Dunlop, M.G., Thompson, A.M., Green, D.K., Allshire, R.C., 1990. Telomere reduction in human colorectal carcinoma and with ageing. Nature 346, 866–868. https://doi.org/10.1038/346866a0

Hayashi, M.T., Cesare, A.J., Fitzpatrick, J.A.J., Lazzerini-Denchi, E., Karlseder, J., 2012. A telomere-dependent DNA damage checkpoint induced by prolonged mitotic arrest. Nat. Struct. Mol. Biol. 19, 387–394. https://doi.org/10.1038/nsmb.2245

Hayflick, L., 1965. The limited in vitro lifetime of human diploid cell strains. Exp. Cell Res. 37, 614–636. https://doi.org/10.1016/0014-4827(65)90211-9

Hazelrigg, T., Levis, R., Rubin, G.M., 1984. Transformation of white locus DNA in Drosophila: Dosage compensation, zeste interaction, and position effects. Cell 36, 469–481. https://doi.org/10.1016/0092-8674(84)90240-X

Heaphy, C.M., de Wilde, R.F., Jiao, Y., Klein, A.P., Edil, B.H., Shi, C., Bettegowda, C., Rodriguez, F.J., Eberhart, C.G., Hebbar, S., Offerhaus, G.J., McLendon, R., Rasheed, B.A., He, Y., Yan, H., Bigner, D.D., Oba-Shinjo, S.M., Marie, S.K.N., Riggins, G.J., Kinzler, K.W., Vogelstein, B., Hruban, R.H., Maitra, A., Papadopoulos, N., Meeker, A.K., 2011a. Altered Telomeres in Tumors with ATRX and DAXX Mutations. Science 333, 425–425. https://doi.org/10.1126/science.1207313

Heaphy, C.M., Subhawong, A.P., Hong, S.-M., Goggins, M.G., Montgomery, E.A., Gabrielson, E., Netto, G.J., Epstein, J.I., Lotan, T.L., Westra, W.H., Shih, I.-M., Iacobuzio-Donahue, C.A., Maitra, A., Li, Q.K., Eberhart, C.G., Taube, J.M., Rakheja, D., Kurman, R.J., Wu, T.C., Roden, R.B., Argani, P., De Marzo, A.M., Terracciano, L., Torbenson, M., Meeker, A.K., 2011b. Prevalence of the Alternative Lengthening of Telomeres Telomere

Maintenance Mechanism in Human Cancer Subtypes. Am. J. Pathol. 179, 1608–1615. https://doi.org/10.1016/j.ajpath.2011.06.018

Henderson, E.R., Blackburn, E.H., 1989. An Overhanging 3' Terminus Is a Conserved Feature of Telomeres. Mol. Cell. Biol. 9, 345–348. https://doi.org/10.1128/mcb.9.1.345-348.1989

Henderson, P.T., Delaney, J.C., Muller, J.G., Neeley, W.L., Tannenbaum, S.R., Burrows, C.J., Essigmann, J.M., 2003. The Hydantoin Lesions Formed from Oxidation of 7,8-Dihydro-8-oxoguanine Are Potent Sources of Replication Errors in Vivo. Biochemistry 42, 9257–9262. https://doi.org/10.1021/bi0347252

Henle, E.S., Han, Z., Tang, N., Rai, P., Luo, Y., Linn, S., 1999. Sequence-specific DNA Cleavage by Fe2+-mediated Fenton Reactions Has Possible Biological Implications. J. Biol. Chem. 274, 962–971. https://doi.org/10.1074/jbc.274.2.962

Henson, J.D., Cao, Y., Huschtscha, L.I., Chang, A.C., Au, A.Y.M., Pickett, H.A., Reddel, R.R., 2009. DNA C-circles are specific and quantifiable markers of alternative-lengthening-of-telomeres activity. Nat. Biotechnol. 27, 1181–1185. https://doi.org/10.1038/nbt.1587

Henson, J.D., Hannay, J.A., McCarthy, S.W., Royds, J.A., Yeager, T.R., Robinson, R.A., Wharton, S.B., Jellinek, D.A., Arbuckle, S.M., Yoo, J., Robinson, B.G., Learoyd, D.L., Stalley, P.D., Bonar, S.F., Yu, D., Pollock, R.E., Reddel, R.R., 2005. A Robust Assay for Alternative Lengthening of Telomeres in Tumors Shows the Significance of Alternative Lengthening of Telomeres in Sarcomas and Astrocytomas. Clin. Cancer Res. 11, 217–225. https://doi.org/10.1158/1078-0432.217.11.1

Hodson, C., van Twest, S., Dylewska, M., O'Rourke, J.J., Tan, W., Murphy, V.J., Walia, M., Abbouche, L., Nieminuszczy, J., Dunn, E., Bythell-Douglas, R., Heierhorst, J., Niedzwiedz, W., Deans, A.J., 2022. Branchpoint translocation by fork remodelers as a general mechanism of R-loop removal. Cell Rep. 41, 111749. https://doi.org/10.1016/j.celrep.2022.111749

Hogrebe, A., von Stechow, L., Bekker-Jensen, D.B., Weinert, B.T., Kelstrup, C.D., Olsen, J.V., 2018. Benchmarking common quantification strategies for large-scale phosphoproteomics. Nat. Commun. 9, 1045. https://doi.org/10.1038/s41467-018-03309-6

Horn, S., Figl, A., Rachakonda, P.S., Fischer, C., Sucker, A., Gast, A., Kadel, S., Moll, I., Nagore, E., Hemminki, K., Schadendorf, D., Kumar, R., 2013. TERT Promoter Mutations in Familial and Sporadic Melanoma. Science 339, 959. https://doi.org/10.1126/science.1230062

Houghtaling, B.R., Cuttonaro, L., Chang, W., Smith, S., 2004. A Dynamic Molecular Link between the Telomere Length Regulator TRF1 and the Chromosome End Protector TRF2. Curr. Biol. 14, 1621–1631. https://doi.org/10.1016/j.cub.2004.08.052

Huang, F.W., Hodis, E., Xu, M.J., Kryukov, G.V., Chin, L., Garraway, L.A., 2013. Highly recurrent TERT promoter mutations in human melanoma. Science 339, 957–959.

Huda, A., Arakawa, H., Mazzucco, G., Galli, M., Petrocelli, V., Casola, S., Chen, L., Doksani, Y., 2023. The telomerase reverse transcriptase elongates reversed replication forks at telomeric repeats. Sci. Adv. 9, eadf2011. https://doi.org/10.1126/sciadv.adf2011

Huertas, P., Aguilera, A., 2003. Cotranscriptionally Formed DNA:RNA Hybrids Mediate Transcription Elongation Impairment and Transcription-Associated Recombination. Mol. Cell 12, 711–721. https://doi.org/10.1016/j.molcel.2003.08.010

Itoh, T., Tomizawa, J., 1980. Formation of an RNA primer for initiation of replication of ColE1 DNA by ribonuclease H. Proc. Natl. Acad. Sci. 77, 2450–2454. https://doi.org/10.1073/pnas.77.5.2450

Jang, Y., Elsayed, Z., Eki, R., He, S., Du, K.-P., Abbas, T., Kai, M., 2020. Intrinsically disordered protein RBM14 plays a role in generation of RNA:DNA hybrids at double-strand break sites. Proc. Natl. Acad. Sci. 117, 5329–5338. https://doi.org/10.1073/pnas.1913280117

Jonkers, I., Lis, J.T., 2015. Getting up to speed with transcription elongation by RNA polymerase II. Nat. Rev. Mol. Cell Biol. 16, 167–177. https://doi.org/10.1038/nrm3953

Kaul, Z., Cesare, A.J., Huschtscha, L.I., Neumann, A.A., Reddel, R.R., 2012. Five dysfunctional telomeres predict onset of senescence in human cells. EMBO Rep. 13, 52–59. https://doi.org/10.1038/embor.2011.227

Kelleher, C., Kurth, I., Lingner, J., 2005. Human Protection of Telomeres 1 (POT1) Is a Negative Regulator of Telomerase Activity In Vitro. Mol. Cell. Biol. 25, 808–818. https://doi.org/10.1128/MCB.25.2.808-818.2005

Keskin, H., Shen, Y., Huang, F., Patel, M., Yang, T., Ashley, K., Mazin, A.V., Storici, F., 2014. Transcript-RNA-templated DNA recombination and repair. Nature 515, 436–439. https://doi.org/10.1038/nature13682

Killela, P.J., Reitman, Z.J., Jiao, Y., Bettegowda, C., Agrawal, N., Diaz Jr, L.A., Friedman, A.H., Friedman, H., Gallia, G.L., Giovanella, B.C., 2013. TERT promoter mutations occur frequently in gliomas and a subset of tumors derived from cells with low rates of self-renewal. Proc. Natl. Acad. Sci. 110, 6021–6026.

Kim, S., Kaminker, P., Campisi, J., 1999. TIN2, a new regulator of telomere length in human cells. Nat. Genet. 23, 405–412. https://doi.org/10.1038/70508

Klobutcher, L.A., Swanton, M.T., Donini, P., Prescott, D.M., 1981. All gene-sized DNA molecules in four species of hypotrichs have the same terminal sequence and an unusual 3’ terminus. Proc. Natl. Acad. Sci. 78, 3015–3019. https://doi.org/10.1073/pnas.78.5.3015

König, P., Fairall, L., Rhodes, D., 1998. Sequence-specific DNA recognition by the Myb-like domain of the human telomere binding protein TRF1: A model for the protein-DNA complex. Nucleic Acids Res. 26, 1731–1740. https://doi.org/10.1093/nar/26.7.1731

Krokan, H.E., Bjoras, M., 2013. Base Excision Repair. Cold Spring Harb. Perspect. Biol. 5. https://doi.org/10.1101/cshperspect.a012583

Lafuente-Barquero, J., García-Rubio, M.L., Martin-Alonso, M.S., Gómez-González, B., Aguilera, A., 2020. Harmful DNA:RNA hybrids are formed in cis and in a Rad51-independent manner. eLife 9, e56674. https://doi.org/10.7554/eLife.56674

Lee, Arora, R., Wischnewski, H., Azzalin, C.M., 2018. TRF1 participates in chromosome end protection by averting TRF2-dependent telomeric R loops. Nat. Struct. Mol. Biol. 25, 147–153. https://doi.org/10.1038/s41594-017-0021-5

Lee, J.-H., Paull, T.T., 2005. ATM Activation by DNA Double-Strand Breaks Through the Mre11-Rad50-Nbs1 Complex. Science 308, 551–554. https://doi.org/10.1126/science.1108297

Lee, M., Hills, M., Conomos, D., Stutz, M.D., Dagg, R.A., Lau, L.M.S., Reddel, R.R., Pickett, H.A., 2013. Telomere extension by telomerase and ALT generates variant repeats by mechanistically distinct processes. Nucleic Acids Res. 42, 1733–1746. https://doi.org/10.1093/nar/gkt1117

Leman, A.R., Dheekollu, J., Deng, Z., Lee, S.W., Das, M.M., Lieberman, P.M., Noguchi, E., 2012. Timeless preserves telomere length by promoting efficient DNA replication through human telomeres. Cell Cycle 11, 2337–2347. https://doi.org/10.4161/cc.20810

Lerner, L.K., Sale, J.E., 2019. Replication of G Quadruplex DNA. Genes 10. https://doi.org/10.3390/genes10020095

Lewis, P.W., Elsaesser, S.J., Noh, K.-M., Stadler, S.C., Allis, C.D., 2010. Daxx is an H3.3-specific histone chaperone and cooperates with ATRX in replication-independent chromatin assembly at telomeres. Proc. Natl. Acad. Sci. 107, 14075–14080. https://doi.org/10.1073/pnas.1008850107

Li, B., Oestreich, S., de Lange, T., 2000. Identification of Human Rap1: Implications for Telomere Evolution. Cell 101, 471–483. https://doi.org/10.1016/S0092-8674(00)80858-2

Li, L., Germain, D.R., Poon, H.-Y., Hildebrandt, M.R., Monckton, E.A., McDonald, D., Hendzel, M.J., Godbout, R., 2016. DEAD Box 1 Facilitates Removal of RNA and Homologous Recombination at DNA Double-Strand Breaks. Mol. Cell. Biol. 36, 2794–2810. https://doi.org/10.1128/MCB.00415-16

Lin, C.-Y.G., Näger, A.C., Lunardi, T., Vančevska, A., Lossaint, G., Lingner, J., 2021. The human telomeric proteome during telomere replication. Nucleic Acids Res. 49, 12119–12135. https://doi.org/10.1093/nar/gkab1015

Lingner, J., Hughes, T.R., Shevchenko, A., Mann, M., Lundblad, V., Cech, T.R., 1997. Reverse Transcriptase Motifs in the Catalytic Subunit of Telomerase. Science 276, 561. https://doi.org/10.1126/science.276.5312.561

Liu, D., O'Connor, M.S., Qin, J., Songyang, Z., 2004a. Telosome, a Mammalian Telomere-associated Complex Formed by Multiple Telomeric Proteins*. J. Biol. Chem. 279, 51338–51342. https://doi.org/10.1074/jbc.M409293200

Liu, D., Safari, A., O'Connor, M.S., Chan, D.W., Laegeler, A., Qin, J., Songyang, Z., 2004b. PTOP interacts with POT1 and regulates its localization to telomeres. Nat. Cell Biol. 6, 673–680. https://doi.org/10.1038/ncb1142

Loayza, D., de Lange, T., 2003. POT1 as a terminal transducer of TRF1 telomere length control. Nature 423, 1013–1018. https://doi.org/10.1038/nature01688

Londoño-Vallejo, J.A., Der-Sarkissian, H., Cazes, L., Bacchetti, S., Reddel, R.R., 2004. Alternative Lengthening of Telomeres Is Characterized by High Rates of Telomeric Exchange. Cancer Res. 64, 2324–2327. https://doi.org/10.1158/0008-5472.CAN-03-4035

Lonkar, P., Dedon, P.C., 2011. Reactive species and DNA damage in chronic inflammation: reconciling chemical mechanisms and biological fates. Int. J. Cancer 128, 1999–2009. https://doi.org/10.1002/ijc.25815

Loor, G., Kondapalli, J., Schriewer, J.M., Chandel, N.S., Vanden Hoek, T.L., Schumacker, P.T., 2010. Menadione triggers cell death through ROS-dependent mechanisms involving PARP activation without requiring apoptosis. Free Radic. Biol. Med. 49, 1925–1936. https://doi.org/10.1016/j.freeradbiomed.2010.09.021

Lopes, M., 2009. Electron Microscopy Methods for Studying In Vivo DNA Replication Intermediates, in: Vengrova, S., Dalgaard, J.Z. (Eds.), DNA Replication: Methods and Protocols. Humana Press, Totowa, NJ, pp. 605–631. https://doi.org/10.1007/978-1-60327-815-7_34

López-Otín, C., Blasco, M.A., Partridge, L., Serrano, M., Kroemer, G., 2013. The Hallmarks of Aging. Cell 153, 1194–1217. https://doi.org/10.1016/j.cell.2013.05.039

Lovejoy, C.A., Li, W., Reisenweber, S., Thongthip, S., Bruno, J., de Lange, T., De, S., Petrini, J.H.J., Sung, P.A., Jasin, M., Rosenbluh, J., Zwang, Y., Weir, B.A., Hatton, C., Ivanova, E., Macconaill, L., Hanna, M., Hahn, W.C., Lue, N.F., Reddel, R.R., Jiao, Y., Kinzler, K., Vogelstein, B., Papadopoulos, N., Meeker, A.K., for the ALT Starr Cancer Consortium, 2012. Loss of ATRX, Genome Instability, and an Altered DNA Damage Response Are Hallmarks of the Alternative Lengthening of Telomeres Pathway. PLOS Genet. 8, e1002772. https://doi.org/10.1371/journal.pgen.1002772

Lu, R., Pickett, H.A., 2022. Telomeric replication stress: the beginning and the end for alternative lengthening of telomeres cancers. Open Biol. 12, 220011. https://doi.org/10.1098/rsob.220011

Lu, W.-T., Hawley, B.R., Skalka, G.L., Baldock, R.A., Smith, E.M., Bader, A.S., Malewicz, M., Watts, F.Z., Wilczynska, A., Bushell, M., 2018. Drosha drives the formation of DNA:RNA hybrids around DNA break sites to facilitate DNA repair. Nat. Commun. 9, 532. https://doi.org/10.1038/s41467-018-02893-x

Luke, B., Panza, A., Redon, S., Iglesias, N., Li, Z., Lingner, J., 2008. The Rat1p 5′ to 3′ Exonuclease Degrades Telomeric Repeat-Containing RNA and Promotes Telomere Elongation in Saccharomyces cerevisiae. Mol. Cell 32, 465–477. https://doi.org/10.1016/j.molcel.2008.10.019

Maciejowski, J., de Lange, T., 2017. Telomeres in cancer: tumour suppression and genome instability. Nat. Rev. Mol. Cell Biol. 18, 175–186. https://doi.org/10.1038/nrm.2016.171

MacNeill, S., 2012. Composition and Dynamics of the Eukaryotic Replisome: A Brief Overview, in: MacNeill, S. (Ed.), The Eukaryotic Replisome: A Guide to Protein Structure and Function. Springer Netherlands, Dordrecht, pp. 1–17. https://doi.org/10.1007/978-94-007-4572-8_1

Majerska, J., Feretzaki, M., Glousker, G., Lingner, J., 2018. Transformation-induced stress at telomeres is counteracted through changes in the telomeric proteome including SAMHD1. Life Sci. Alliance 1, e201800121. https://doi.org/10.26508/lsa.201800121

Majerská, J., Redon, S., Lingner, J., 2017. Quantitative telomeric chromatin isolation protocol for human cells. Telomeres Telomerase 114, 28–38. https://doi.org/10.1016/j.ymeth.2016.08.003

Makarov, V.L., Hirose, Y., Langmore, J.P., 1997. Long G Tails at Both Ends of Human Chromosomes Suggest a C Strand Degradation Mechanism for Telomere Shortening. Cell 88, 657–666. https://doi.org/10.1016/S0092-8674(00)81908-X

Marin-Vicente, C., Domingo-Prim, J., Eberle, A.B., Visa, N., 2015. RRP6/EXOSC10 is required for the repair of DNA double-strand breaks by homologous recombination. J. Cell Sci. 128, 1097–1107. https://doi.org/10.1242/jcs.158733

Marnef, A., Legube, G., 2021. R-loops as Janus-faced modulators of DNA repair. Nat. Cell Biol. 23, 305–313. https://doi.org/10.1038/s41556-021-00663-4

Matsuoka, S., Ballif, B.A., Smogorzewska, A., McDonald, E.R., Hurov, K.E., Luo, J., Bakalarski, C.E., Zhao, Z., Solimini, N., Lerenthal, Y., Shiloh, Y., Gygi, S.P., Elledge, S.J., 2007. ATM and ATR Substrate Analysis Reveals Extensive Protein Networks Responsive to DNA Damage. Science 316, 1160–1166. https://doi.org/10.1126/science.1140321

Matsuoka, S., Rotman, G., Ogawa, A., Shiloh, Y., Tamai, K., Elledge, S.J., 2000. Ataxia telangiectasia-mutated phosphorylates Chk2 in vivo and in vitro. Proc. Natl. Acad. Sci. 97, 10389–10394. https://doi.org/10.1073/pnas.190030497

Mattiroli, F., Vissers, J.H.A., van Dijk, W.J., Ikpa, P., Citterio, E., Vermeulen, W., Marteijn, J.A., Sixma, T.K., 2012. RNF168 Ubiquitinates K13-15 on H2A/H2AX to Drive DNA Damage Signaling. Cell 150, 1182–1195. https://doi.org/10.1016/j.cell.2012.08.005

Mazzucco, G., Huda, A., Galli, M., Piccini, D., Giannattasio, M., Pessina, F., Doksani, Y., 2020. Telomere damage induces internal loops that generate telomeric circles. Nat. Commun. 11, 5297. https://doi.org/10.1038/s41467-020-19139-4

Mazzucco, G., Huda, A., Galli, M., Zanella, E., Doksani, Y., 2022. Purification of mammalian telomeric DNA for single-molecule analysis. Nat. Protoc. 17, 1444–1467. https://doi.org/10.1038/s41596-022-00684-9

McKerlie, M., Zhu, X.-D., 2011. Cyclin B-dependent kinase 1 regulates human TRF1 to modulate the resolution of sister telomeres. Nat. Commun. 2, 371. https://doi.org/10.1038/ncomms1372

McNulty, J.M., Jerkovic, B., Bolton, P.H., Basu, A.K., 1998. Replication Inhibition and Miscoding Properties of DNA Templates Containing a Site-Specific cis-Thymine Glycol or Urea Residue. Chem. Res. Toxicol. 11, 666–673. https://doi.org/10.1021/tx970225w

Meers, C., Keskin, H., Banyai, G., Mazina, O., Yang, T., Gombolay, A.L., Mukherjee, K., Kaparos, E.I., Newnam, G., Mazin, A., Storici, F., 2020. Genetic Characterization of Three Distinct Mechanisms Supporting RNA-Driven DNA Repair and Modification Reveals Major Role of DNA Polymerase ζ. Mol. Cell 79, 1037-1050.e5. https://doi.org/10.1016/j.molcel.2020.08.011

Meers, C., Keskin, H., Storici, F., 2016. DNA repair by RNA: Templated, or not templated, that is the question. Cut.-Edge Perspect. Genomic Maint. III 44, 17–21. https://doi.org/10.1016/j.dnarep.2016.05.002

Meselson, M., Stahl, F.W., 1958. The replication of DNA in Escherichia coli*. Proc. Natl. Acad. Sci. 44, 671–682. https://doi.org/10.1073/pnas.44.7.671

Michelini, F., Pitchiaya, S., Vitelli, V., Sharma, S., Gioia, U., Pessina, F., Cabrini, M., Wang, Y., Capozzo, I., Iannelli, F., Matti, V., Francia, S., Shivashankar, G.V., Walter, N.G., d'Adda di Fagagna, F., 2017. Damage-induced lncRNAs control the DNA damage response through interaction with DDRNAs at individual double-strand breaks. Nat. Cell Biol. 19, 1400–1411. https://doi.org/10.1038/ncb3643

Miglietta, G., Russo, M., Capranico, G., 2020. G-quadruplex–R-loop interactions and the mechanism of anticancer G-quadruplex binders. Nucleic Acids Res. 48, 11942–11957. https://doi.org/10.1093/nar/gkaa944

Moyzis, R.K., Buckingham, J.M., Cram, L.S., Dani, M., Deaven, L.L., Jones, M.D., Meyne, J., Ratliff, R.L., Wu, J.R., 1988. A highly conserved repetitive DNA sequence, (TTAGGG)n, present at the telomeres of human chromosomes. Proc. Natl. Acad. Sci. 85, 6622–6626. https://doi.org/10.1073/pnas.85.18.6622

Muller, 1938. The remaking of chromosomes. Collect. Net 8, 198.

Nakamura, T.M., Morin, G.B., Chapman, K.B., Weinrich, S.L., Andrews, W.H., Lingner, J., Harley, C.B., Cech, T.R., 1997. Telomerase Catalytic Subunit Homologs from Fission Yeast and Human. Science 277, 955–959. https://doi.org/10.1126/science.277.5328.955

Nandakumar, J., Bell, C.F., Weidenfeld, I., Zaug, A.J., Leinwand, L.A., Cech, T.R., 2012. The TEL patch of telomere protein TPP1 mediates telomerase recruitment and processivity. Nature 492, 285–289. https://doi.org/10.1038/nature11648

Nassour, J., Aguiar, L.G., Correia, A., Schmidt, T.T., Mainz, L., Przetocka, S., Haggblom, C., Tadepalle, N., Williams, A., Shokhirev, M.N., Akincilar, S.C., Tergaonkar, V., Shadel, G.S., Karlseder, J., 2023. Telomere-to-mitochondria signalling by ZBP1 mediates replicative crisis. Nature 614, 767–773. https://doi.org/10.1038/s41586-023-05710-8

Nassour, J., Radford, R., Correia, A., Fusté, J.M., Schoell, B., Jauch, A., Shaw, R.J., Karlseder, J., 2019. Autophagic cell death restricts chromosomal instability during replicative crisis. Nature 565, 659–663. https://doi.org/10.1038/s41586-019-0885-0

Nergadze, S.G., Farnung, B.O., Wischnewski, H., Khoriauli, L., Vitelli, V., Chawla, R., Giulotto, E., Azzalin, C.M., 2009. CpG-island promoters drive transcription of human telomeres. RNA 15, 2186–2194. https://doi.org/10.1261/rna.1748309

O'Connell, J.D., Paulo, J.A., O'Brien, J.J., Gygi, S.P., 2018. Proteome-Wide Evaluation of Two Common Protein Quantification Methods. J. Proteome Res. 17, 1934–1942. https://doi.org/10.1021/acs.jproteome.8b00016

Ohki, R., Ishikawa, F., 2004. Telomere-bound TRF1 and TRF2 stall the replication fork at telomeric repeats. Nucleic Acids Res. 32, 1627–1637. https://doi.org/10.1093/nar/gkh309

Ohle, C., Tesorero, R., Schermann, G., Dobrev, N., Sinning, I., Fischer, T., 2016. Transient RNA-DNA Hybrids Are Required for Efficient Double-Strand Break Repair. Cell 167, 1001-1013.e7. https://doi.org/10.1016/j.cell.2016.10.001

Oikawa, S., Tada-Oikawa, S., Kawanishi, S., 2001. Site-Specific DNA Damage at the GGG Sequence by UVA Involves Acceleration of Telomere Shortening. Biochemistry 40, 4763–4768. https://doi.org/10.1021/bi002721g

Okamoto, K., Bartocci, C., Ouzounov, I., Diedrich, J.K., Yates III, J.R., Denchi, E.L., 2013. A two-step mechanism for TRF2-mediated chromosome-end protection. Nature 494, 502–505. https://doi.org/10.1038/nature11873

Olson, E., Nievera, C.J., Klimovich, V., Fanning, E., Wu, X., 2006. RPA2 Is a Direct Downstream Target for ATR to Regulate the S-phase Checkpoint*. J. Biol. Chem. 281, 39517–39533. https://doi.org/10.1074/jbc.M605121200

Ong, S.-E., Mann, M., 2006. A practical recipe for stable isotope labeling by amino acids in cell culture (SILAC). Nat. Protoc. 1, 2650–2660. https://doi.org/10.1038/nprot.2006.427

Opresko, P.L., Fan, J., Danzy, S., Wilson, D.M., III, Bohr, V.A., 2005. Oxidative damage in telomeric DNA disrupts recognition by TRF1 and TRF2. Nucleic Acids Res. 33, 1230–1239. https://doi.org/10.1093/nar/gki273

Orthwein, A., Fradet-Turcotte, A., Noordermeer, S.M., Canny, M.D., Brun, C.M., Strecker, J., Escribano-Diaz, C., Durocher, D., 2014. Mitosis Inhibits DNA Double-Strand Break Repair to Guard Against Telomere Fusions. Science 344, 189–193. https://doi.org/10.1126/science.1248024

Osterod, M., Hollenbach, S., Hengstler, J.G., Barnes, D.E., Lindahl, T., Epe, B., 2001. Age-related and tissue-specific accumulation of oxidative DNA base damage in 7, 8-dihydro-8-oxoguanine-DNA glycosylase (Ogg1) deficient mice. Carcinogenesis 22, 1459–1463.

O'Sullivan, R.J., Arnoult, N., Lackner, D.H., Oganesian, L., Haggblom, C., Corpet, A., Almouzni, G., Karlseder, J., 2014. Rapid induction of alternative lengthening of telomeres by

depletion of the histone chaperone ASF1. Nat. Struct. Mol. Biol. 21, 167–174. https://doi.org/10.1038/nsmb.2754

Perkins, A., Nelson, K.J., Parsonage, D., Poole, L.B., Karplus, P.A., 2015. Peroxiredoxins: guardians against oxidative stress and modulators of peroxide signaling. Trends Biochem. Sci. 40, 435–445. https://doi.org/10.1016/j.tibs.2015.05.001

Pessina, F., Giavazzi, F., Yin, Y., Gioia, U., Vitelli, V., Galbiati, A., Barozzi, S., Garre, M., Oldani, A., Flaus, A., Cerbino, R., Parazzoli, D., Rothenberg, E., d'Adda di Fagagna, F., 2019. Functional transcription promoters at DNA double-strand breaks mediate RNA-driven phase separation of damage-response factors. Nat. Cell Biol. 21, 1286–1299. https://doi.org/10.1038/s41556-019-0392-4

Petersen, S., Saretzki, G., Zglinicki, T. von, 1998. Preferential Accumulation of Single-Stranded Regions in Telomeres of Human Fibroblasts. Exp. Cell Res. 239, 152–160. https://doi.org/10.1006/excr.1997.3893

Petti, E., Buemi, V., Zappone, A., Schillaci, O., Broccia, P.V., Dinami, R., Matteoni, S., Benetti, R., Schoeftner, S., 2019. SFPQ and NONO suppress RNA:DNA-hybrid-related telomere instability. Nat. Commun. 10, 1001. https://doi.org/10.1038/s41467-019-08863-1

Pickett, H.A., Reddel, R.R., 2015. Molecular mechanisms of activity and derepression of alternative lengthening of telomeres. Nat. Struct. Mol. Biol. 22, 875–880. https://doi.org/10.1038/nsmb.3106

Porro, A., Feuerhahn, S., Delafontaine, J., Riethman, H., Rougemont, J., Lingner, J., 2014a. Functional characterization of the TERRA transcriptome at damaged telomeres. Nat. Commun. 5, 5379. https://doi.org/10.1038/ncomms6379

Porro, A., Feuerhahn, S., Lingner, J., 2014b. TERRA-Reinforced Association of LSD1 with MRE11 Promotes Processing of Uncapped Telomeres. Cell Rep. 6, 765–776. https://doi.org/10.1016/j.celrep.2014.01.022

Porro, A., Feuerhahn, S., Reichenbach, P., Lingner, J., 2010. Molecular Dissection of Telomeric Repeat-Containing RNA Biogenesis Unveils the Presence of Distinct and Multiple Regulatory Pathways. Mol. Cell. Biol. 30, 4808. https://doi.org/10.1128/MCB.00460-10

Prakash, A., Borgstahl, G.E.O., 2012. The Structure and Function of Replication Protein A in DNA Replication, in: MacNeill, S. (Ed.), The Eukaryotic Replisome: A Guide to Protein Structure and Function. Springer Netherlands, Dordrecht, pp. 171–196. https://doi.org/10.1007/978-94-007-4572-8_10

Rauniyar, N., Yates, J.R.I., 2014. Isobaric Labeling-Based Relative Quantification in Shotgun Proteomics. J. Proteome Res. 13, 5293–5309. https://doi.org/10.1021/pr500880b

Reaban, M.E., Lebowitz, J., Griffin, J.A., 1994. Transcription induces the formation of a stable RNA.DNA hybrid in the immunoglobulin alpha switch region. J. Biol. Chem. 269, 21850–21857. https://doi.org/10.1016/S0021-9258(17)31881-1

Redon, S., Reichenbach, P., Lingner, J., 2010. The non-coding RNA TERRA is a natural ligand and direct inhibitor of human telomerase. Nucleic Acids Res. 38, 5797–5806. https://doi.org/10.1093/nar/gkq296

Redon, S., Zemp, I., Lingner, J., 2013. A three-state model for the regulation of telomerase by TERRA and hnRNPA1. Nucleic Acids Res. 41, 9117–9128. https://doi.org/10.1093/nar/gkt695

Reichert, S., Stier, A., 2017. Does oxidative stress shorten telomeres in vivo? A review. Biol. Lett. 13, 20170463. https://doi.org/10.1098/rsbl.2017.0463

Ribes-Zamora, A., Indiviglio, S.M., Mihalek, I., Williams, C.L., Bertuch, A.A., 2013. TRF2 Interaction with Ku Heterotetramerization Interface Gives Insight into c-NHEJ Prevention at Human Telomeres. Cell Rep. 5, 194–206. https://doi.org/10.1016/j.celrep.2013.08.040

Richter, T., Zglinicki, T. von, 2007. A continuous correlation between oxidative stress and telomere shortening in fibroblasts. Exp. Gerontol. 42, 1039–1042. https://doi.org/10.1016/j.exger.2007.08.005

Riethman, H., Ambrosini, A., Paul, S., 2005. Human subtelomere structure and variation. Chromosome Res. 13, 505–515. https://doi.org/10.1007/s10577-005-0998-1

Ronson, G.E., Piberger, A.L., Higgs, M.R., Olsen, A.L., Stewart, G.S., McHugh, P.J., Petermann, E., Lakin, N.D., 2018. PARP1 and PARP2 stabilise replication forks at base excision repair intermediates through Fbh1-dependent Rad51 regulation. Nat. Commun. 9, 746. https://doi.org/10.1038/s41467-018-03159-2

Roy, D., Zhang, Z., Lu, Z., Hsieh, C.-L., Lieber, M.R., 2010. Competition between the RNA Transcript and the Nontemplate DNA Strand during R-Loop Formation In Vitro: a Nick Can Serve as a Strong R-Loop Initiation Site. Mol. Cell. Biol. 30, 146–159. https://doi.org/10.1128/MCB.00897-09

Rudd, S.G., Valerie, N.C.K., Helleday, T., 2016. Pathways controlling dNTP pools to maintain genome stability. Cut.-Edge Perspect. Genomic Maint. III 44, 193–204. https://doi.org/10.1016/j.dnarep.2016.05.032

Sabharwal, S.S., Schumacker, P.T., 2014. Mitochondrial ROS in cancer: initiators, amplifiers or an Achilles' heel? Nat. Rev. Cancer 14, 709.

Sagie, S., Toubiana, S., Hartono, S.R., Katzir, H., Tzur-Gilat, A., Havazelet, S., Francastel, C., Velasco, G., Chédin, F., Selig, S., 2017. Telomeres in ICF syndrome cells are vulnerable to DNA damage due to elevated DNA:RNA hybrids. Nat. Commun. 8, 14015. https://doi.org/10.1038/ncomms14015

Salas-Armenteros, I., Pérez-Calero, C., Bayona-Feliu, A., Tumini, E., Luna, R., Aguilera, A., 2017. Human THO–Sin3A interaction reveals new mechanisms to prevent R-loops that cause genome instability. EMBO J. 36, 3532–3547. https://doi.org/10.15252/embj.201797208

Sanz, L.A., Hartono, S.R., Lim, Y.W., Steyaert, S., Rajpurkar, A., Ginno, P.A., Xu, X., Chédin, F., 2016. Prevalent, Dynamic, and Conserved R-Loop Structures Associate with Specific Epigenomic Signatures in Mammals. Mol Cell 63, 167–178. https://doi.org/10.1016/j.molcel.2016.05.032

Sarek, G., Kotsantis, P., Ruis, P., Van Ly, D., Margalef, P., Borel, V., Zheng, X.-F., Flynn, H.R., Snijders, A.P., Chowdhury, D., Cesare, A.J., Boulton, S.J., 2019. CDK phosphorylation of TRF2 controls t-loop dynamics during the cell cycle. Nature 575, 523–527. https://doi.org/10.1038/s41586-019-1744-8

Sarek, G., Vannier, J.-B., Panier, S., Petrini, J.H.J., Boulton, S.J., 2015. TRF2 Recruits RTEL1 to Telomeres in S Phase to Promote T-Loop Unwinding. Mol. Cell 57, 622–635. https://doi.org/10.1016/j.molcel.2014.12.024

Savoca, V., Rivosecchi, J., Gaiatto, A., Rossi, A., Mosca, R., Gialdini, I., Zubovic, L., Tebaldi, T., Macchi, P., Cusanelli, E., 2023. TERRA stability is regulated by RALY and polyadenylation in a telomere-specific manner. Cell Rep. 42. https://doi.org/10.1016/j.celrep.2023.112406

Scheibe, M., Arnoult, N., Kappei, D., Buchholz, F., Decottignies, A., Butter, F., Mann, M., 2013. Quantitative interaction screen of telomeric repeat-containing RNA reveals novel

TERRA regulators. Genome Res. 23, 2149–2157. https://doi.org/10.1101/gr.151878.112

Schoeftner, S., Blasco, M.A., 2008. Developmentally regulated transcription of mammalian telomeres by DNA-dependent RNA polymerase II. Nat. Cell Biol. 10, 228–236. https://doi.org/10.1038/ncb1685

Schreiber, V., Amé, J.-C., Dollé, P., Schultz, I., Rinaldi, B., Fraulob, V., Ménissier-de Murcia, J., de Murcia, G., 2002. Poly(ADP-ribose) Polymerase-2 (PARP-2) Is Required for Efficient Base Excision DNA Repair in Association with PARP-1 and XRCC1*. J. Biol. Chem. 277, 23028–23036. https://doi.org/10.1074/jbc.M202390200

Schwanhäusser, B., Busse, D., Li, N., Dittmar, G., Schuchhardt, J., Wolf, J., Chen, W., Selbach, M., 2011. Global quantification of mammalian gene expression control. Nature 473, 337–342. https://doi.org/10.1038/nature10098

Schwartzentruber, J., Korshunov, A., Liu, X.-Y., Jones, D.T.W., Pfaff, E., Jacob, K., Sturm, D., Fontebasso, A.M., Quang, D.-A.K., Tönjes, M., Hovestadt, V., Albrecht, S., Kool, M., Nantel, A., Konermann, C., Lindroth, A., Jäger, N., Rausch, T., Ryzhova, M., Korbel, J.O., Hielscher, T., Hauser, P., Garami, M., Klekner, A., Bognar, L., Ebinger, M., Schuhmann, M.U., Scheurlen, W., Pekrun, A., Frühwald, M.C., Roggendorf, W., Kramm, C., Dürken, M., Atkinson, J., Lepage, P., Montpetit, A., Zakrzewska, M., Zakrzewski, K., Liberski, P.P., Dong, Z., Siegel, P., Kulozik, A.E., Zapatka, M., Guha, A., Malkin, D., Felsberg, J., Reifenberger, G., von Deimling, A., Ichimura, K., Collins, V.P., Witt, H., Milde, T., Witt, O., Zhang, C., Castelo-Branco, P., Lichter, P., Faury, D., Tabori, U., Plass, C., Majewski, J., Pfister, S.M., Jabado, N., 2012. Driver mutations in histone H3.3 and chromatin remodelling genes in paediatric glioblastoma. Nature 482, 226–231. https://doi.org/10.1038/nature10833

Sfeir, A., de Lange, T., 2012. Removal of Shelterin Reveals the Telomere End-Protection Problem. Science 336, 593–597. https://doi.org/10.1126/science.1218498

Sfeir, A., Kosiyatrakul, S.T., Hockemeyer, D., MacRae, S.L., Karlseder, J., Schildkraut, C.L., de Lange, T., 2009. Mammalian Telomeres Resemble Fragile Sites and Require TRF1 for Efficient Replication. Cell 138, 90–103. https://doi.org/10.1016/j.cell.2009.06.021

Sharma, S., Anand, R., Zhang, X., Francia, S., Michelini, F., Galbiati, A., Williams, H., Ronato, D.A., Masson, J.-Y., Rothenberg, E., Cejka, P., d'Adda di Fagagna, F., 2021. MRE11-RAD50-NBS1 Complex Is Sufficient to Promote Transcription by RNA Polymerase II at Double-Strand Breaks by Melting DNA Ends. Cell Rep. 34, 108565. https://doi.org/10.1016/j.celrep.2020.108565

Shatkin, A.J., 1976. Capping of eucaryotic mRNAs. Cell 9, 645–653. https://doi.org/10.1016/0092-8674(76)90128-8

Shay, J.W., Bacchetti, S., 1997. A survey of telomerase activity in human cancer. Eur. J. Cancer 33, 787–791.

Silva, B., Arora, R., Azzalin, C.M., 2022. The alternative lengthening of telomeres mechanism jeopardizes telomere integrity if not properly restricted. Proc. Natl. Acad. Sci. 119, e2208669119. https://doi.org/10.1073/pnas.2208669119

Silva, B., Arora, R., Bione, S., Azzalin, C.M., 2021. TERRA transcription destabilizes telomere integrity to initiate break-induced replication in human ALT cells. Nat. Commun. 12, 3760. https://doi.org/10.1038/s41467-021-24097-6

Silva, B., Pentz, R., Figueira, A.M., Arora, R., Lee, Y.W., Hodson, C., Wischnewski, H., Deans, A.J., Azzalin, C.M., 2019. FANCM limits ALT activity by restricting telomeric replication

stress induced by deregulated BLM and R-loops. Nat. Commun. 10, 2253. https://doi.org/10.1038/s41467-019-10179-z

Smith, S., de Lange, T., 2000. Tankyrase promotes telomere elongation in human cells. Curr. Biol. 10, 1299–1302. https://doi.org/10.1016/S0960-9822(00)00752-1

Smith, S., Giriat, I., Schmitt, A., de Lange, T., 1998. Tankyrase, a Poly(ADP-Ribose) Polymerase at Human Telomeres. Science 282, 1484. https://doi.org/10.1126/science.282.5393.1484

Soudet, J., Jolivet, P., Teixeira, M.T., 2014. Elucidation of the DNA End-Replication Problem in Saccharomyces cerevisiae. Mol. Cell 53, 954–964. https://doi.org/10.1016/j.molcel.2014.02.030

Srivastava, D.K., Vande Berg, B.J., Prasad, R., Molina, J.T., Beard, W.A., Tomkinson, A.E., Wilson, S.H., 1998. Mammalian Abasic Site Base Excision Repair: IDENTIFICATION OF THE REACTION SEQUENCE AND RATE-DETERMINING STEPS. J. Biol. Chem. 273, 21203–21209. https://doi.org/10.1074/jbc.273.33.21203

Stagno d´Alcontres, M., Palacios, A., Mejias, D., Blasco, M.A., 2014. TopoIIα prevents telomere fragility and formation of ultra thin DNA bridges during mitosis through TRF1-dependent binding to telomeres. Cell Cycle 13, 1463–1481. https://doi.org/10.4161/cc.28419

Statello, L., Guo, C.-J., Chen, L.-L., Huarte, M., 2021. Gene regulation by long non-coding RNAs and its biological functions. Nat. Rev. Mol. Cell Biol. 22, 96–118. https://doi.org/10.1038/s41580-020-00315-9

Stuckey, R., García-Rodríguez, N., Aguilera, A., Wellinger, R.E., 2015. Role for RNA:DNA hybrids in origin-independent replication priming in a eukaryotic system. Proc. Natl. Acad. Sci. 112, 5779–5784. https://doi.org/10.1073/pnas.1501769112

Sun, H., Treco, D., Szostak, J.W., 1991. Extensive 3'-overhanging, single-stranded DNA associated with the meiosis-specific double-strand breaks at the ARG4 recombination initiation site. Cell 64, 1155–1161. https://doi.org/10.1016/0092-8674(91)90270-9

Svendsen, J.M., Smogorzewska, A., Sowa, M.E., O'Connell, B.C., Gygi, S.P., Elledge, S.J., Harper, J.W., 2009. Mammalian BTBD12/SLX4 Assembles A Holliday Junction Resolvase and Is Required for DNA Repair. Cell 138, 63–77. https://doi.org/10.1016/j.cell.2009.06.030

Takai, H., Smogorzewska, A., de Lange, T., 2003. DNA Damage Foci at Dysfunctional Telomeres. Curr. Biol. 13, 1549–1556. https://doi.org/10.1016/S0960-9822(03)00542-6

Tan, J., Duan, M., Yadav, T., Phoon, L., Wang, X., Zhang, J.-M., Zou, L., Lan, L., 2020a. An R-loop-initiated CSB–RAD52–POLD3 pathway suppresses ROS-induced telomeric DNA breaks. Nucleic Acids Res. 48, 1285–1300. https://doi.org/10.1093/nar/gkz1114

Tan, J., Wang, X., Phoon, L., Yang, H., Lan, L., 2020b. Resolution of ROS-induced G-quadruplexes and R-loops at transcriptionally active sites is dependent on BLM helicase. FEBS Lett. 594, 1359–1367. https://doi.org/10.1002/1873-3468.13738

Tan, R., Nakajima, S., Wang, Q., Sun, H., Xue, J., Wu, J., Hellwig, S., Zeng, X., Yates, N.A., Smithgall, T.E., Lei, M., Jiang, Y., Levine, A.S., Su, B., Lan, L., 2017. Nek7 Protects Telomeres from Oxidative DNA Damage by Phosphorylation and Stabilization of TRF1. Mol. Cell 65, 818-831.e5. https://doi.org/10.1016/j.molcel.2017.01.015

Tang, M., Li, Y., Zhang, X., Deng, T., Zhou, Z., Ma, W., Songyang, Z., 2014. Structural Maintenance of Chromosomes Flexible Hinge Domain Containing 1 (SMCHD1) Promotes Non-homologous End Joining and Inhibits Homologous Recombination

Repair upon DNA Damage *. J. Biol. Chem. 289, 34024–34032. https://doi.org/10.1074/jbc.M114.601179

Tardat, M., Déjardin, J., 2018. Telomere chromatin establishment and its maintenance during mammalian development. Chromosoma 127, 3–18. https://doi.org/10.1007/s00412-017-0656-3

Teng, Y., Yadav, T., Duan, M., Tan, J., Xiang, Y., Gao, B., Xu, J., Liang, Z., Liu, Y., Nakajima, S., Shi, Y., Levine, A.S., Zou, L., Lan, L., 2018. ROS-induced R loops trigger a transcription-coupled but BRCA1/2-independent homologous recombination pathway through CSB. Nat. Commun. 9, 4115. https://doi.org/10.1038/s41467-018-06586-3

Tomlinson, R.L., Ziegler, T.D., Supakorndej, T., Terns, R.M., Terns, M.P., 2006. Cell Cycle-regulated Trafficking of Human Telomerase to Telomeres. Mol. Biol. Cell 17, 955–965. https://doi.org/10.1091/mbc.e05-09-0903

Van Ly, D., Low, R.R.J., Frölich, S., Bartolec, T.K., Kafer, G.R., Pickett, H.A., Gaus, K., Cesare, A.J., 2018. Telomere Loop Dynamics in Chromosome End Protection. Mol. Cell 71, 510-525.e6. https://doi.org/10.1016/j.molcel.2018.06.025

van Steensel, B., Smogorzewska, A., de Lange, T., 1998. TRF2 Protects Human Telomeres from End-to-End Fusions. Cell 92, 401–413. https://doi.org/10.1016/S0092-8674(00)80932-0

Vančevska, A., Ahmed, W., Pfeiffer, V., Feretzaki, M., Boulton, S.J., Lingner, J., 2020. SMCHD1 promotes ATM-dependent DNA damage signaling and repair of uncapped telomeres. EMBO J. 39, e102668. https://doi.org/10.15252/embj.2019102668

Vannier, J.-B., Pavicic-Kaltenbrunner, V., Petalcorin, M.I.R., Ding, H., Boulton, S.J., 2012. RTEL1 Dismantles T Loops and Counteracts Telomeric G4-DNA to Maintain Telomere Integrity. Cell 149, 795–806. https://doi.org/10.1016/j.cell.2012.03.030

Vannier, J.-B., Sandhu, S., Petalcorin, M.IR., Wu, X., Nabi, Z., Ding, H., Boulton, S.J., 2013. RTEL1 Is a Replisome-Associated Helicase That Promotes Telomere and Genome-Wide Replication. Science 342, 239–242. https://doi.org/10.1126/science.1241779

Vítor, A.C., Sridhara, S.C., Sabino, J.C., Afonso, A.I., Grosso, A.R., Martin, R.M., de Almeida, S.F., 2019. Single-molecule imaging of transcription at damaged chromatin. Sci. Adv. 5, eaau1249. https://doi.org/10.1126/sciadv.aau1249

Wahba, L., Gore, S.K., Koshland, D., 2013. The homologous recombination machinery modulates the formation of RNA–DNA hybrids and associated chromosome instability. eLife 2, e00505. https://doi.org/10.7554/eLife.00505

Wallace, S.S., 2014. Base excision repair: A critical player in many games. Cut.-Edge Perspect. Genomic Maint. 19, 14–26. https://doi.org/10.1016/j.dnarep.2014.03.030

Wang, Z., Rhee, D.B., Lu, J., Bohr, C.T., Zhou, F., Vallabhaneni, H., de Souza-Pinto, N.C., Liu, Y., 2010. Characterization of Oxidative Guanine Damage and Repair in Mammalian Telomeres. PLOS Genet. 6, e1000951. https://doi.org/10.1371/journal.pgen.1000951

Watson, J.D., Crick, F.H.C., 1953. Molecular Structure of Nucleic Acids: A Structure for Deoxyribose Nucleic Acid. Nature 171, 737–738. https://doi.org/10.1038/171737a0

Weinhold, N., Jacobsen, A., Schultz, N., Sander, C., Lee, W., 2014. Genome-wide analysis of noncoding regulatory mutations in cancer. Nat. Genet. 46, 1160–1165.

Wellinger, R.E., Prado, F., Aguilera, A., 2006. Replication Fork Progression Is Impaired by Transcription in Hyperrecombinant Yeast Cells Lacking a Functional THO Complex. Mol. Cell. Biol. 26, 3327–3334. https://doi.org/10.1128/MCB.26.8.3327-3334.2006

White, C.I., Haber, J.E., 1990. Intermediates of recombination during mating type switching in Saccharomyces cerevisiae. EMBO J. 9, 663–673. https://doi.org/10.1002/j.1460-2075.1990.tb08158.x

Wu, L., Hickson, I.D., 2003. The Bloom's syndrome helicase suppresses crossing over during homologous recombination. Nature 426, 870–874. https://doi.org/10.1038/nature02253

Wu, L., Multani, A.S., He, H., Cosme-Blanco, W., Deng, Yu, Deng, J.M., Bachilo, O., Pathak, S., Tahara, H., Bailey, S.M., Deng, Yibin, Behringer, R.R., Chang, S., 2006. Pot1 Deficiency Initiates DNA Damage Checkpoint Activation and Aberrant Homologous Recombination at Telomeres. Cell 126, 49–62. https://doi.org/10.1016/j.cell.2006.05.037

Wu, P., Takai, H., de Lange, T., 2012. Telomeric 3' Overhangs Derive from Resection by Exo1 and Apollo and Fill-In by POT1b-Associated CST. Cell 150, 39–52. https://doi.org/10.1016/j.cell.2012.05.026

Xu, B., Clayton, D.A., 1996. RNA-DNA hybrid formation at the human mitochondrial heavy-strand origin ceases at replication start sites: an implication for RNA-DNA hybrids serving as primers. EMBO J. 15, 3135–3143. https://doi.org/10.1002/j.1460-2075.1996.tb00676.x

Yang, L., Sun, L., Teng, Y., Chen, H., Gao, Y., Levine, A.S., Nakajima, S., Lan, L., 2017. Tankyrase1-mediated poly(ADP-ribosyl)ation of TRF1 maintains cell survival after telomeric DNA damage. Nucleic Acids Res. 45, 3906–3921. https://doi.org/10.1093/nar/gkx083

Yang, Z., Sharma, K., de Lange, T., 2022. TRF1 uses a noncanonical function of TFIIH to promote telomere replication. Genes Dev. 36, 956–969. https://doi.org/10.1101/gad.349975.122

Ye, J.Z.-S., Hockemeyer, D., Krutchinsky, A.N., Loayza, D., Hooper, S.M., Chait, B.T., de Lange, T., 2004. POT1-interacting protein PIP1: a telomere length regulator that recruits POT1 to the TIN2/TRF1 complex. Genes Dev. 18, 1649–1654. https://doi.org/10.1101/gad.1215404

Yeager, T.R., Neumann, A.A., Englezou, A., Huschtscha, L.I., Noble, J.R., Reddel, R.R., 1999. Telomerase-negative Immortalized Human Cells Contain a Novel Type of Promyelocytic Leukemia (PML) Body1. Cancer Res. 59, 4175–4179.

Yeh, T.-Y.J., Meyer, T.N., Schwesinger, C., Tsun, Z.-Y., Lee, R.M., Chi, N.-W., 2006. Tankyrase recruitment to the lateral membrane in polarized epithelial cells: regulation by cell–cell contact and protein poly (ADP-ribosyl) ation. Biochem. J. 399, 415–425.

Yehezkel, S., Segev, Y., Viegas-Péquignot, E., Skorecki, K., Selig, S., 2008. Hypomethylation of subtelomeric regions in ICF syndrome is associated with abnormally short telomeres and enhanced transcription from telomeric regions. Hum. Mol. Genet. 17, 2776–2789. https://doi.org/10.1093/hmg/ddn177

Yu, G.-L., Bradley, J.D., Attardi, L.D., Blackburn, E.H., 1990. In vivo alteration of telomere sequences and senescence caused by mutated Tetrahymena telomerase RNAs. Nature 344, 126–132. https://doi.org/10.1038/344126a0

Yu, K., Chedin, F., Hsieh, C.-L., Wilson, T.E., Lieber, M.R., 2003. R-loops at immunoglobulin class switch regions in the chromosomes of stimulated B cells. Nat. Immunol. 4, 442–451. https://doi.org/10.1038/ni919

Yu, Z., Mersaoui, S.Y., Guitton-Sert, L., Coulombe, Y., Song, J., Masson, J.-Y., Richard, S., 2020. DDX5 resolves R-loops at DNA double-strand breaks to promote DNA repair and

avoid chromosomal deletions. NAR Cancer 2, zcaa028. https://doi.org/10.1093/narcan/zcaa028

Zhang, C., Chen, Liping, Peng, D., Jiang, A., He, Y., Zeng, Y., Xie, C., Zhou, H., Luo, X., Liu, H., Chen, Liang, Ren, J., Wang, W., Zhao, Y., 2020. METTL3 and N6-Methyladenosine Promote Homologous Recombination-Mediated Repair of DSBs by Modulating DNA-RNA Hybrid Accumulation. Mol. Cell 79, 425-442.e7. https://doi.org/10.1016/j.molcel.2020.06.017

Zhang, J.-M., Yadav, T., Ouyang, J., Lan, L., Zou, L., 2019. Alternative Lengthening of Telomeres through Two Distinct Break-Induced Replication Pathways. Cell Rep. 26, 955-968.e3. https://doi.org/10.1016/j.celrep.2018.12.102

Zhong, Z., Shiue, L., Kaplan, S., de Lange, T., 1992. A Mammalian Factor That Binds Telomeric TTAGGG Repeats In Vitro. Mol. Cell. Biol. 12, 4834–4843. https://doi.org/10.1128/mcb.12.11.4834-4843.1992

Zhou, J., Liu, M., Fleming, A.M., Burrows, C.J., Wallace, S.S., 2013. Neil3 and NEIL1 DNA Glycosylases Remove Oxidative Damages from Quadruplex DNA and Exhibit Preferences for Lesions in the Telomeric Sequence Context. J. Biol. Chem. 288, 27263–27272. https://doi.org/10.1074/jbc.M113.479055

Zimmermann, M., Kibe, T., Kabir, S., de Lange, T., 2014. TRF1 negotiates TTAGGG repeat-associated replication problems by recruiting the BLM helicase and the TPP1/POT1 repressor of ATR signaling. Genes Dev. 28, 2477–2491. https://doi.org/10.1101/gad.251611.114

Zou, L., Elledge, S.J., 2003. Sensing DNA damage through ATRIP recognition of RPA-ssDNA complexes. Science 300, 1542–1548.

NGUYEN Thu Trang

trang.nguyen@epfl.ch | +41 77 947 1632

EDUCATION

- **Swiss Institute for Experimental Cancer Research, EPFL, Switzerland** — Sep 2018 – Present
  PhD in Molecular Life Science
- **National University of Singapore, Singapore** — Aug 2014 – Jun 2018
  BSc in Life Science
  GPA: 4.80/5.00
  Graduated with Honors - Highest Distinction

RESEARCH EXPERIENCES

- **PhD Project: *Telomere protection against oxidative stress*** — Sept 2018 – Present

  Supervisor: Dr. Joachim Lingner — Professor for Life Sciences
  Swiss Institute for Experimental Cancer Research
  School of Life Sciences
  Ecole Polytechnique Fédérale de Lausanne
  Switzerland

- **Undergraduate Honors Project: *Identification of CCND3 as a downstream target of TAL1 oncogene in T-cell acute lymphoblastic leukemia*** — Sept 2017 – Jun 2018

  Supervisors: Dr. Takaomi Sanda — Assistant Professor
  Department of Medicine
  National University of Singapore, Singapore

  Dr. Sudhakar Jha — Assistant Professor
  Department of Biochemistry
  National University of Singapore, Singapore

- **Summer Research Project in Kyoto University Amgen Scholars Program: *Histone H3.3 Chaperone HIRA Induces Acquired Tolerance via Activating Stress-responsive Genes*** — Jun 2017 – Aug 2017

  Supervisor: Dr. Fuyuki Ishikawa — Professor
  Graduate School of Life Science
  Kyoto University, Japan

- **Undergraduate Research Project: *Interaction between DDX3 protein and cGAS-STING pathway*** — Jan 2016 – Nov 2016

  Supervisors: Dr. Stephan Gasser — Associate Professor
  Department of Microbiology and Immunology
  National University of Singapore, Singapore
  Current Position: Principal Scientist
  Roche Glycart AG, Switzerland

  Dr. Zhang Yongliang — Associate Professor
  Department of Microbiology and Immunology
  National University of Singapore, Singapore

SELECTED HONORS & AWARDS

- **MSCA Fellowship (aDDRess - ITN)** — Aug 2019 – Aug 2022
- **Singapore Society for Biochemistry and Molecular Biology prize** — June 2018
  The prize is awarded to the best student in Life Sciences with concentration in Biomedical Science or Molecular and Cell Biology.
- **Kyoto University Amgen Scholarship** — June 2017 – Aug 2017
  The scholarship from Amgen Foundation covers travel cost and living expenses for undergraduate students to work full-time in a laboratory in Kyoto University during 8 weeks.
- **Oversea Undergraduate Scholarship** — Aug 2014 – June 2018
  The scholarship is from the Ministry of Education, Vietnam to support students to continue their study overseas. It covers tuition fee, travel allowance and living expenses.
- **Silver Medal in the 23rd International Biology Olympiad** — July 2012
- **Bronze Medal in the 22nd International Biology Olympiad** — July 2011
  The International Biology Olympiad is a science olympiad for high school students worldwide.

REFERENCES

Prof. Joachim Lingner

Professor for Life Sciences
Swiss Institute for Experimental Cancer Research (ISREC)
School of Life Sciences
Ecole Polytechnique Fédérale de Lausanne (EPFL), Switzerland
Phone: +41-21-693 0721
Email: joachim.lingner@epfl.ch

Dr. Stephan Gasser

Principal Scientist
Roche Pharma Research and Early Development
Roche Innovation Center Zurich
Roche Glycart AG, Switzerland
Phone: +41 44 755 69 53
Email: stephan.gasser@roche.com